

**STUDY ON CORROSION INHIBITION EFFICIENCY OF
ESSENTIAL OILS EXTRACTED FROM SOME SELECTED
PLANTS AVAILABLE IN MIZORAM**

**A THESIS SUBMITTED IN PARTIAL FULFILLMENT OF THE
REQUIREMENTS FOR THE DEGREE OF DOCTOR OF
PHILOSOPHY**

LALRINTLUANGI

MZU REGISTRATION NO.: 5440 of 2013

Ph.D REGISTRATION NO. : MZU/Ph.D./732 of 11.05.2015



**DEPARTMENT OF INDUSTRIAL CHEMISTRY
SCHOOL OF PHYSICAL SCIENCES**

JUNE, 2023

**STUDY ON CORROSION INHIBITION EFFICIENCY OF ESSENTIAL
OILS EXTRACTED FROM SOME SELECTED PLANTS
AVAILABLE IN MIZORAM**

BY

Lalrintluangi

Department of Chemistry

Under the supervision of

Dr. VED PRAKASH SINGH

Joint supervisors

Prof., RAJ KUMAR MISHRA

Dr. RAGHVENDU PATHAK

Dr. ASHISH KUMAR SINGH

Submitted

**In partial fulfillment of the requirement of the Degree of Doctor of Philosophy
in industrial Chemistry of Mizoram University, Aizawl.**

(A central University under the Act of Parliament)

Department of Industrial Chemistry

School of Physical Sciences

Dr. Ved Prakash Singh

Associate Professor

CERTIFICATE

This is to certify that the thesis entitled “*Study on Corrosion inhibition efficiency of Essential oils extracted from some selected Plants available in Mizoram*” submitted by **Lalrintluangi**, for the award of the degree of ***Doctor of Philosophy*** in the Mizoram University, Tanhril, Aizawl, embodies therecord of the original investigations carried out by her under my supervision. She has been duly registered and the thesis presented is worthy of being considered for the award of the Ph.D. degree. This work has not been submitted for any degree in any other university.

Dated: June, 2023

(Dr. VED PRAKASH SINGH)

Supervisor



DEPARTMENT OF CHEMISTRY

GURU GHASIDAS VISHWAVIDYALAYA, BILASPUAR (C.G.)

(A Central University established by the Central Universities Act, 2009 No.25 of 2009)

Koni, Bilaspur (CG)-495009, Phone-07752-260209, 260435, Fax-07752-260154, 260148

www.ggu.ac.in


Dr. Ashish Kumar Singh

Associate Professor

CERTIFICATE

This is to certify that the thesis entitled “*Study on Corrosion inhibition efficiency of Essential oils extracted from some selected Plants available in Mizoram*” submitted by **Lalrintluangi**, for the award of the degree of *Doctor of Philosophy* in the Mizoram University, Tanhril, Aizawl, embodies the record of the original investigations carried out by her under my supervision. She has been duly registered and the thesis presented is worthy of being considered for the award of the Ph.D. degree. This work has not been submitted for any degree in any other university.

Dated : June, 2023


Dr. Ashish Kumar Singh
Associate Professor
Department of Chemistry
Guru Ghasidas Vishwavidyalaya
(A Central University)
Bilaspur (C.G.) 495009

(Dr. ASHISH KUMAR SINGH)

Joint Supervisor

(A central University under the Act of Parliament)

Department of Chemistry

Banaras Hindu University

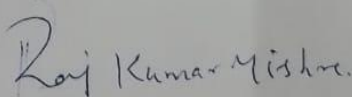
Institute of Sciences

Prof., Raj kumar Mishra

CERTIFICATE

This is to certify that the thesis entitled "*Study on Corrosion inhibition efficiency of Essential oils extracted from some selected Plants available in Mizoram*" submitted by **Lalrintluangi**, for the award of the degree of *Doctor of Philosophy* in the Mizoram University, Tanhril, Aizawl, embodies therecord of the original investigations carried out by her under my joint supervision. She has been duly registered and the thesis presented is worthy of being considered for the award of the Ph.D. degree. This work has not been submitted for any degree in any other university.

Dated: December, 2022


(Prof., RAJ KUMAR MISHRA)

Joint Supervisor

Dr. Raj Kumar Mishra
Professor Department of Chemistry
Institute of Science
Banaras Hindu University
Varanasi-221005, India
Mobile No. +91-9774379665

(A central University under the Act of Parliament)

Department of Chemistry
Pachhunga University college
Aizawl, Mizoram

Dr. RaghvenduPathak

CERTIFICATE

This is to certify that the thesis entitled "*Study on Corrosion inhibition efficiency of Essential oils extracted from some selected Plants available in Mizoram*" submitted by Lalrintluangi, for the award of the degree of *Doctor of Philosophy* in the Mizoram University, Tanhril, Aizawl, embodies therecord of the original investigations carried out by her under my supervision. She has been duly registered and the thesis presented is worthy of being considered for the award of the Ph.D. degree. This work has not been submitted for any degree in any other university.

Dated: December, 2022

Raghvendu Pathak
16/12/2022
(Dr. RaghvenduPathak)
Joint Supervisor

Declaration of the Candidate

Mizoram University

June, 2023

I, Lalrintluangi, hereby declare that the subject matter of this thesis is the record of work done by me, that the contents of this thesis did not form basis of the award of any previous degree to me or to do the best of my knowledge to anybody else, and that the thesis has not been submitted by me for any research degree in any other University/ Institute.

This is being submitted to the Mizoram University for the degree of Doctor of Philosophy in Industrial Chemistry.

(LALRINTLUANGI)

Candidate

(Dr. VED PRAKASH SINGH)

Head

(Dr. VED PRAKASH SINGH)

Supervisor

ACKNOWLEDGEMENT

First of all, I thank Almighty God for blessing me with health, strength and knowledge to accomplish my work. Without his grace and mercy, this work would not have been possible.

I would like to acknowledge and give my warmest appreciation to my supervisor, **Dr. Ved Prakash Singh**, Associate Professor, Department of Industrial Chemistry, Mizoram University. His dedication, genuine interest, and, most of all, his overwhelming attitude to assist his students had been solely responsible for the completion of my work. He is always ready to provide a fresh perspective and scholarly advice during my entire tenure. I admire his timely advice, scrutiny, and scientific approach, which have greatly aided me in completing this work.

I sincerely thank and give respect to *Prof. Muthukumuran R., Head, Department of Chemistry, MZU*, and other faculty members viz., *Prof. Diwakar Tiwari, Dr. N. Mohondas Singh, Dr. Zodinpuia Pachuau, Dr. A. Bimolini Devi* and non-teaching staff, *Mr. Brojendro Singh Shagolsem, Sr. Laboratory Technician, and Mr. John Vanlalhrauaia, Technical Assistant, Chemistry Department. MZU*, for their endless help and support throughout my academic career.

I appreciate the good cooperation I have experienced from my fellow research scholar of the department. I would like to give credit to my fellow labmate *Dr. Jayanta Dowarah, Dr. Lalhrauaizela Mr. Brilliant N. Marak, Mr. Laldingluaia Khiangte, Mr. Biki Hazarika, Mr. Lalropuia, Mr. Saurabh Chetia and Ms. Lalremruati* for their limitless assistance in my research work. They were my devoted friends and never fail to comfort me during my times of difficulties. Their good deeds would be remembered during my entire life.

My sincere thanks go to my co-guides viz., *Dr. Raj Kumar Mishra, BHU, Varanasi, Dr. Ashish Kumar Singh, Guru Ghasidas University, Bilaspur, Chhattisgarh, Dr. Raghvendu Pathak, Pachhunga University college, Aizawl* for their constant encouragement and useful advice they have offered me throughout my academic career in the University.

I heartfelt thanks to *Dr. Jay Prakash*, Pachhunga University College, Aizawl, Mizoram, for his incentive, helpful work and suggestions in completing my research works.

I also express my deepest gratitude to *Dr. Manisha Malviya*, Department of Chemistry, IIT BHU, Varanasi, *Dr. S.K. Mishra*, Department of Chemistry, IIT BHU, Varanasi, *Dr. Awadhesh Kumar*, HAMP Department, MZU, Aizawl and all the faculties of Pachhunga University college (PUC), Aizawl, Mizoram for the collaboration of performing the experiment of Electrochemical studies of my samples and extraction of Essential oils.

I also thank Central Instrument (CIF), IIT(BHU), Varanasi and Banaras Hindu University, Institute of Science, Department of Chemistry, Varanasi for collecting spectroscopic GC-MS, SEM-EDS, and FT-IR.

I acknowledge NFST- UGC, New Delhi for their financial support in funding the research work and the fellowship I enjoy during my research period.

It is my pleasure to thank my parents and all of my family members for their prayers, love and support during my tenure for the degree. I also give my heartfelt thanks to my husband for her courage, strength and hard labour he went through for the accomplishment of the degree I sought for.

(LALRINTLUANGI)

CONTENTS

Title of the Thesis
Certificate
Declaration of the Candidate
Acknowledgement
Table of Contents
List of Tables
List of Figures

CHAPTER 1

	Pages
1. INTRODUCTION	1
1.1 FACTORS WHICH AFFECT CORROSIONS	3
1.2 TYPES OF CORROSION	4
1.3 CORROSION INHIBITORS	6
1.3.1 Classification or Types of inhibitors	7
1.3.2 Mechanism of corrosion inhibition	8
1.3.3 Thermodynamics Inhibition process	10
1.4 EFFECT AND ECONOMIC IMPACT OF CORROSION	10
1.5 PROPERTIES OF CORROSION INHIBITORS	11
1.6 GREEN CORROSION INHIBITORS	11
1.7 REVIEW OF LITERATURE	12
1.8 OBJECTIVE	18
1.9. SCOPE OF STUDY	19
1.9.1 Importance of acid in industrial process	19
1.9.2 Sustainability and Corrosion Inhibition	19

CHAPTER-2

	Pages
2 EXTRACTION OF ESSENTIAL OILS AND	
IDENTIFICATION OF MAJOR PHYTOCHEMICALS	21
2.1 OUTLOOK OF THE PRESENT WORK	22
2.1.1 <i>Zingiber Mioga</i> (ZM)	22
2.1.2 <i>Zingiber Officinale</i> (ZO)	23
2.1.3 <i>Eryngium Foetidum</i> (EF)	24
2.1.4 <i>Mentha Piperita</i> (MP)	24
2.1.5 <i>Allium Sativum</i> (AS)	25
2.2 EXTRACTION OF ESSENTIAL OILS	26
2.2.1 <i>Extraction of oils from Zingiber mioga buds</i>	27
2.2.2 <i>Extraction of oils from Zingiber officinale rhizome</i>	28
2.2.3 <i>Extraction of oils from Eryngium foetidum leaves</i>	28
2.2.4 <i>Extraction of oils from Mentha piperita leaves</i>	29
2.2.5 <i>Extraction of oils from Garlic Allium sativum scaly bulb</i>	29
2.3 SOLUTION PREPARATION	30
2.4 SPECIMEN PREPARATION	30
2.5 IDENTIFICATION OF MAJOR PHYTOCHEMICALS	
OF ESSENTIAL OILS	31
2.6 CHARACTERIZATION OF (FT- IR) SPECTROSCOPY	
2.5.1 <i>GC-MS analysis of EOs extract</i>	31
2.5.2 <i>FT-IR analysis of EOs extract</i>	44

CHAPTER-3

	Pages
3. CORROSION INHIBITION EFFICIENCY	53
3.1 Weight loss measurement	53
3.1.1 <i>ZingiberMioga(ZM)</i>	54
3.1.2 <i>ZingiberOfficinale(ZO)</i>	55
3.1.3 <i>EryngiumFoetidum(EF)</i>	57
3.1.4 <i>Mentha Piperita(MP)</i>	59
3.1.5 <i>Allium Sativum(AS)</i>	61
3.2 Electrochemical measurements	64
3.2.1 <i>ZingiberMioga(ZM)</i>	65
3.2.2 <i>ZingiberOfficinale(ZO)</i>	71
3.2.3 <i>EryngiumFoetidum(EF)</i>	78
3.2.4 <i>Mentha Piperita(MP)</i>	84
3.2.5 <i>Allium Sativum(AS)</i>	90

CHAPTER-4

	Pages
4. STUDY ON SURFACE MORPHOLOGY	97
4.1. EFFECT OF TEMPERATURE, ADSORPTION ISOTHERM AND THERMODYNAMIC PARAMETERS	

OF ZINGIBER MIOGA (ZM)	98
4.2 EFFECT OF TEMPERATURE, ADSORPTION ISOTHERM AND THERMODYNAMIC PARAMETERS OF ZINGIBER OFFICINALE (ZO)	104
4.3 EFFECT OF TEMPERATURE, ADSORPTION ISOTHERM AND THERMODYNAMIC PARAMETERS OF ERYNGIUM FOETIDUM (EF)	110
4.4 EFFECT OF TEMPERATURE, ADSORPTION ISOTHERM AND THERMODYNAMIC PARAMETERS OF MENTHA × PIPERITA (MP)	116
4.5 EFFECT OF TEMPERATURE, ADSORPTION ISOTHERM AND THERMODYNAMIC PARAMETERS ALLIUM SATIVUM (AS)	121
4.6 FOURIER TRANSFORM INFRARED SPECTROSCOPY (FTIR SPECTROSCOPY) STUDY	126
4.6.1 <i>Zingiber mioga</i>	126
4.6.2 <i>Zingiber officinale</i>	128
4.6.3 <i>Eryngium foetidum</i>	129
4.6.4 <i>Mentha piperita</i>	130
4.6.5 <i>Allium sativum</i>	131
4.7 SCANNING ELECTRON MICROSCOPE (SEM) ANALYSIS	131

4.7.1	<i>Zingibermyoga</i>	132
4.7.2	<i>Zingiberofficinale</i>	132
4.7.3	<i>Mentha piperita</i>	133
4.7.4	<i>Eryngiumfoetidum</i>	134
4.7.5	<i>Allium sativum</i>	134
4.8	MECHANISM OF CORROSION INHIBITION	135
4.8.1	Mechanism of Corrosion Inhibition of ZM Extract	135
4.8.2	Mechanism of Corrosion Inhibition of ZO Extract	136
4.8.3	Mechanism of Corrosion Inhibition of EF Extract	137
4.8.4	Mechanism of Corrosion Inhibition of MP Extract	138
4.8.5	Mechanism of Corrosion Inhibition of AS Extract	139

CHAPTER – 5

	Pages
5. SUMMARY AND CONCLUSIONS	141
5.1 <i>ZingiberMyoga (ZM) Extract</i>	141
5.2 <i>ZingiberOfficinale(ZO) Extract</i>	143
5.3 <i>Eryngiumfoetidum(EF) Extract</i>	144
5.4 <i>MenthaPiperita (MP) oils extract</i>	146
5.5 <i>Allium Sativum (AS) oils extract</i>	148

FUTURE WORK	150
REFERENCES	151
BIODATA	167
PARTICULARS OF THE CANDIDATE	169
LIST OF PUBLICATIONS	171
CONFERENCE/SEMINARS	172

LIST OF TABLES

TABLE	PAGES
2.5.1.1 Phytochemical constituents of extracted oils from <i>Zingiber Mioga</i> (ZM).	32
2.5.1.2 Phytochemical constituents of extracted oils from <i>Zingiber Officinale</i> (ZO).	34
2.5.1.3 Phytochemical constituents of extracted oils from <i>Eryngium Foetidum</i> (EF).	36
2.5.1.4 Phytochemical constituents of extracted oils from <i>Mentha Piperita</i> (MP).	39
2.5.1.5 Phytochemical constituents of extracted oils from garlic <i>Allium Sativum</i> (AS).	42

2.5.2.1 FT-IR characterization of <i>ZingiberMioga</i> (ZM).	44
2.5.2.2 FT-IR characterization of <i>ZingiberOfficinale</i> (ZO).	45
2.5.2.3: FT-IR characterization of <i>EryngiumFoetidum</i> (EF).	47
2.5.2.4: FT-IR characterization of <i>MenthaPiperita</i> (MP).	49
2.5.2.5: FT-IR characterization of <i>Allium Sativum</i> (AS).	51
3.1.1 Weight loss measurement for mild steel in 1M HCl without and with inhibitors indifferent concentrations of <i>ZingiberMioga</i> EO extract at 30°C.	54
3.1.2 Weight loss measurement for mild steel in 1M HCl without and with inhibitors indifferent concentrations of <i>Zingiberofficinale</i> EO extract at 30°C.	56
3.1.3 Weight loss measurement for mild steel in 1M HCl without and with inhibitorsin different concentrations of <i>Eryngiumfoetidum</i> EO extract at 30°C.	58
3.1.4 Weight loss measurement for mild steel in 1M HCl without and with inhibitors indifferent concentrations of <i>MenthaPiperita</i> EO extract at 30°C.	60
3.1.5 Gravimetric analysis for mild steel in an acidic medium with differenttemperatures in the absence and presence of various concentrations of <i>Allium sativum</i> EOextract at 30 ° C.	62
3.2.1.1 Values of potentiodynamic polarization obtained for mild steel in the absenceand presence of several concentrations of <i>Zingibermioga</i> EO extract at 30 ° C.	66
3.2.1.2 Values of impedance parameters obtained from fitting EIS data withR(QR)(QR) equivalent circuit for Myoga Ginger (<i>Zingibermioga</i>) EO extract in 1M HCl inthe absence and presence of inhibitors of various concentrations at 30 ° C.	68
3.2.1.3 Inhibition efficiency and surface coverage obtained from R_{ct} with increasingconcentration of inhibitor.	69
3.2.2.1 Values of potentiodynamic polarization obtained for mild steel	

in the absence and presence of several concentrations of <i>Zingiber officinale</i> EO extract at 30°C	72
3.2.2.2 Values of impedance parameters obtained from fitting EIS data with R(QR)(QR) equivalent circuit for <i>Zingiber officinale</i> EO extract in 1M HCl in the absence and presence of various concentrations of inhibitor at 30°C.	74
3.2.2.3 Inhibition efficiency and surface coverage obtained from R_{ct} with increasing concentration of inhibitor.	75
3.2.3.1 Values of potentiodynamic polarization obtained for mild steel in the absence and presence of several concentrations of <i>Eryngium foetidum</i> EO extract at 30°C.	79
3.2.3.2 Values of impedance parameters obtained from <i>Eryngium foetidum</i> EO extract in 1M HCl in the absence and presence of inhibitors of various concentrations at 30°C.	81
3.2.3.3 Inhibition efficiency and surface coverage obtained from R_{ct} with increasing concentration of inhibitor.	82
3.2.4.1 Values of potentiodynamic polarization were obtained for mild steel in the absence and presence of several concentrations of M. Piperita EO extract at 30°C.	85
3.2.4.2 Values of impedance parameters obtained from M. Piperita EO extract in 1M HCl in the absence and presence of inhibitors of various concentrations at 30°C.	87
3.2.4.3. Inhibition efficiency and surface coverage obtained from R_{ct} with increasing concentration of inhibitor.	88
3.2.5.1. Values of potentiodynamic polarization were obtained for mild steel in the absence and presence of several concentrations of <i>Allium sativum</i> EO extract at 30°C.	90
3.2.5.2. Values of impedance parameters obtained from <i>Allium sativum</i> EO extract in 1M HCl in the absence and presence of inhibitors of various concentrations at 30°C by fitting with R(QR)(QR) equivalent circuit.	93
3.2.5.3. Inhibition efficiency and surface coverage obtained from	

R_c with increasing concentration of inhibitor.	93
4.1.1 Values of Corrosion rate and Inhibition efficiency without and with inhibitors (concentration = 5g/L) at various temperatures in the <i>Zingiber mioga</i> EO extracts.	98
4.1.2 Thermodynamic parameters for mild steel in 1M HCl acidic medium in various concentrations of <i>Zingiber mioga</i> EO extract at a temperature range (303K - 333K).	100
4.1.3 Thermodynamics parameters of <i>Zingiber mioga</i> EO for mild steel in the acidic medium at different temperatures.	100
4.2.1 Variations of corrosion rate and inhibition efficiency with different temperatures in the presence of <i>Zingiber officinale</i> EO and without inhibitor.	105
4.2.2 Thermodynamics parameters for mild steel in the acidic medium in various concentration of <i>Zingiber officinale</i> EO at temperature ranges between 303–333 K.	107
4.2.3 Thermodynamics parameters for mild steel in an acidic medium of <i>Zingiber officinale</i> EO extract at different temperatures.	107
4.3.1 Variation of corrosion rate and inhibition efficiency in <i>Eryngium foetidum</i> EO at different temperatures and without inhibitor.	111
4.3.2 Thermodynamics parameters for mild steel in the acidic medium in various concentration of <i>Eryngium foetidum</i> EO at a temperature range between (303 – 333)K.	112
4.3.3 Thermodynamics parameters for mild steel in the acidic medium in <i>Eryngium foetidum</i> EO at different temperatures	112
4.4.1 Variation of corrosion rate and inhibition efficiency with different temperatures in the presence of 5g/L of <i>Mentha piperita</i> EO extract and without inhibitor.	116
4.4.2 Thermodynamics parameters for mild steel in the acidic medium in various concentrations of <i>Mentha piperita</i> EO	

extract at a temperature range between (303 – 333) K	118
4.4.3 Thermodynamics parameters of <i>Menthapiperita</i> for mild steel in the acidic medium at different temperatures.	118
4.5.1. Variation of corrosion rate and inhibition efficiency with different temperatures in the presence of 5g/L of <i>Allium sativum</i> oils extract and without inhibitor.	122
4.5.2. Thermodynamics parameters for mild steel in the acidic medium in various concentrations of <i>Allium sativum</i> oils extract at a temperature range between (303 – 333) K	123
4.5.3 Thermodynamics parameters of <i>Allium sativum</i> for mild steel in the acidic medium at different temperatures.	124

LIST OF FIGURES

FIGURE	PAGES
1.1 Schematic representation of the mechanism of Rusting of Iron.	2
1.2 Schematic diagram of adsorption inhibitors classification.	7
1.3 A schematic representation of the double layer that develops between an electrode and electrolyte interface.	9
2.1 Hydro-distillation by using Clevenger apparatus.	27
2.5.1.1(a): Main phytochemical constituents in ZM extract.	33
2.5.1.2(a): Main phytochemical constituents in ZO extract.	35
2.5.1.3(a): Main phytochemical constituents in EF extract.	38
2.5.1.4(a): Main phytochemical constituents in MP extract.	41

2.5.1.5(a): Main phytochemical constituents in AS extract.	43
2.5.1.1(b): GC-MS Spectra of <i>Zingiber mioga</i> (ZM) essential oil extract.	
2.5.1.2 (b): GC-MS Spectra of <i>Zingiber officinale</i> (ZO) essential oil extract.	
2.5.1.3(b) : GC-MS Spectra of <i>Eryngium foetidum</i> (EF) essential oil extract.	
2.5.1.4(b): GC-MS Spectra of <i>Mentha piperita</i> (MP) essential oil extract.	
2.5.1.5(b): GC-MS Spectra of <i>Allium Sativum</i> (AS) essential oil extract.	
2.5.2.1 FTIR Spectra of ZM essential oils extract.	45
2.5.2.2 FTIR Spectra of ZO essential oils extract.	46
2.5.2.3 FTIR Spectra of EF essential oils extract.	48
2.5.2.4 FTIR Spectra of MP essential oils extract.	50
2.5.2.5 FTIR Spectra of AS essential oils extract.	51
3.1.1 Gravimetric plot of mild steel with and without inhibitor in various concentrations in 1M HCl solution of <i>Zingiber mioga</i> EO extract at temperature 30°C.	55
3.1.2 Gravimetric plot of mild steel with and without inhibitor in various concentrations in 1M HCl solution of EO (<i>Zingiber officinale</i>) extract at a temperature of 30°C.	57
3.1.3 Gravimetric plot of mild steel with and without inhibitor in various concentrations in 1M HCl solution of <i>Eryngium foetidum</i> L. EO extract at temperature 30°C.	59
3.1.4 Gravimetric plot of mild steel with and without inhibitor in various concentrations in 1M HCl solution of EOs (<i>M. Piperita</i>) extract at temperature 30°C.	61
3.1.5 Gravimetric plot of mild steel with and without inhibitor in various concentrations in 1M HCl solution of <i>Allium sativum</i> EO extract at temperature 30°C.	63
3.2.1.1 Tafel-polarisation curves for mild steel in 1M HCl without and	

with inhibitors of various concentrations of <i>Zingiber mioga</i> EO extract at 30°C.	67
3.2.1.2 (a) Nyquist plot for mild steel without and with different concentration of <i>Zingiber mioga</i> EO extract in 1M HCl at 30°C and (b) bode plots for mild steel in 1M HCl with and without inhibitors of different concentrations in <i>Zingiber mioga</i> EO extract at 30°C.	69
3.2.1.3 Impedance modulus vs. frequency of bode plots for mild steel in 1M HCl with and without inhibitors of different concentrations in <i>Zingiber mioga</i> EO extract at 30°C.	70
3.2.1.4 Equivalent electrical circuit model for EIS measurement.	71
3.2.1.5. Inhibition efficiency for mild steel in 1M HCl containing different concentrations of <i>Zingiber mioga</i> EO extracted by weight loss (Gravimetric analysis), Polarization curves, and the Nyquist plot.	71
3.2.2.1 Tafel-polarisation curves for mild steel in 1M HCl without and with inhibitors of various concentrations of <i>Zingiber officinale</i> EO extract at 30°C.	73
3.2.2.2 Nyquist plot for mild steel without and with different concentrations of <i>Zingiber officinale</i> EO extract in 1M HCl at 30°C and (b) bode plots for mild steel in 1M HCl with and without inhibitors of different concentrations in <i>Zingiber officinale</i> EO extract at 30°C.	76
3.2.2.3 Impedance modulus vs. frequency of bode plots for mild steel in 1M HCl with and without inhibitors of different concentrations in <i>Zingiber officinale</i> EO extract at 30°C.	77
3.2.2.4 Equivalent electrical circuit model for EIS measurement.	77
3.2.2.5 Inhibition efficiency for mild steel in 1M HCl containing different concentrations of <i>Zingiber officinale</i> EO extracted by weight loss (Gravimetric analysis), Polarization curves, and the Nyquist plot (Kumari et al., 2017).	78
3.2.3.1 Tafel-polarisation curves for mild steel in 1M HCl without and	

with inhibitors of various concentrations of <i>Eryngiumfoetidum</i> L. EO extract at 30°C.	80
3.2.3.2 Impedance of Nyquist plot for mild steel without and with inhibitors of various concentrations of <i>Eryngiumfoetidum</i> L. EO extract in 1M HCl at 30°C. (b) bode plots for mild steel in 1M HCl with and without inhibitors of different concentrations in <i>Eryngiumfoetidum</i> L. EO extract at 30°C.	83
3.2.3.3. Impedance modulus vs. frequency of bodeplots for mild steel in 1M HCl with and without inhibitors of different concentrations in <i>Eryngiumfoetidum</i> L. EO extract at 30°C.	83
3.2.3.4. Equivalent electrical circuit model for EIS measurement.	83
3.2.3.5 Inhibition efficiency for mild steel in 1M HCl containing different concentrations of <i>EryngiumFoetidum</i> essential oils extracted by weight loss (Gravimetric analysis), Polarization curves, and the Nyquist plot(Zhang & Hua, 2009).	84
3.2.4.1 Tafel-polarisation curves for mild steel in 1M HCl without and with inhibitors of various concentrations of <i>M. Piperita</i> EO extract30°C.	86
3.2.4.2 (a) Nyquist plot for mild steel without and with inhibitors of various concentrations of <i>M. Piperita</i> EO extract in 1M HCl at 30° C. (b) bode plots for mild steel in 1M HCl with and without inhibitors of different concentrations in <i>M. Piperita</i> EO extract at 30°C.	89
3.2.4.3 Impedance modulus vs. frequency of bode plots for mild steel in 1M HCl with and without inhibitors of different concentrations in <i>M. Piperita</i> EO extract at 30°C.	89
3.2.4.4 Equivalent electrical circuit model for EIS measurement.	89
3.2.4.5 Inhibition efficiency for mild steel in 1M HCl containing different concentrations of <i>M. Piperita</i> EO extract by weight loss (Gravimetric analysis), Polarization curves, and the Nyquist plot.	90

3.2.5.1 Tafel-polarisation curves for mild steel in 1M HCl without and with inhibitors of various concentrations of <i>Allium sativum</i> EO extract at 30°C.	92
3.2.5.2 (a) Nyquist plot for mild steel without and with inhibitors of various concentrations of <i>Allium sativum</i> EO extract in 1M HCl at 30°C. (b) Bode plots for mild steel in 1M HCl with and without inhibitors of different concentrations in <i>Allium sativum</i> EO extract at 30°C.	94
3.2.5.3 Impedance modulus vs. frequency of bode plots for mild steel in 1M HCl with and without inhibitors of different concentrations in <i>Allium sativum</i> EO extract at 30°C.	95
3.2.5.4 Equivalent electrical circuit model for EIS measurement.	95
3.2.5.5 Inhibition efficiency for mild steel in 1M HCl containing different concentrations of <i>Allium sativum</i> EO extracted by weight loss (Gravimetric analysis), Polarization curves, and the Nyquist plot.	96
4.1.1 Inhibitor efficiency with various concentrations of ZM extracted oils at different temperatures.	99
4.1.2 Langmuir adsorption isotherm for inhibitor extracted from <i>Zingiber mioga</i> EO at various temperatures.	101
4.1.3 Arrhenius plots for corrosion rates ($\log C_R$ versus $1/T$) on the mild steel in 1M HCl solution without and with inhibitors of <i>Zingiber mioga</i> EO extract at different concentrations at 30°C.	102
4.1.4 Transition state plots for corrosion rates ($\ln (C_R/T)$ versus $1/T$) on the mild steel in 1M HCl solution without and with inhibitors <i>Zingiber mioga</i> EO extract at different concentrations at 30°C.	103
4.2.1 Inhibitor efficiency with various concentrations of ginger extracted oils at different temperatures.	106
4.2.2 Langmuir adsorption isotherm for inhibitor of various concentrations extracted from <i>Zingiber officinale</i> EO at different temperatures.	108

4.2.3 Arrhenius plots for Mild steel corrosion rates $\log C_R$ versus $1/T$ in acidic in the absence and presence of <i>Zingiberofficinale</i> EO.	108
4.2.4 Transition ($\log (C_R/T)$ versus $1/T$) plots for Mild steel corrosion in acidic medium in the absence and presence of <i>Zingiberofficinale</i> EO.	109
4.3.1 Inhibitor efficiency with various concentrations of ginger extracted oils at different temperatures.	111
4.3.2 Langmuir adsorption isotherm for inhibitor of various concentrations extracted from <i>Eryngiumfoetidum</i> EO at different temperatures.	113
4.3.3. Arrhenius plots for Mild steel corrosion rates $\log C_R$ versus $1/T$ in acidic in the absence and presence of <i>Eryngiumfoetidum</i> EO.	114
4.3.4 Transition ($\log (C_R/T)$ versus $1/T$) plots for Mild steel corrosion in acidic medium in the absence and presence of <i>Eryngiumfoetidum</i> EO.	114
4.4.1 Inhibitor efficiency with various concentrations of peppermint extracted oils at different temperatures.	117
4.4.2 Langmuir adsorption isotherm for inhibitor of various concentrations extracted from <i>Menthapiperita</i> EO at different temperatures.	119
4.4.3 Arrhenius plots for Mild steel corrosion rates $\log C_R$ versus $1/T$ in acidic in the absence and presence of peppermint extracted oils.	119
4.4.4 Transition state plots for Mild steel corrosion rates $\log (C_R/T)$ versus $1/T$ in acidic in the absence and presence of <i>Menthapiperita</i> extracted oils.	120
4.5.1 Inhibitor efficiency at various concentrations of garlic extracted oils at different temperatures.	122
4.5.2 Langmuir adsorption isotherm for inhibitor of various concentrations extracted from <i>Allium sativum</i> EO at different temperatures.	124
4.5.3 Arrhenius plots for Mild steel corrosion rates $\log C_R$ versus $1/T$ in acidic in the absence and presence of <i>Allium sativum</i>	

extracted oils.	125
4.5.4 Transition state plots for Mild steel corrosion rates $\log(C_R/T)$ versus $1/T$ in acidic in the absence and presence of <i>Allium sativum</i> extracted oils	125
4.6.1 FT-IR spectra of (a) Pure <i>Zingiber mioga</i> (Aidu oils) and (b) protective layer developed on MSS after immersion for 6 h in 1 M HCl containing 5 g/L <i>Zingiber mioga</i> (Aiduoil)	127
4.6.2 FT-IR spectra of (a) pure <i>Zingiber officinale</i> (Ginger oil) and (b) protective layer developed on MSS after immersion for 6 h in 1 M HCl containing 5 g/L <i>Zingiber officinale</i> (Ginger oil).	128
4.6.3 FT-IR spectra of (a) pure <i>Eryngium foetidum</i> (Spiny coriander oil) and (b) protective layer developed on MSS after immersion for 6 h in 1 M HCl containing 5 g/L <i>Eryngium foetidum</i> (spiny coriander oil).	129
4.6.4 FT-IR spectra of (a) pure Peppermint oil and (b) protective layer developed on MSS after immersion for 6 h in 1 M HCl containing 5 g/L Menthe Piperita (Peppermint oil).	130
4.6.5 FT-IR spectra of (a) pure <i>Allium sativum</i> (Garlic oil) and (b) protective layer developed on MSS after immersion for 6h in 1 M HCl containing 5 g/L <i>Allium sativum</i> (Garlic oil).	131
4.7.1 SEM images of MSS: (a) before immersion in corrosive solution; (b) after immersion in 1 M HCl for 6 h; (c) after immersion in 1M HCl solution containing 5 g/L <i>Zingiber mioga</i> extracted oils for 6 h.	132
4.7.2 SEM images of MSS: (a) before immersion in corrosive solution; (b) after immersion in 1 M HCl for 6 h; (c) after immersion in 1M HCl solution containing 5 g/L <i>Zingiber officinale</i> extracted oils for 6 h.	133
4.7.3 SEM images of MSS: (a) before immersion in corrosive solution; (b) after immersion in 1 M HCl for 6 h; (c) after immersion in 1M HCl solution containing 5 g/L <i>Mentha piperita</i> extracted oils for 6 h.	133

4.7.4 SEM images of MSS: (a) before immersion in corrosive solution; (b) after immersion in 1 M HCl for 6h; (c) after immersion in 1M HCl solution containing 5 g/L <i>Eryngiumfoetidum</i> extracted oils for 6 h.	134
4.7.5 SEM images of MSS: (a) before immersion in corrosive solution; (b) after immersion in 1 M HCl for 6 h; (c) after immersion in 1N HCl solution containing 5 g/L <i>Allium sativum</i> extracted oils for 6 h.	135
4.8.1 Postulated corrosion inhibition mechanism of main constituent compounds in ZM extract	136
4.8.2 Postulated corrosion inhibition mechanism of main constituent compounds in ZO extract	137
4.8.3 Postulated corrosion inhibition mechanism of main constituent compounds in EF extract	138
4.8.4 Postulated corrosion inhibition mechanism of main constituent compounds in MP extract	139
4.8.5 Postulated corrosion inhibition mechanism of main constituent compounds in AS extract	140

BIO-DATA

- 1. NAME** : Lalrintluangi
- 2. DATE OF BIRTH** : 21st October, 1987
- 3. FATHER'S NAME** : C. Rohmingthanga
- 4. PERMANENT ADDRESS** : Ruantlang, Champhai
- 5. EMAIL ADDRESS** : tluangs.toik@gmail.com

6. EDUCATIONAL QUALIFICATIONS :

Examination passed	Year of Passing	Board/University	Division	% of marks	Subjects
HSLC	2002	Mizoram Board of School Education	II	57.8	English, Mizo, Mathematics, Science, Social sciences
HSSLC(Sc)	2005	Mizoram Board of School Education	II	51.2	English, Mizo, Physics, Chemistry, Mathematics
B.SC (Chemistry)	2008	Mizoram University	II	55	Chemistry, Botany, Zoology, FGC
M.Sc (Chemistry)	2010	Madras University	I	61.30	Organic Chemistry, Physical Chemistry, Inorganic Chemistry

1. INTRODUCTION

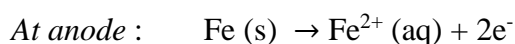
Corrosion is the deterioration of materials due to their exposure to air, moisture, or a chemical (such as acid or base). During the corrosion process, a pure metal will convert to a naturally more stable form, such as metal oxide, hydroxide, or sulfide, which causes metals to rust and deteriorate; and eventually result in a functional failure of equipments. Iron rust is a reddish, orangey, or reddish-brown material that forms on iron when exposed to moist air for an extended period. Rusting is the term used to describe the corrosion of iron. The common theories of corrosion/rusting are (i) Direct Chemical Attack theory, (ii) Electrochemical theory, and (iii) Acid theory. (Deng et al., 2014).

Direct Chemical Attack theory: Direct Chemical Attack: Direct chemical attack, or pure chemical corrosion, is an attack resulting from a direct exposure of a bare surface to caustic liquid or gaseous agents.

Mechanism for rusting of iron: Electrochemical theory

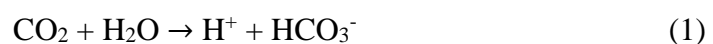
According to electrochemical theory, following actions contribute to the overall rusting,

(i) At anodes of every electrochemical cells, oxidation process occurs. As a result, ferrous ions are formed by oxidation of iron atom.



Due to oxidation, the metal atoms in the lattice dissolved as ions in the solution, leaving the metal with electrons. These electrons travel through the metal toward the cathode region.

(ii) The hydrogen ions at the cathodes of each cell are responsible for the collection of electrons (reduction). The H^{+} ions can be acquired from water or acidic substances (e.g., CO_2 in water as in eq. 1)



At cathode : $H^+ + e^- \rightarrow H$

On the iron surface, hydrogen atoms reduce the dissolved oxygen.

Consequently, the overall response at the cathode of various electrochemical cells can be expressed as in eq. 2,



(iii) The total redox reaction can be expressed by multiplying the anode reaction by two and adding the cathode reaction to equalize the number of electrons lost and gained.

The ferrous ions are oxidized even more by the oxygen in the air, which results in the formation of rust as per eq. 3 & 4 and Fig. 1.1.

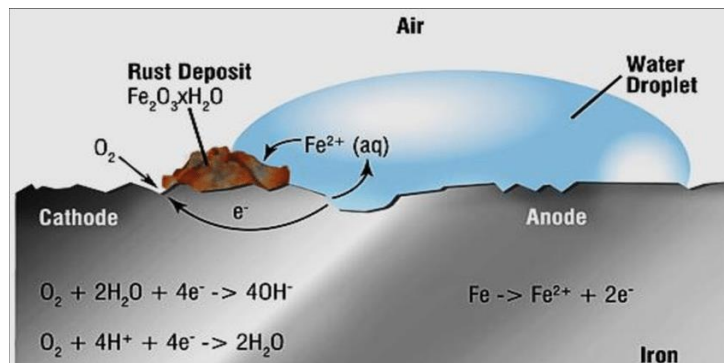
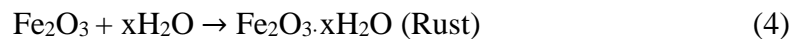
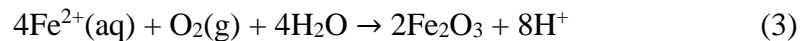


Fig 1.1 Schematic representation of the mechanism of Rusting of Iron

Even though corrosion is unavoidable, it is still often studied because of its practical, aesthetic, and economic significance. Protecting metals and alloys against corrosion with some materials also known as corrosion inhibitors is a common and cost-effective practice.

Acid theory: Acid theory of corrosion considers acid to be the main cause. Rusting takes place faster in acid solutions than in neutral or basic solutions. Oxygen and water are necessary for rusting of iron. This is not true for all the metals like Zn etc.

1.1 Factors that affect corrosion

The following are the most important elements that contribute to corrosion:

- (i) **Reactivity of the metals:** Each metal has a different reactivity depending on their position in the electrochemical series. The possibility of corrosion will increase with the metal's reactivity i.e. lower reduction potential of metal preferred the oxidation or corrosion.
- (ii) **Presence of impurities in metals:** The contaminants form a voltaic cells accelerate the corrosion rate.
- (iii) **Presence of electrolytes:** The presence of electrolytes in water also speeds up the rate at which corrosion occurs. For instance, the corrosion of iron occurs in a more significant amount naturally in seawater compared to distilled water.
- (iv) **Presence of CO₂CO₂ in water:** The presence of CO₂CO₂ in natural water increases rusting of iron. Water containing CO₂CO₂ acts as an electrolyte and increases the flow of electrons from one place to another.
- (v) **Presence of protective coatings:** When the surface of the metal is coated with layers of other metals that are more active than the metal of the substrate, the corrosion rate is slowed down significantly. For example, Rusting is prevented on iron by a zinc coating.
- (vi) **Temperature:** It is common knowledge that corrosion is an electrochemical reaction that follows the Arrhenius equation. Consequently, metal corrosion accelerates as temperature rises.
- (vii) **Presence of moisture:** Moisture is adsorbed on metal surfaces in various ways. It is possible to trap acidic gas from the surrounding environment on the metal surface. Therefore, it increases the rate of material deterioration because it creates a conductive path for electrochemical reaction on the metal's surface.
- (viii) **Effect of pH:** Exposure to alkaline or acidic medium causes rapid deterioration of metallic objects. When hydrogen ion or anion

concentrations are more significant, corrosion products are formed that directly impact the cathodic and anodic processes.

1.2 Types of Corrosion

Uniform corrosion, pitting, crevice corrosion, filiform corrosion, galvanic corrosion, environmental cracking, and fretting corrosion are a few examples of different types of corrosion that are visible to the naked eye. Here, we will discuss the various types of corrosion that might occur and how they can affect carbon steel.

(i) Crevice Corrosion

Crevice corrosion is a localized form of corrosion that occurs whenever there is a difference in ionic concentration between any two locations of a metal substrate. Corrosion of this type, for example, is common in closed environments (crevices). Crevice corrosion can happen in several places, including gaskets, washer undersides, and bolt heads. It occurs in all forms of aluminum alloys and stainless steel. The main reason is that corrosion can grow inside the cracks due to differential aeration.

(ii) Stress Corrosion Cracking

Stress Corrosion Cracking (SCC) refers to metal cracking due to its corrosive environment and the tensile stresses. It frequently happens in hot climates.

Example: Cracking of austenitic stainless steel in chloride solution described by SCC.

(iii) Intergranular Corrosion

Intergranular corrosion happens when impurities are present in the grain boundaries, which separate the grains generated during the metal alloy's solidification. It causes corrosion to occur between the grains. It can also happen when the alloy is depleted or enriched at the grain boundaries.

Example: The influence of IGC can be seen in aluminum-based alloys.

(iv) Galvanic Corrosion

Galvanic corrosion occurs when two metals with different electrochemical properties come into electrical contact with each in an electrolytic environment. Deterioration of one of these metals at a joint or junction is describes as Galvanic corrosion.

Example: Breakdown of copper in a saltwater environment when it comes in contact with steel.

(iv) Pitting Corrosion

Pitting Corrosion is hard to spot because of its unpredictability and is considered among the most harmful forms of corrosion. It begins at a specific place and spreads outward, eventually leading to the formation of a corrosion cell that is surrounded by the regular metallic surface. Once developed, this 'Pit' grows and takes several shapes. The pit steadily penetrates metal in a vertical trajectory from the surface, eventually causing structural failure if left abandoned.

Example: Consider a water droplet on a steel surface; pitting will commence at the droplet's center (anodic site).

(v) Uniform Corrosion

This type of corrosion, in which the environment attacks the metal's surface, is thought to be the most prevalent. It is simple to determine the corrosion's extent. This kind of corrosion only minimally impacts the material's performance.

Example: A piece of zinc and steel immersed in diluted sulphuric acid would usually dissolve at a constant rate over its entire surface.

(vi) Hydrogen Grooving

This type of piping corrosion is caused by grooves generated by the interaction of a corrosive chemical, corroded pipe constituents, and hydrogen gas bubbles. When the bubbles come in contact with the substance, they typically destroy the protective layer.

(vii) Metal Dusting

Corrosion, known as "metal dusting," happens when susceptible materials are exposed to environments with high carbon activity, such as synthesis gas. Corrosion causes metal to deteriorate to a powdery state. Owing to corrosion caused by carbon monoxide (CO) in the gaseous state, graphite forms on the surface of the metals. This graphite layer transforms into meta-stable M_3C species (where M is the metal), which typically migrate away from the metal's surface. However, M_3C species may only be observed in some cases. This corrosion result by direct transfer of metal atom on graphite layer.

(viii) Microbial Corrosion

Corrosion brought on by microorganisms is called "microbial corrosion" or "microbiologically influenced corrosion" (MIC). The most common one is termed chemoautotrophs. This corrosion can impact metallic and non-metallic materials in the presence or absence of oxygen.

(viii) High-temperature Corrosion

As the name suggests, high-temperature corrosion is a type of heat-induced corrosion of materials (primarily metals). Metals are susceptible to chemical degradation in a heated environment with gases like oxygen, sulfur, or other chemicals. These chemicals can readily oxidize the materials (metals in this example). Materials in automotive engines, for instance, must be able to withstand prolonged exposure to high temperatures and an atmosphere that may contain acidic combustion by-products.

1.3. Corrosion inhibitors

Substances that limit corrosion when introduced to an corrosive environment at low concentrations are known as corrosion inhibitors. In some ways, an inhibitor is a substrate similar to a catalyst that retards the oxidation reaction of metals. Even though corrosion is a preventable aspect of life (Trabanelli, 1991), it nonetheless commands attention because of its significance in the economy, technology, and aesthetics. One of the most popular and economically practical strategies for preventing corrosion is using corrosion inhibitors to preserve metal and alloys (Ambrish Singh, 2009). A corrosion inhibitor is an inorganic or organic molecule that

significantly slows the corrosion rate when introduced to a corrosive environment. Corrosion inhibitors must be compatible with a specific corrosive environment and are often employed in tiny concentrations. Two mechanisms are known via which corrosion inhibitors work to prevent corrosion, i.e. (i) by interacting with corrosive species to change the corrosive environment into one that is less corrosive or noncorrosive and (ii) by interacting with the metal surface to generate a protective layer. These inhibitors are termed environmental modifiers and adsorption inhibitors, respectively. Adsorption inhibitor relates to eco-friendly or green corrosion inhibitors. It deals with green corrosion inhibitors. Figure 1.1 is a schematic diagram of adsorption inhibitors classification (Sastri, 2011):

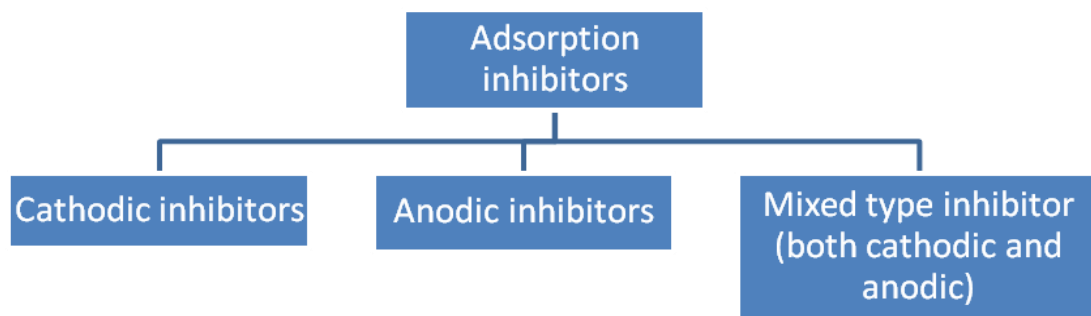


Figure 1.2: schematic diagram of the adsorption inhibitors classification.

1.3.1 Classification or Types of inhibitors

Inhibitors can be categorized according to Fig. 1.2. Characterization may be based on the materials used as an inhibitor, such as inorganic, organic, or hybrid. The corrosion inhibitor can be categorized as cathodic, anodic, or mixed, depending on whether they mainly retard the cathodic or anodic reaction of the corrosion process. The anodic inhibitors function by becoming strongly polarised and shifting the metal's mixed corrosion potential in the noble direction to control the rate of oxidation processes (Deng et al., 2014). Anodic inhibitors work better in corrosive environments that are neutral or alkaline. Anodic inorganic inhibitors include chromates, nitrites, molybdates, and phosphates. Cathodic inhibitors prevent or reduce the reduction reaction rate by decreasing the mixed corrosion potential and reducing the corrosion current (Deng et al., 2014). These inhibitors have an inhibitory effect on the cathodic side of the polarisation curve, either by lowering oxygen in

neutral or alkaline corrosive environments or by hydrogen evolution in the acidic environment. Examples of cathodic inorganic inhibitors include inorganic phosphates, silicates, or borates in alkaline solutions, zinc salts, and calcium and magnesium carbonates. Among them, industrially important covalent cathodic inhibitors are zinc salts and polyphosphates. Organic corrosion inhibitors provide a protective coating that displaces water and prevents deterioration. Amines, amine salts, imidazolines-sodium benzoate, mercaptans, esters, and ammonia derivatives make up the majority of organic inhibitors. Adsorption-type inhibitors change the cathode's or anode's surface by adhering to it, e.g., **organic amines**. Many organic compounds act like mixed-type inhibitors, which affect both the anodic and cathodic branches of polarisation curves. For example, Organic compounds with an amino group (-NH₂), carboxyl group (-COOH), or phosphonate group (-PO₄).

Several synthetic inorganic and organic inhibitors are currently being phased out due to various environmental concerns. Because of this, corrosion scientists and engineers have spent the last two decades developing "green" or biocompatible corrosion inhibitors (Roy et al., 2014). Plant extracts were tested to see if they could prevent steel from rusting in an acid solution. These included chamomile, halfa bar, black cumin, and kidney bean (Raja & Sethuraman, 2008). Many plant extracts have been found to reduce corrosion by various writers, which are addressed by (Raja & Sethuraman, 2008)

1.3.2 Mechanism of corrosion inhibition

Creating a coating, usually a passivation layer that blocks the corrosive chemical from reaching the metal is a common mechanism for inhibiting corrosion. There are three ways in which an inhibitor can protect metals from corrosion:

- (1) By chemical adsorption (chemisorption) on the surface of the metal, a protective thin film forms with inhibitor or inhibitor ions.
- (2) By leading a film formation through oxide protection of the base metal.
- (3) By Reacting with a potential corrosive component in aqueous media and producing a complex.

Organic inhibitors primarily cause inhibition through a change in the potential difference between the metal electrode and the solution, which is caused by

adsorption at the metal-solution interface. Potential shifts are due to the non-uniform distribution of charges across the interface between the metal electrode and solution. It is confirmed by an electrical double-layer or, in a few cases, by forming an electrical triple-layer. A simplified representation of the electrical double layer is shown in Figure 1.2 (Christensen *et al.*, 1994; Sastri, 2011).

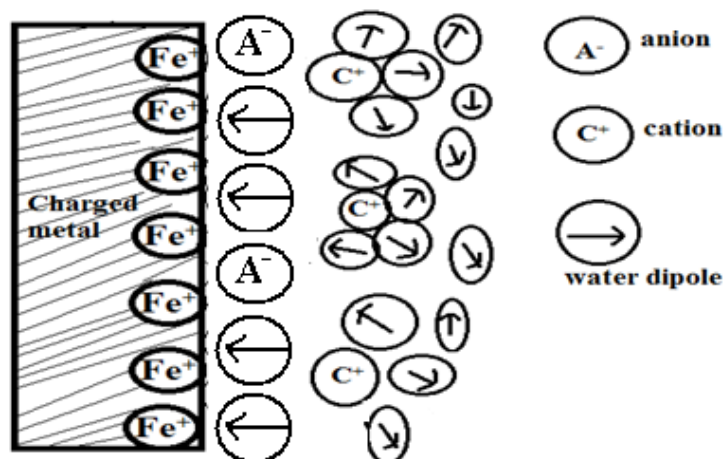


Figure 1.3 A schematic representation of the double layer that develops between an electrode and electrolyte interface

Free energy of solvation, hence, hydration of cation depends on charge/size ratio. Due to the small radii of cations, they are easily hydrated (Christensen *et al.*, 1994). The plane formed by the nuclei of anions directly adsorbed on the metal surface is termed the Inner Helmholtz Plane (IHP). The composition and structure of the electric double layer are altered when a corrosion inhibitor is introduced into it. As a result, the adsorption of the inhibitor may be tracked by measuring the capacitance of the double layer before and after its addition.

Several factors influence the adsorption process, but one of the most important factors is the chemical structure of the organic inhibitors. It is described by different spectroscopic techniques, including Fourier Transform Infrared Spectroscopy (FTIR) and Gas Chromatography combined with Mass Spectroscopy (GC-MS). Researchers mainly considered two distinct interactions, including physisorption and chemisorption, to understand the mechanism of corrosion inhibition by organic molecules. Physisorption occurs when an electrically charged metal surface comes into contact with charged species in the bulk of an electrolytic solution. In comparison, chemisorption occurs when inhibitor molecules share or

transfer charges with the metal surface (Deyab, 2014). These adsorption processes can also be interpreted in terms of interaction energy. The interaction energy between organic inhibitor molecules and metal surfaces is larger than between water molecules and metal surfaces because the interaction energy between organic inhibitor molecules and the metal surface is higher than between a water molecule and metal surface. So, the effect of organic molecules to inhibit corrosion is caused by their ability to bind to metal surfaces through functional groups.

1.3.3 Thermodynamics Inhibition process

Thermodynamics, which determines the electrochemical basis of corrosion, provides a valuable framework for analyzing the corrosion process. Corrosion rates and inhibition efficiency both depend on thermodynamic variables such as temperature. This topic deserves careful attention because by analyzing the activation energy and free energy of the adsorption, the rate of corrosion can be calculated. Adsorption mechanisms for inhibitor compounds onto a metal surface can also be understood using these thermodynamic parameters. (Yadav & Quraishi, 2012)

1.4. Effect and Economic impact of corrosion

Some economic effects of corrosion include the following:

- Replacing the damaged machinery.
- Taking preventative measures, such as painting.
- Equipment breakdown brought on by corrosion.
- Excessive design to compensate for corrosion loss of efficiency.
- Damage to nearby equipment where corrosion failure occurs.

A total of over \$300 billion annually at today's values is lost due to metal corrosion in the United States. Broader use of corrosion-resistant materials and implementation of best practices in the field of corrosion technology might cut these expenses by around a third (Zarras & Stenger-Smith, 2015). The current global cost of corrosion is estimated to be \$2.5 trillion, roughly equivalent to 3.4% of the world's gross domestic product investigated by NACE. Corrosion causes an annual loss of about 5-7% of India's GDP. It is estimated that savings of 15% to 35% of the cost of corrosion could be realized;(Koch et al., 2016), i.e., US\$375 and US\$875 billion

yearly by applying availability corrosion prevention and control on a global basis. Every nation has to spend a considerable amount of money on protecting the metallic structures corroded by high environmental risk, developing anti-corrosive measures, and repairing or replacing the corroded systems. Corrosion accounts for over half of India's defense budget and perhaps quadruple the country's annual education spending. Thus, this vast sum necessitates immediate action and long-term planning to reduce it and make our industry safer and accident-free (Singh et al., 2017)

Therefore, corrosion inhibitors are in high demand all around the world. Leakage of corrosive metals or alloys that are used in machinery can cause severe ecological concerns, such as oil spills, fire incidents, and human casualties following explosions. The National Association for Corrosion Engineering (NACE) assessment study cites corrosion as the leading cause of damage to expensive machinery and historic structures (Dillon et al., 2015). NACE is a professional organization that aims to safeguard human health and the natural environment while minimizing the economic costs of corrosion. For decades, those working in corrosion control have developed innovative technologies, implemented efficient management practices, raised public awareness of the importance of corrosion control, and implemented effective strategies for controlling corrosion to save money, the environment, and lives (Espallargas, 2015).

1.5. Properties of Corrosion Inhibitors

The following variables affect how well a corrosion inhibitor works:

- (i) Strong adsorption onto the metal surface
- (ii) Altering the degree of anodic as well as cathodic reactions
- (iii) By reducing the rate of diffusion of reactants to the surface of the metal
- (iv) By reducing the electrical resistance to the metal surface.

1.6. Green Corrosion Inhibitors

Eco-friendly corrosion inhibitors break down naturally and are free of carcinogens and other toxins. Anti-corrosion products that are "green" are safe for the environment since they are free of potentially harmful ingredients like lead or mercury. Corrosion can be stopped or reduced by treating the metal's exposed surface

with an inhibitor, a chemical (or mixture of compounds) supplied at extremely low concentrations. Green corrosion inhibitors are low-cost, less toxic, environmentally benign, renewable, and readily available. "Green chemistry," also called sustainable chemistry, enables scientists and engineers to protect humans and the environment using renewable raw materials. It benefits the economy by finding creative and discovering replacements for hazardous substances, innovative ways to reduce waste materials, and energy conservation.

Some researchers have reported that using green corrosion inhibitors is a successful strategy to utilize naturally occurring compounds that are quite effective for inhibitors controlling the corrosion of metals in acidic and alkaline environments (Al-Schaibani, 2000);(El-Etre, 2007). Neem leaves (*Azadirachta indica*) extracts inhibited the corrosion of mild steel in the H₂SO₄ solution (Ekpe et al.,1994). The inhibitive effect of the extracts *Delonix regia* on the corrosion of aluminum in hydrochloric acid solution was determined using weight loss measurements as well as the potentiostat technique (Abiola et al., 2007)

Many biodegradable organic substances used as green inhibitors over the years have been reported as available from various natural sources and can be used as corrosion inhibitors (El-Haddad, 2016). They are natural honey, onion, low-grade gram flour, garlic, potato, coriander leaves, seeds (castor, fennel, and mustard), flowers, gums gelatine and plant roots, etc. Most of them have been investigated for their corrosion inhibition property and have been very effective in mild acidic or basic media (Y. Zhou et al., 2017). Due to heterocyclic constituents like flavonoids, alkaloids, tannins, cellulose, and polycyclic compounds, the corrosion inhibition efficiency in plant extracts increases. Typically, due to the formation of a protective film barrier over the metal surfaces, thus preventing, retarding, or decreasing the corrosion rate to a considerable extent (Gadiyar *et al.*; 1991).

1.7. Review of Literature

The direct economic loss and environmental damage caused by the corrosion of mild steel have made it one of the most important subjects to study in recent

decades (Garcia-Arriaga et al., 2010). Leakage due to corrosion causes major environmental issues like oil spills, fire mishaps, and human deaths by explosions. Grills, metal equipment, and transportation systems are everyday objects where corrosion is an obvious problem (bridges and roads). Steel corrosion is a major cause of the abrupt collapse of the highway, electrical towers, and building infrastructure, which can cause devastating financial losses and human casualties (www.nace.org).

Science and technology are based on thinking, skill, observations, and from learning subjects. They explore new ideas for the uses of humanity and meet the needs of human beings are fulfilled (Maqbool et al., 2014). (Wilbertz, 2013) Humans have always been curious about nature and innovating new technology. It is a skill to canalize some processes and improve material quality. Research is always solving a specific problem, and our desires are connected to it and push research into a more fruitful direction to benefit society (Wilbertz, 2013). In modern society, the increasing importance of material sciences has an important role in improving the quality of materials. The exchange of ideas from various researchers facilitates the industry's progress (L. Zhou et al., 2008). This tendency arises from the constant and better change in industry, development, and technology modernization. The success of research has a significant impact on existing functions and modifies some functions. It creates new options for improvement and increases the performance of the material. It establishes prominent growth in the industry as it facilitates further development that can be sustained by other options (Mulder, 2007).

During chemical processes, contaminants can be deposited in the machinery and boost the efficacy of an assault due to corrosion. As a result of adhesion and deposition, this can lead to significant corrosion issues. Due to this, the equipment may experience localized corrosion and the development of pin holes. Cleaning by acidic solutions like sulphuric acid (H_2SO_4), hydrochloric acid (HCl), and phosphoric acid (H_3PO_4) are standard methods. Organic acids such as Formic acid, acetic acid, and citric acid, along with basic solutions, may also be used as cleaning agents. Cleaning techniques are necessary yet harmful to the equipment because they are corrosive and can cause damage to the equipment. As a result, corrosion inhibitors

are introduced to cleaning agents to prevent metal from corrosion(Gadiyar et al., 1991)

Rapid urbanization and expanding companies based on petrochemical processes might influence corrosion owing to the usage of crude petrochemicals that contain organic and inorganic acids, reducing the life of the equipment. (Wanklyn, 1982); (Papavinasam, 2021); (Miksic et al., 2009). As a result of the rapid growth of the transportation sector, the oil refining and petrochemical sectors have had to expand significantly to keep up with the demand for reliable fuel for the increasing number of vehicles used in these modes of transportation. The refinery business uses metallic equipment frequently exposed to corrosive mediums like water, atmosphere, and soil (Naemnezhad et al., 2017). There must be careful management and constant monitoring to prevent corrosion and mishaps. The units of crude petroleum refineries are susceptible to corrosion due to the natural elements. The presence of HCl and H₂S gases below 373 K or NaCl and Na₂SO₄ salts below 473 K, for example, are more aggressive and can harm refinery equipment (Gutzeit et al., 1987);(Groysman, 2014).

A corrosive agent like HCl is produced during the hydrolysis of calcium and magnesium and is found in crude oil as a by-product. Inorganic salts are the most common corrosive pollutant found in marine tankers and pipelines, even though they are eliminated during the early processing of crude oils (CaCl₂, MgCl₂, and NaCl). Even after desalting, this is still present in crude oil. There is a significant issue with these corrosive chemicals still present in the crude oil after it has passed through the distillation column and risen with the light hydrocarbons. Damage to the refinery's machinery is possible with both the reforming and hydro-treating process units (Garverick, 1994);(Lai, 1990); (Lewandowski, 2017). Organochlorine is present in crude petroleum products and is employed in catalytic reformers in the petrochemical process (Groysman, 2014). The corrosive quality of these comes from the HCl that is produced when organochlorine is hydrolyzed. Inorganic solid acid like this is harmful to expensive machinery since it causes corrosion and breakdowns.

For cleanliness, alkaline, acidic, strong, or weak oxidizing and reducing chemicals are used to remove contaminants. These corrosive conditions and robust

chemicals harm equipment. Humans and other organisms are most at risk from metal allergies and their release into the food chain (Valdez, 2012).

Right from the beginning of the invention of iron, it is indeed accompanied by rust, which gradually degrades the iron after coming into contact with air and water (Rao, 2000).

Fertilizer is agriculture's most vital industry. Water, air, hydrogen sulfide, nitrogen-containing compounds, polythionic acids, organic chloride compounds, sulphuric acid, and alkaline solutions (sodium hydroxide, sodium carbonate, ammonium hydroxide, amines, sour water, and wasted caustic) are used to make fertilizers. Sometimes these compounds disintegrate or react to produce corrosive chemicals like ammonia or hydrogen sulfide, di-hydrogen ammonium phosphate, or ammonium nitrate, which increase metal corrosion. Fertilizer firms use phosphorus, sulfur, and chloride-rich chemicals (Kim & Kim, 2017).

Since the metal is thermodynamically unstable and tends to revert to its thermodynamically stable native oxide state (Davis, 1989) after exposing to the surrounding atmosphere, it must be heated to be extracted from its ore (G, 1989). Eco-friendly corrosion inhibitors have recently gained popularity due to their accessibility, low toxicity, biodegradability, and compatibility. Numerous researchers have observed the efficacy of plant extracts as suitable corrosion inhibitors for mild steel in acidic environments (Davis, 1989)

Considering their availability, low toxicity, bio-degradability, and compatibility, eco-friendly corrosion inhibitors have recently received greater attention. Many studies have investigated the inhibition effectiveness of plant extracts as suitable corrosion inhibitors for mild steel in acidic environments. Interestingly, plant extracts contain a wide variety of phytochemical constituents, such as polyphenols, amino acids, terpenes, carboxylic acid, pigment resins, and alkaloids (Deyab et al., 2017). Most of these compounds contain heteroatom and multiple bonds, which possess similar electronic structures as conventional organic corrosion inhibitors; hence, they are found to be potential corrosion inhibitors.

Haldhar group tested the corrosion inhibition effectiveness of *Valeriana wallichii* extract for mild steel in an acidic solution (Haldhar et al., 2018). It is reported that plant extract shows good inhibition performance of 93.47% at 500 mg/L at 298 K. The phytochemical studies confirmed that the naphthoic acid and iridoid derivative are the main active constituents of the *Valeriana wallichii* extract. Based on polarization measurements suggested that the inhibitor molecule acts as a mixed type of inhibitor.

Umoren group studied the inhibition efficiency of synthetic polymer (polyethylene glycol), naturally occurring polymers (gum arabic), and synergistic halide additives for mild steel in H₂SO₄ solution (Umoren et al., 2008). The resulting polyethylene glycol was a more effective inhibitor than gum arabic. Also determined, *Raphia hookeri* exudates gum—halide mixtures for aluminum corrosion in an acidic medium (Umoren & Ebenso, 2008). The corrosion property of *Raphia hookeri* exudates gum obeys Freundlich, Langmuir, and Temkin adsorption isotherms, which is physical adsorption. The ethanolic extract of *Vernonia amygdalina* for the corrosion inhibition of mild steel in acidic media H₂SO₄ was found to be a better corrosion inhibitor, and it forms an adsorption layer on the said steel following the traditional Langmuir adsorption isotherm (Odiogenyi et al., 2009).

Chalchat group found rosemary oils were rich in 1,8-cineole camphor, bornyl acetate, and a long chain of hydrocarbons (Chalchat et al., 1993). Rosemary extracts of organic compounds contain borneol, bornyl acetate, camphor, cineole, camphene, and alpha-pinene. *Rosmarinus officinalis* L. leaves extract as corrosion inhibitor of Al-Mg alloy corrosion in chloride solution (Kliškić et al., 2000). Adsorption properties and inhibition effect of *Rosmarinus officinalis* L oil as green corrosion inhibitors on C38 steel in 0.5 M in an acidic medium of H₂SO₄ were investigated by (Quariachi et al., 2010).

Recently, some researchers have reported some drugs as corrosion inhibitors because these drugs are heterocyclic in nature, do not contain any heavy metals or other toxic compounds, and are environmentally non-hazardous. Sethuraman & Raja reported preliminary results of corrosion inhibition of mild steel in HCl solution by the crude methanolic extract of *A. pallens* (Sethuraman & Raja, 2005). (Chetouani

& Hammouti, 2014) studied the inhibition effect of extract of *S. Officinalis* leaves and essential oils for steel in 1M HCl solution by using gravimetric measurement, PDP and EIS. PDP study revealed that the extract of *S. officinalis* leaves and essential oils acts as a mixed-type inhibitor. EIS measurement showed that essential oil extract of *S. Officinalis* formed thin film barriers on the mild steel surface in HCl solution. By decreasing the active surface area of corrosion that takes place by adsorption of the inhibitors and lowering the degradation of the metal. The inhibition efficiency of essential oil extract of *Salvia Officinalis* decreases with temperature rise (Soltani et al., 2012). Ginkgo (Yingxing) leaf extract (Deng & Li, 2012) in corrosive medium HCl and H₂SO₄ solutions on mild steel surface acted as cathodic-type inhibitors with mainly mixed-type corrosion inhibitors and follows Langmuir adsorption isotherm. Adsorption of Trifoliate fenugreek (Noor, 2008) on mild steel surface predominately acts as an anodic inhibitor and follows Langmuir and Temkin adsorption isotherms in both HCl and H₂SO₄ acidic solutions, respectively. Similarly, the adsorption of lupine (*Lupinus albus* L) on the metal surface acts as a mixed-type inhibitor in HCl corrosive media (Abdel-Gaber et al., 2009). It obeys the kinetic thermodynamic model in both the HCl and H₂SO₄ acid solutions. Also, the effect of the addition of potassium halides was found to be in the order of KCl < KBr < KI, and the results obtained have shown that the increase in efficiency was due to synergism among different reactants involved during corrosion inhibition. Extract of *Justicia gendarussa* on mild steel in 1 M HCl medium was studied (Satapathy et al., 2009) and can inhibit corrosion, and inhibition efficiency up to 93% was achieved with 150ppm extract of *J. gendarussa* at 298K. The potentiodynamic polarization measurement showed that it acts as a mixed-type inhibitor and follows the Langmuir adsorption isotherm. Rocha examined the aqueous extract of mango and orange peels as corrosion inhibitors for carbon steel in 1M HCl (Da Rocha, 2010). They showed that the inhibition efficiencies of oranges are higher than mango in the concentration range between (200-400) mg L⁻¹. The adsorption of the extract on the surface of carbon steel obeys Langmuir's adsorption isotherm.

The inhibiting effect of the extract of *Punica granatum* (PG) was studied in 2M HCl and 1M H₂SO₄ solutions at 30°C. Ellagic acid (EA) and tannic acid (TA)

were the main constituents involved as mild steel corrosion inhibitors. The Tafel curves indicate mixed-type inhibition behaviour and follows Langmuir adsorption isotherm (Behpour et al., 2012).

Mobin and Rizvi reported inhibition effect by Polysaccharide obtained from *Plantago* on carbon steel in acidic medium by electrochemical methods (Mobin & Rizvi, 2017). It is found that Polysaccharide is a cathodic inhibitors. Raja et al. found that *Kopsia singapurenensis* and *Xylofia Ferrungina* extracts have an inhibitory effect on the corrosion behaviour of mild steel in acid media (Raja et al., 2010 2013)

The Anti-corrosive activity of *Emblica officianilis*, *Terminalia chebula*, *Sapindus trifolianu* and *Accacia conicianna* has been investigated by (Sanghavi et al., 1996). Gadow and coworkers studied the extract of *Eruca sativa* seeds as corrosion inhibitor for carbon steel corrosion in 1M HCl solution (Gadow & Fakeeh, 2022). Avwiri and co-workers (Avwiri & Igho, 2003) investigated the inhibitive action of *Vernonia amygdalina* on the corrosion of Aluminium alloys in HCl and HNO₃. The extract of *Fucus spiralis* was tested as a corrosion inhibitor of carbon steel in a 1M HCl medium by Afrokh et al., 2021). Gravimetric and electrochemical methods, including potentiodynamic polarisation (PDP) and electrochemical impedance spectroscopy (EIS) were utilized to investigate the corrosion-inhibition properties of the samples. UV-Visible, UV-Vis-NIR, and Optical Microscopy analyses were used to assess the surface of carbon steel in the optimum solution.

1.8 Objective

- i. An effort will be made to assess the corrosion inhibition efficiency of extracted essential oil on the mild steel in an acidic medium by gravimetric (weight loss) as well as electrochemical methods, i.e., Potentiodynamic and Electrochemical Impedance Spectroscopy (EIS) studies.
- ii. Essential oils contain organic compounds were characterized by Gas Chromatography-Mass Spectrometry (GC/MS) and Fourier Transform Infrared (FTIR) spectroscopic technique.

- iii. Analysing the effect of inhibitors on the surface morphology of the metal by using the method of SEM and FTIR analysis.
- iv. Temperature effect on corrosion inhibition by essential oil extract were studied for determination of adsorption parameter such as the nature of inhibitor adsorption on metal surface (physisorption and chemisorption) and physical and thermodynamic properties (free energy, enthalpy, entropy, activation energy).

1.9. Scope of Study

1.9.1. Importance of acid in industrial process

In the chemical industry, acids are the most valuable chemical for producing various types of drugs, textiles, cosmetics, herbicides, insecticides, polymers, and the formation of composite materials. In this context, organic acids are among the most versatile ingredients in the food and textile industries. Citric, acetic, lactic, tartaric, malic, gluconic, propionic, and fumaric acids are some of the organic acids used widely in various industries (Pandey et al., 2008). Without using these organic acids, the productions of various valuable materials become impossible, which are useful for human beings. For example, chemical industries use chloroacetic acid to manufacture carboxymethyl cellulose, carboxymethyl starch derivatives, and herbicides such as aryl hydroxyl acetic acid. The same is used for making the insecticide dimethoate and the herbicides Benazoline and methyl β -naphthoxyacetate. A large amount of chloroacetic acid is used to produce polyvinyl chloride (PVC). Chloroacetic acid is also used for manufacturing drugs such as coumarin and vitamin B6. It is corrosive in nature and damages the equipment (Heitz et al., 1992).

1.9.2. Sustainability and Corrosion Inhibition

Researchers have devoted much effort and time in understanding corrosion and its prevention over the past two decades. The increasing demand for high-quality goods at reasonable prices, the depletion of non-renewable natural resources, and stringent rules meant to protect the environment are all significant factors in deciding the choice for corrosion inhibition processes. Scientists are exploring innovative

approaches to improve performance, reduce costs, and conform to rules and regulations. Using naturally available resources as corrosion inhibitor is the ultimate solution for corrosion inhibition process owing to the low-cost, sustainable, and environmentally friendly nature and valorisations of bio-waste materials. In addition, these renewable resources can be easily transformed chemically for a plethora of applications, particularly in corrosion resistance against various aggressive mediums (Oguzie, 2006); (Eddy & Odoemelam, 2009); (Johnsirani et al., 2013); (Mourya et al., 2014a)

**2. EXTRACTION OF ESSENTIAL OILS AND IDENTIFICATION OF
MAJOR PHYTOCHEMICALS**

Mild steel and alloys are widely used for electrical appliances, industry, vehicle parts, construction, medical equipment, and different applications due to their high malleability and excellent structural and mechanical strength (Gadow & Fakeeh, 2022). However, due to its thermodynamic instability, especially in aggressive acid solutions, it is vulnerable to corrosion attack (Lavanya et al., 2020). Surface modification is therefore required to reduce its corrosion and make it longer life of same in the corrosive environment. There are a variety of physical and chemical treatments like coating, anodizing, and inhibitors, which are used for the metal–solution interface and act as a barrier by separating the metal surface from the corroding. The most valuable method for protecting against metal corrosion is applying inhibitors in the aggressive medium.

Acid solutions are often used in industry for cleaning, descaling, and pickling of steel structures, processes which are generally followed by considerable metal dissolution. The two most common acids HCl and H₂SO₄ used in the industrial pickling of iron and its alloys to eliminate unnecessary corrosion (Stratmann et al., 2003). A valuable method to protect metals and alloys in aggressive environments against corrosion is the addition of corrosion inhibitors to the solution in contact with the surface to inhibit the corrosion reaction and to reduce the corrosion rate.

The weak corrosion resistance of mild steel in an acidic solution requires corrosion inhibitors during the reaction process. The literature survey reveals that inhibitors (organic compounds) containing hetero-atoms have heterocyclic rings, several polar functional groups, and extensively conjugated substructures. It draws great attention as they slow down metal corrosion by adsorbing on the metal surface, increasing solubility and inhibiting efficiency (Rajeswari et al., 2014). Moreover, the adsorption of organic inhibitors on a metal surface in an acid solution depends upon some factors such as the electronic structure of the inhibitor molecule, steric factors, presence of functional groups, nature of substituents present in the inhibitors,

aromaticity, presence of conjugation, molecular weight, solution temperature, and electrochemical potential at metal/electrolyte interfaces (Shabani-Nooshabadi et al., 2015).

The present chapter describes methods used to characterize the plant material and the corrosion monitoring technique. The corrosion-inhibitive effect of some selected plants found in Mizoram was analyzed. We have chosen five plants for the present study to evaluate anti-corrosive properties. The extracted oils were collected from buds of *Zingiber mioga*, the rhizome of *Zingiber officinale*, leaves of *Mentha piperita L*, leaves of *Eryngium foetidum L*, and the scaly bulb of *Allium sativum*. The anti-corrosion effect studied in 1M HCl on mild steel was carried out using weight loss, potentiodynamic polarization, and electrochemical impedance methods. Furthermore, samples' surface morphology and characterization were conducted by FT-IR and scanning electron microscopy (SEM). The phytochemical presence in the sample was investigated by using GC-MS.

2.1 Outlook of the present work

2.1.1 *Zingiber mioga* (ZM)

Classification

Family	<i>Zingiberaceae</i>
Order	<i>Zingiberales</i>
Genus	<i>Zingiber</i>
Species	<i>Z. Mioga</i>

Zingiber mioga, also called Japanese ginger, is a deciduous plant and herbaceous perennial firstly found in the region of eastern and native to Japan, China, and the southern part of Korea. It is also found in Mizoram, North East India. *Z. mioga* is also a traditional medicine used medicinally to treat coughs and relieve insect bites, eye inflammation, and rheumatism (Sharifi-Rad et al., 2017);(Wiar, 2012). Several components of *Zingiber mioga* are cytotoxic, have anti-carcinogenic properties, and are used for cancer treatment. It was previously reported that *Z. mioga* exerts an anti-obesity effect (IWASHITA et al., 2001). However, the

mechanism underlying obesity inhibition remains unclear. Only its edible flower buds and flavourful shoots are used in cooking. The flower buds are finely frayed and used for making soup and dishes such as roasted egg plant. The flower buds are pierced interchangeably with meat and then pan-fried (Abe et al., 2008).

2.1.2 *Zingiber officinale* (ZO)

Classification

Family	<i>Zingiberaceae</i>
Order	<i>Zingiberales</i>
Genus	<i>Zingiber</i>
Species	<i>Z. Officinale</i>

Zingiber officinale is a flowering and herbaceous perennial plant predominantly found in Mizoram and the north-eastern region, root whose rhizome is generally used as a fragrant kitchen (Dalia Mustafa M Elbashir et al., 2021) spice and folk medicine.(Dafaalla, 2022) *Zingiber officinale* has been used for many years to treat several ailments, such as cough and cold, sore throat, vomiting, arthritis, migraines, and hypertension. Even though it is used as traditional medicine and a dietary supplement, there are no good facts that consuming ginger or its extracts has any effect on human health or as a treatment for various diseases(Nair, 2019). It can be used with numerous food items such as vegetables, soda, and alcoholic beverages.

Young *Zingiber officinale* rhizomes are delicious, moist, and soft solid with a gentle taste. They are often used to make pickles with vinegar or sherry as a snack or cooked as an ingredient in many dishes. They can be sheer the herb in boiling water to make ginger tea and also used for making candy and ginger wine by adding honey.

Mature *Zingiber officinale* rhizomes are fibre and nearly dry. The juice from ginger roots is often used as a seasoning in Indian recipes. It is a common ingredient

in Chinese, Korean, Japanese, Vietnamese, and many South Asian cuisines for flavoring dishes such as seafood, meat, and vegetarian dishes.

2.1.3 *Eryngium foetidum* (EF)

Classification

Family	<i>Apiaceae</i>
Order	<i>Apiales</i>
Genus	<i>Eryngium</i>
Species	<i>E. foetidum</i>

Eryngium foetidum L. is a green spicy leafy herb found in different places of Mizoram, and it is usually used for marinating, garnishing, and flavoring food. It is also used as a medicinal plant for the treatment of a number of an illness such as fevers, chills, vomiting, burns, fevers, hypertension, headache, earache, stomachache, asthma, arthritis, snake bites, scorpion stings, diarrhea, malaria, cancer, diabetic, epilepsy (Boonsong, 2005). Many medicinal investigations have been studied, and they are anti-parasitic, anti-inflammatory, painkiller, antiepileptic or antiseizure, and anti-biotic bio-activity. It would be the best scheme to raise the yield and to support industrial uses of *Eryngium foetidum* L. as an inexpensively relevant and applicable crop (B. K. Singh et al., 2014).

2.1.4 *Mentha piperita* (MP)

Classification

Family	<i>Lamiaceae</i>
Order	<i>Lamiales</i>
Genus	<i>Mentha</i>
Species	<i>M. piperita</i>

Mentha Piperita is a cross hybrid between spearmint and water mint, so it is a hybrid species. It is originally from Europe and the Middle East and the plant is

now broadly extended and civilized in many regions of the world and cultivated in the north eastern region of India, including Mizoram. It is rarely found in the wild uncultivated with its close relative species (Ng & Gilotra, 2020).

Now a day, *Mentha Piperita* is applicable for the treatment of IBS (irritable bowel syndrome) and ailments of digestive problems, the common cold, sinus infections, headaches, and allergies. *Mentha Piperita* oils are almost colorless; a volatile essential oil distilled with leaves and steam from the aromatic plant is generally used for flavoring sweetmeat, chewing gum, dentifrices, and medicine. Oils are applied to the skin to solve the problems such as headaches, muscle aches, joint pain, and itching (Dixit, 2021).

2.1.5 *Allium sativum* (AS)

Classification

Family	Amaryllidaceae
Order	Asparagales
Genus	<i>Allium</i>
Species	<i>A. sativum</i>

Allium sativum is a species of bulbous flowering plant in the genus *Allium*. It is closely related to the onion, shallot, leek, chive, Welsh onion, and Chinese onion (Block, 2010). It originates in South, Central, and north eastern Asia and is also found in Mizoram. It has been used as both a food flavoring and traditional medicine. *Allium sativum* usually makes used for high blood pressure, high levels of cholesterol or other fats in the blood, and hardening of the arteries. It is also used for the common cold, osteoarthritis, and many other conditions, but no good scientific evidence supports it. A pharmacological investigation recently determined it is promoted for treating cardiovascular. In garlic, diallyl thiosulfinate is the major component in the bulb root of the garlic plant and is used for antimicrobial properties, anti-bacterial and anti-fungal activity (Ng & Gilotra, 2020).

2.2 Extraction of essential oils

Essential oils are types of oils that capture the scent, flavor, or essence of a plant. For thousands of years, they've been widely used for various applications from medicinal purposes to cosmetic use. The plant's active constituents are extracted to collect essential oil.

The extraction of essential oils is commonly done by following two methods:

1. Azeotropic distillation (hydro-distillation, hydro diffusion, and steam distillation) and
2. Extraction with solvents.

Each extraction method needs to apply various amounts of pressure and temperature, which eventually impacts the result of the essential oil being the best quality. Depending on the essential oil being produced, some essential oil extraction methods are better suited to certain plant types and parts. In our present work, we are going to extract by Clevenger apparatus using the method of hydro-distillation. Some of the reasons steam distillation is such a widespread process of extracting essential oils are because the volatile compounds can be distilled at temperatures lower than their boiling point. As such, the natural qualities of the plant material are less likely to become altered or diminished during the process. For this reason, essential oil distillation is often regarded as the only extraction method that allows for purity.

Hydro-distillation is the most frequently applied method of essential oil extraction (Figure 1). The heat from the steam vaporizes into volatile compounds of the pieces of the collected plant. The vaporized compounds enter a cooling chamber known as a condenser. As the vapors cool, they condense from steam into a liquid form.

After being condensed, the essential oil and water from the water-soluble parts of the plant known as hydrosols or floral water are collected into a receiver with two separate outflows. Because oil and water do not mix, the essential oil floats above the water. As such, the lower outflow will draw out the water, and the upper outflow will draw out the essential oil.

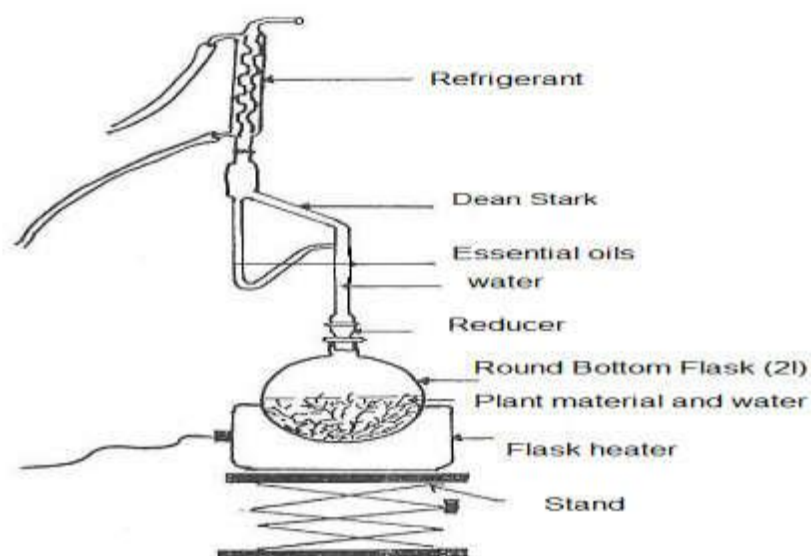


Figure 1: Hydro-distillation by using Clevenger apparatus.

2.2.1 Extraction of oils from *Zingiber mioga* buds

Zingiber mioga flower buds used in this extraction were purchased from the market, Aizawl. The buds were peeled; 500g washed thoroughly, and kept in a tray to drop out water, chopped into small pieces, and then grinded. The grind is placed in the Clevenger apparatus with levelling water. The steam is allowed to pass through the plant material under pressure, softening the cells and allowing the essential oils to escape in vapor. The temperature of the stem must be high enough to vaporize the oil present, yet not so high sufficient that it destroys the therapeutic properties of plants or burns the essential oils meant for corrosion inhibition property present in plant material. The temperature is adjusted 70°C till it boils; after boiling lowers, the temperature is to 50°C and keeps boiling for 5 to 6 hours. The tiny droplets of essential oils evaporating along with the stem molecule travel through a tube into the condensation chamber. As the steam cools, it condenses into water. The essential oil forms a film on the surface of the water. The film is decanted or skimmed off to separate the essential oil from the water. The *Zingiber mioga* oil is kept in a capping tube for experimental use.

2.2.2 Extraction of oils from *Zingiber officinale* rhizome

The roots of *Zingiber officinale* used in this extraction were purchased from the market, Aizawl. Take 1kg of *Zingiber officinale* rhizome, washed thoroughly and kept in a tray to drop out of the water, and the fresh *Zingiber officinale* was sliced into pieces and then grinded. Using "Clevenger apparatus" by hydro-distillation method, extracted the essential oil from the *Zingiber officinale* rhizomes was done. The apparatus consists of a round-bottomed flask. The steam is allowed to pass through the plant material under pressure which softens the cells and allows the essential oils to escape in vapor form. The temperature of the stem must be high enough to vaporize the oil present, yet not so high enough that it destroys the therapeutic properties of plants or burns the essential oils meant for corrosion inhibition property present in plant material. The temperature is adjusted 70°C till it boils; after boiling lowers, the temperature is to 50°C and keeps boiling for 5 to 6 hours. The tiny droplets of essential oils evaporating along with the stem molecule travel through a tube into the condensation chamber. As the steam cools, it condenses into water. The essential oil forms a film on the surface of the water. The film is decanted or skimmed off to separate the essential oil from the water. The *Zingiber officinale* oil was kept in a capping tube for experimental use.

2.2.3 Extraction of oils from *Eryngium foetidum* leaves

The *Eryngium foetidum* leaves used in this extraction were purchased from the market Aizawl. 500g of leaves were washed thoroughly and kept in a tray to drop out water, and the fresh leaves of *Eryngium foetidum* were chopped into small pieces and then grinded. Fresh leaves are placed in the Clevenger apparatus, and the steam is allowed to pass through the plant material under pressure, softening the cells and allowing the essential oils to escape in vapor form. The temperature of the stem must be high enough to vaporize the oil present, yet not so high enough that it destroys the beneficial properties of plants or burns the essential oils meant for corrosion inhibition property present in plant material. The temperature is adjusted 70°C till it boils; after boiling lowers, the temperature is to 40°C, and it keeps boiling for 5 to 6 hours. The tiny droplets of essential oils evaporating along with the stem molecule

travel through a tube into the condensation chamber. As the steam cools, it condenses into water. The essential oil forms a film on the surface of the water. The film is decanted or skimmed off the top to separate the essential oil from the water. The extracted oil was kept in a capping tube for experimental use.

2.2.4 Extraction of oils from *Mentha Piperita* leaves

The *Mentha Piperita* leaves used in this extraction were purchased from the market Aizawl. The leaves of *Mentha Piperita* 500g were washed thoroughly and kept in a tray to drop out of the water, and the fresh leaves of *Mentha Piperita* were chopped into small pieces and then grinded. Fresh leaves are placed in the Clevenger apparatus, and the steam is allowed to pass through the plant material under pressure, softening the cells and allowing the essential oils to escape in vapor form. The temperature of the stem must be high enough to vaporize the oil present, yet not so high enough that it destroys the therapeutic properties of plants or burns the essential oils meant for corrosion inhibition property present in plant material. The temperature is adjusted 70°C till it boils; after boiling lowers, the temperature is to 40°C, and it keeps boiling for 5 to 6 hours. The tiny droplets of essential oils evaporating along with the stem molecule travel through a tube into the condensation chamber. As the steam cools, it condenses into water. The essential oil forms a film on the surface of the water. The film is decanted or skimmed off the top to separate the essential oil from the water. The extracted oil was kept in a capping tube for experimental use.

2.2.5 Extraction of oils from Garlic *Allium sativum* scaly bulb

The scaly bulb of *Allium sativum* used in this extraction was purchased from the market, Aizawl. The *Allium sativum* bulb was peeled; 500g was washed thoroughly and kept in a tray to drop out water, chopped into small pieces, and then grinded. The grind leaves was placed in the Clevenger apparatus with levelling water. The steam was allowed to pass through the plant material under pressure, softening the cells and allowing the essential oils to escape in vapor form. The temperature of the stem must be high enough to vaporize the oil present, yet not so

high enough that it destroys the therapeutic properties of plants or burns the essential oils meant for corrosion inhibition property present in plant material. The temperature is adjusted 70°C till it boils; after boiling lowers, the temperature is to 50°C and keeps boiling for 5 to 6 hours. The tiny droplets of essential oils evaporating along with the stem molecule travel through a tube into the condensation chamber. As the steam cools, it condenses into water. The essential oil forms a film on the surface of the water. The film is decanted or skimmed off the top to separate the essential oil from the water. The *Allium sativum* oil was kept in a capping tube for experimental use.

2.3 Solution preparation

The aggressive solution of (1M HCl) was prepared by 37% concentrated HCl analytical grade diluting in distilled water. Stalk solution was used for 100ml of various concentrations in each sample, and the selection of inhibitors concentration is from 1g/L to 5g/L of the EOs extract.

2.4 Specimen preparation

The steel sample taken from local steel fabrication containing chemical composition: C = 0.32%, Mn = 0.57%, Si = 0.010%, P = 0.04%, and the remainder Fe = 98.97% with having the dimension of 2.59cm x 1.73cm x 0.28cm was made a small hole near the upper edge of rectangular bar it was used for the gravimetric study while the same metal with the exposure area of 1cm² was used for the electrochemical studies. A small film deposited in the specimen was successfully removed using different grades of abrasive papers 80, 220, 320, 400, 600 and 1200 and rinsed with double distilled water. Finally, it was degreased with acetone, dried in a hot air oven, and kept in moisture-free desiccators for further use.

2.5 Identification of major phytochemicals of essential oils

2.5.1 GC-MS analysis of EOs extract

GC-MS analysis was performed to identify the phytochemicals present in extracted oils, which helps determine the major inhibitive components in the inhibitor. Characterization and chemical composition of essential oil was done by GC-MS (Gas Chromatography and Mass Spectrometry). It is the grouping of Gas-Liquid Chromatography and Mass Spectrometer (Coskun, 2016). GC-MS can help to recognize different substances present in a test sample. It has many usages containing drug detection, fire examination, environmental study, contamination, and explosives analysis. It can also be useful for the identification of unknown compounds. GC-MS can also be helpful in airport security to identify equipment in luggage or on human beings (Patel et al., 2010). Moreover, it can also detect trace elements in worsened materials even when the samples demolish away from each other, and some other inquiries cannot work. GC-MS is the most excellent way for legal experts and forensic researchers to recognize substances because they are specific tests. A specific test sponsor detects the real presence of a particular substance in a tested sample. GC-MS analyzed the sample extract, and the constituent phytochemicals were identified with the help of the NIST library. The results of GC/MS were obtained by measuring the peak area using Turbo Mass software and matched with the hit list spectra of the NIST library (Yuan, 2014).

The analysis of GC-MS data of *Zingiber mioga* EO extracted helps to identify several organic elements of various structures present in Figure 2.5.1.1 shows the GC-MS spectra in are corresponding NIST library database, showing the identification of 15 major components in the oils sample test. Their (RIs) and their RT are reported in Table 2.5.1.1 with their molecular weight.

Table 2.5.1.1 Phytochemical constituents of extracted oils from *Zingiber mioga* (ZM)

S/ No.	RT	RSI	Compound Name	Formula	MW	CAS
1	7.50	713	Diallyl disulfide	C ₆ H ₁₀ S ₂	146	2179-57-9
2	9.47	869	Bicyclo[3.1.1]heptan-3-ol,6,6-dimethyl-2-methylene-	C ₁₀ H ₁₆ O	152	547-61-5
3	11.28	909	α – Terpineol	C ₁₆ H ₁₈ O	154	98-55-5
4	11.61	863	(-)- myrtenol	C ₁₀ H ₁₆ O	152	19894-97-4
5	15.41	766	Trisulphide, di-2-propenyl	C ₆ H ₁₀ S ₃	178	2050-87-5
6	19.82	868	Caryophyllene	C ₁₅ H ₂₄	204	87-44-5
7	22.40	856	α – Longipinene	C ₁₅ H ₂₄	204	41432-70-6
8	23.31	663	Cyclopentanecarboxamide,3-ethenyl-2-(3-pentenylidene)-N-phenyl-	C ₁₉ H ₂₃ NO	281	136091-23-1
9	26.11	854	Caryophyllene oxide	C ₁₅ H ₂₄ O	220	1139-30-6
10	27.10	780	(1R,3E,7E,11R)-1,5,5,8-Tetramethyl-12-oxabicyclo[9.1.0]dodeca-3,7-diene	C ₁₅ H ₂₄ O	220	19888-34-7
11	28.99	641	2-[4-methyl-6-(2,6,6-trimethylcyclohex-1-enyl)hexa-1,3,5-trienyl]cyclohex-1-en-1-carboxaldehyde	C ₂₃ H ₃₂ O	324	NA
12	40.14	802	Chlorpyrifos (Dursban)	C ₉ H ₁₁ Cl ₃ N O ₃ PS	349	2921-88-2

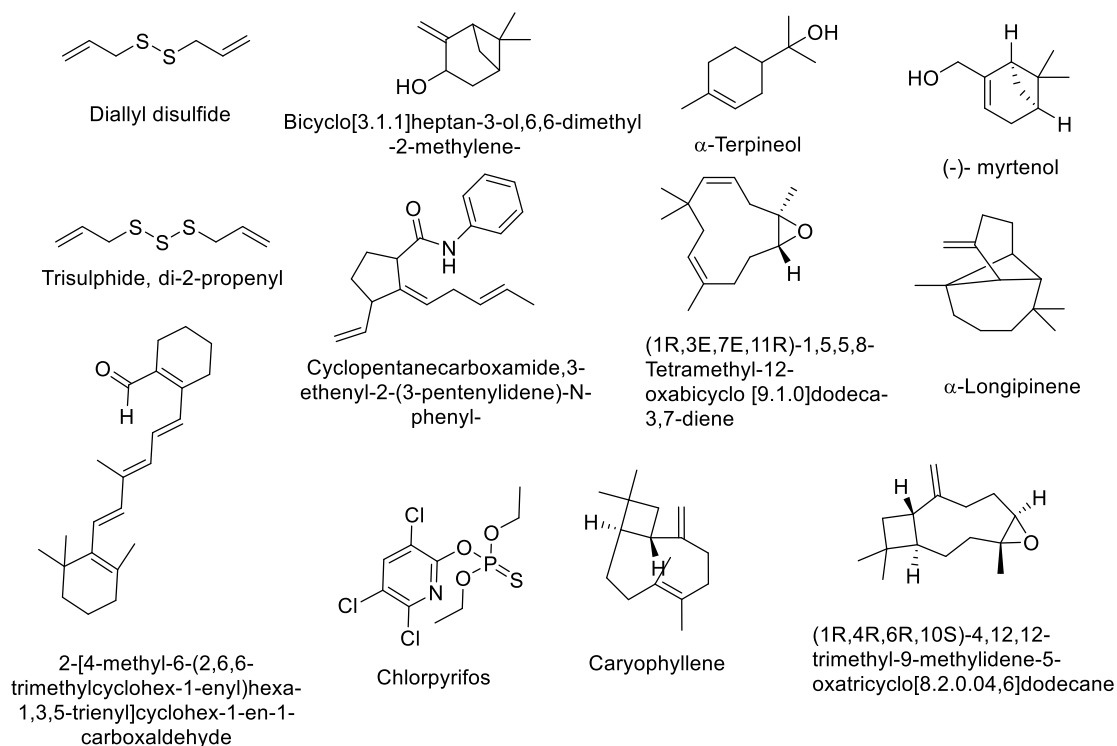


Figure 2.5.1.1: Main phytochemical constituents in ZM extract

Zingiber mioga essential oil was characterized by the high content of α –Terpineol, (-) - myrtenol, α –Pinene, Trisulphide, di-2-propenyl, Caryophyllene, followed by small amounts of α – Longipinene, Cyclopentanecarboxamide with O and N, 3-ethenyl-2-(3-pentenylidene)-N-phenyl. The major components were Allyldisulphide with sulfur atoms and π -bond of extracted oils, and it reveals that π -bond and lone pair interact with the vacant d orbital of Fe atoms (Yadav & Quraishi, 2012) .

Table 2.5.1.2 Phytochemical constituents of extracted oils from *Zingiber officinale* (ZO)

S/ No.	RT	RSI	Compound Name	Formula	MW	CAS
1	4.24	948	Camphene	C ₁₀ H ₁₆	136	79-92-5
2	5.97	8969	α – pinene	C ₁₀ H ₁₆	136	80-56-8
3	6.07	00	(Eucalyptol)	C ₁₀ H ₁₈ O	154	470-82-6
4	10.38	896	Endo – Borneol	C ₁₀ H ₁₈ O	154	507-70-0
5	13.07	845	Cis – Verbinol	C ₁₀ H ₁₆ O	152	1845-30-3
6	14.22	908	2,6-octadienal 3,7-dimethyl-,(E)-	C ₁₀ H ₁₆ O	152	141-27-5
7	15.74	671	Phosphonoacetic acid, 3TMS derivative.	C ₁₀ H ₂₉ O ₅ PSi ₃	356	53044-27-5
8	22.33	889	Benzene,1-(1,5-dimethyl-4-hexenyl) -4-methyl-	C ₁₅ H ₂₂	202	644-30-4
9	22.78	900	1S,5S-2-methyl-5-((R)-6-methylhept -5-en-2-yl)bicyclo[3.1.0]hex-2-ene	C ₁₅ H ₂₄	204	159407-35-9
10	23.28	888	1,3,6,10-Dodecatetraene 3,7,11-trimethyl-,(Z,E)-	C ₁₅ H ₂₄	204	26560-14-5
11	29.06	757	2,4-dihydroxybenzoic acid 3TMS derivative.	C ₁₆ H ₃₀ O ₄ Si ₃	370	10586-16-0
12	34.19	812	Diepicedrene-1-oxide	C ₁₅ H ₂₄ O	220	NA
13	43.33	817	6-methyl-4,6-bis(4-methylpent-3-en-1-yl)cyclohexane- 1,3dienecarbaldehyde	C ₂₀ H ₃₀ O	286	61447-89-0
14	51.40	696	α -D- mannofuranoside, farnesyl-	C ₂₁ H ₃₆ O ₆	384	NA
15	56.12	789	Hexadeca-2,6,10,14-tetraen-1-ol ,3,7,11,16-tetramethyl-	C ₂₀ H ₃₄ O	290	7614-21-3

The analysis of the essential oil of *Zingiber officinale* by chromatography in the gaseous stage coupled with a spectrum of mass enabled us to identify eighteen major compounds (Table 2.5.1.2, Figure 2.5.1.2). The most abundant components are: Geranial (23.30 %), Camphene (12.59 %), Eucalyptol (12.87 %), and alpha-terpineol (7.38 %) and followed by other structures of few organic molecules with their molecular weight. *Zingiber officinale* extracted oils, and its constituent's α -terpineol, cis-verbinol, and 2, 4-dihydroxybenzoic acid. TMS derivative acts as benzene derivatives exhibited an anti-corrosive effect under 1 M HCl solution on uniform corrosion for MS corrosion (Marimuthu et al., 2013).

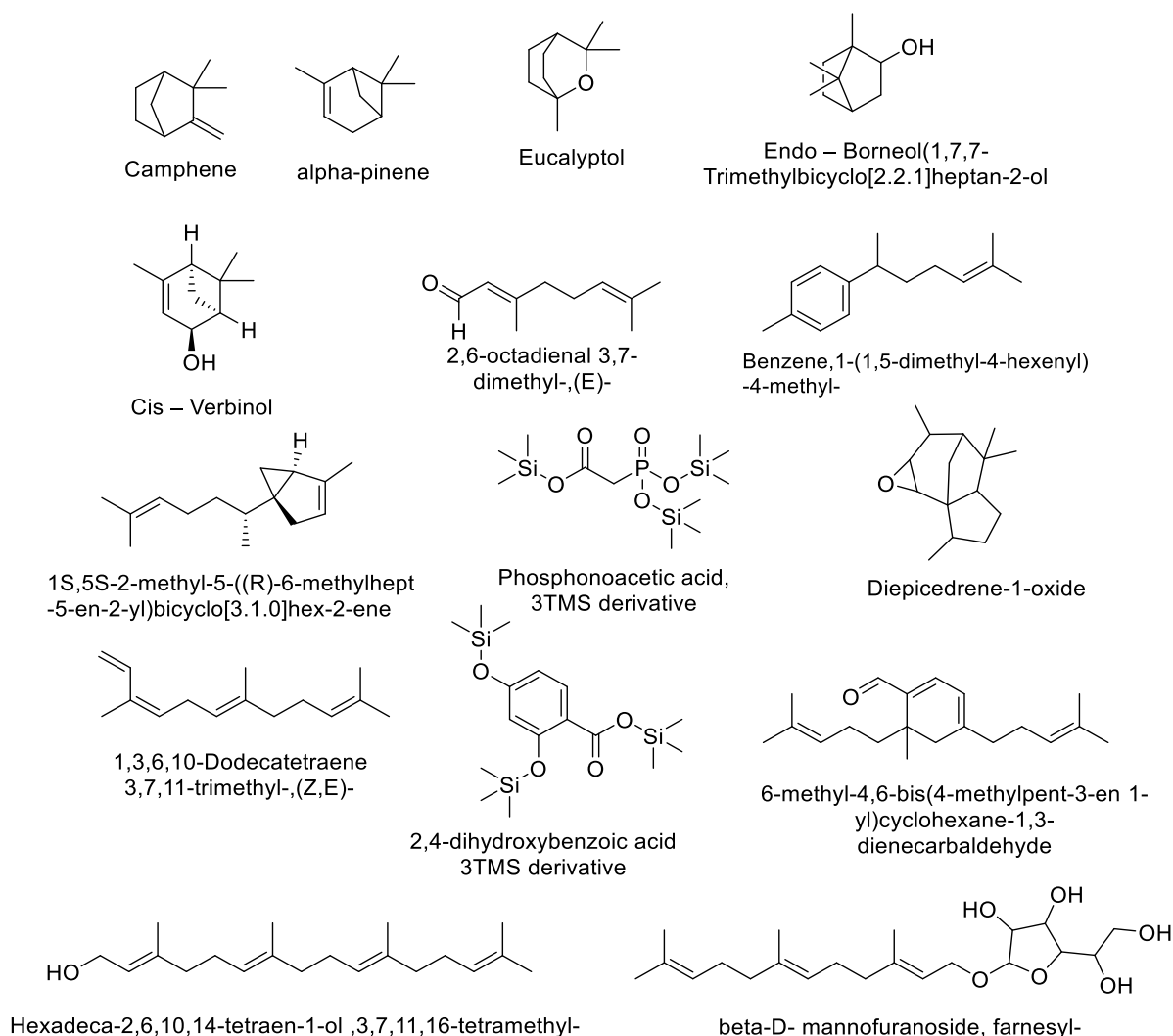


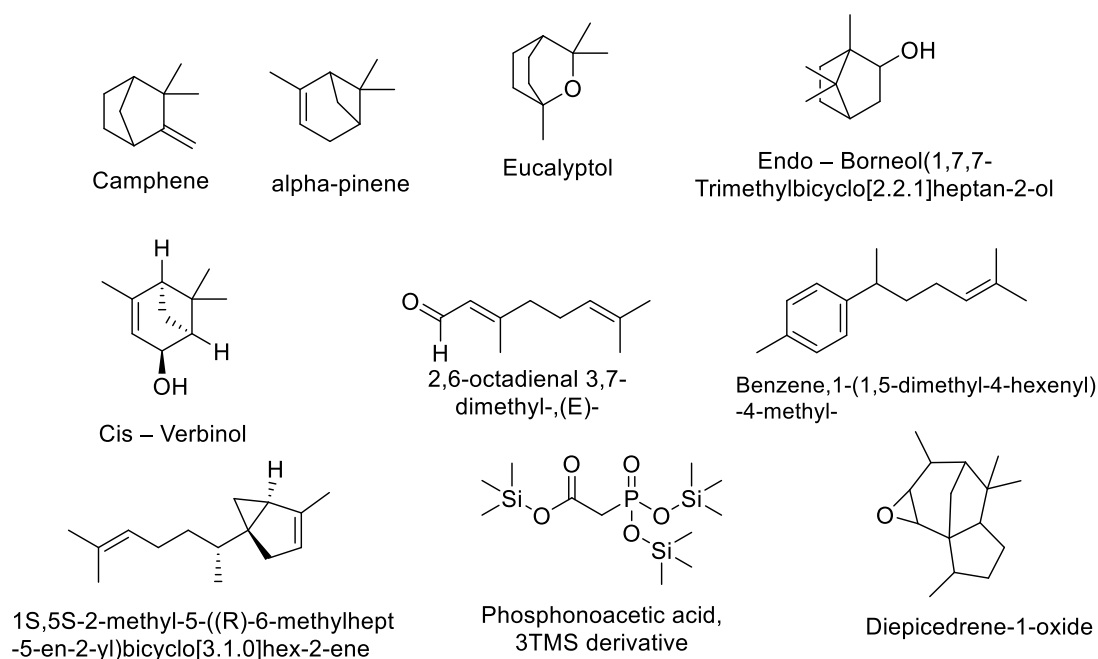
Figure 2.5.1.2: Main phytochemical constituents in ZO extract

Table 2.5.1.3 Phytochemical constituents of extracted oils from *Eryngium foetidum* (EF)

S/No.	RT	RSI	Compound Name	Formula	MW	CAS
1	4.23	962	Camphene	C ₁₀ H ₁₆	136	79-92-5
2	5.95	876	α – pinene	C ₁₀ H ₁₆	136	80-56-8
3	6.06	914	Eucalyptol	C ₁₂ H ₁₇ F ₃ O ₂	250	470-82-6
4	13.05	854	2,6-Octadienal, 3,7-dimethyl-, (Z)-	C ₁₀ H ₁₆ O	152	106-26-3
5	14.19	921	2,6-Octadienal, 3,7-dimethyl-, (E)-	C ₁₀ H ₁₆ O	152	141-27-5
6	17.62	874	Benzaldehyde, 2,4,5-trimethyl-	C ₁₀ H ₁₂ O	148	5779-72-6
7	19.33	970	Dodecanal (Lauraldehyde)	C ₁₂ H ₂₄ O	184	112-54-9
8	22.79	875	1s,5s-2-methyl-5-((R)-6-methylhept-5-en-2-yl)bicyclo[3.1.0]hex-2-ene	C ₁₅ H ₂₄	204	159407-35-9
9	23.29	876	1,3,6,10-Dodecetraene 3,7,11- trimethyl-(Z,E)-	C ₁₅ H ₂₄	204	26560-14-5
10	29.06	919	E-tetra-2-enal	C ₁₄ H ₂₆ O	210	51534-36-2
11	34.21	718	2,7,11-Trimethyl-1-4-phenylthiododec -2,6,10-triene	C ₂₁ H ₃₀ S	314	NA
12	40.12	864	Chlorpyrifos	C ₉ H ₁₁ Cl ₃ NO ₃ PS	349	2921-88-2
13	50.97	652	5-Androsten-17 α -ethynyl-3 α ,17 α -diol	C ₂₁ H ₃₀ O ₂	314	NA
14	53.57	626	Phenylalanine	C ₁₈ H ₂₈ N ₂ O ₄	336	NA
15	56.84	624	Pregn-4-ene-3,20-dione,17-hydroxy-16-methyl-	C ₂₂ H ₃₂ O ₃	344	2868-02-2

The GC-MS analysis was used to identify many groups of non-polar, semi-polar, and any active groups present in the given sample. It is an essential tool in studying specific trace levels of toxic food components that may occur in such complex matrices as foods and feeds.

A combined GC-MS spectral data analysis of *Eryngium foetidum* leaves extracted EO revealed that the major constituents of phytochemical obtained (Table 2.5.1.3 & Figure 2.5.1.3) have the potential to inhibit the acid corrosion of mild steel (Murthy & Vijayaragavan, 2014). The significant phytochemicals camphene and α -Pinene ($C_{10}H_{16}$) are bicyclic mono-terpene. Followed by the organic compounds Trifluoroacetyl α -Terpineol, α -Citral, E-Citral, Duraldehyde, Phenylalanine acts as the presence of oxygen, nitrogen, aromatic rings, and pie-bond can donate electrons to vacant d-orbital to the metal complex (Bhuvaneswari et al., 2018).



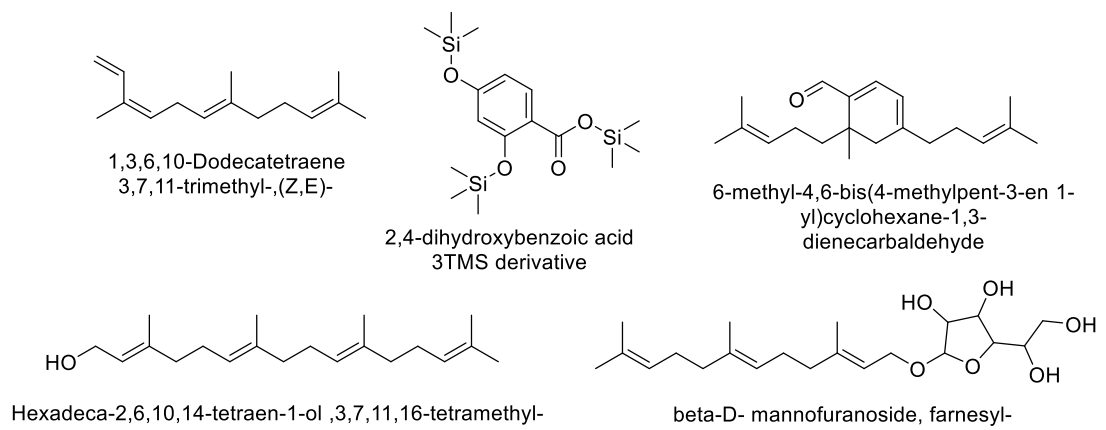


Figure 2.5.1.3: Main phytochemical constituents in EF extract

Table 2.5.1.4 Phytochemical constituents of extracted oils from *Mentha piperita* (MP)

S/No.	RT	RSI	Compound Name	Formula	MW	CAS
1	11.46	855	Bicyclo[6.1.0]nonane,9-(1-methyl ethylidene)-trans-shisool	C ₁₂ H ₂₀	164	56666-90-1
2	12.42	835	Trans-carveol	C ₁₀ H ₁₆ O	152	1197-07-5
3	13.46	859	Carvone	C ₁₀ H ₁₄ O	150	99-49-0
4	19.83	873	Caryophyllene	C ₁₅ H ₂₄	204	87-44-5
5	22.22	929	Germacrene-D	C ₁₅ H ₂₄	204	23986-74-5
6	23.90	836	Cis-calamenene	C ₁₅ H ₂₂	202	72937-55-4
7	28.82	809	Tau-Muurolol	C ₁₅ H ₂₆ O	506	19912-62-0
8	29.12	601	1,1,3,3,5,5,7,7,9,9-Decamethyl-9-(2-ethylpropoxy)pentasiloxan-1-ol	C ₁₄ H ₄₀ O ₆ Si ₅	444	NA
9	34.56	623	Heptasiloxane,1,1,3,3,5,5,7,7,9,9,11,11,13,13-tetradecamethyl-	C ₁₄ H ₄₂ O ₆ Si ₇	504	19095-23-9
10	40.13	796	Chlorpyrifos	C ₉ H ₁₁ Cl ₃ NO ₃ PS	349	2921-88-2
11	43.53	642	Heptadecanoic acid,9-methyl-, methyl ester	C ₁₉ H ₃₈ O ₂	298	54934-57-5
12	58.07	405	Butanoic acid,1a,2,5,5a,6,9,10,10a-octa Hydro-5a-hydroxy-4-(hydroxymethyl) -1,1,7,9-tetramethyl-6,11-dioxo-1H-2,8a- methanocyclopenta[a]Cyclopropa	C ₂₄ H ₃₂ O ₆	416	77508-70-4

13	62.00	414	[e]cyclodecan-5-yl ester. Pregn-16-en-20-one,11.18-bis (acetyloxy)-3,9-epoxy-3-methoxy-	$C_{26}H_{36}O_7$	460	30384-39-5
14	65.83	436	(5alpha)-3-Acetoxypregnan-20-ol-6-one-18-oic acid lactone.	$C_{23}H_{32}O_5$	388	NA

The analysis of GC-MS data of *Mentha piperita* EO extracted helps to identify several organic elements of various structures present in inhibitors. The GC-MS spectra corresponding NIST library database shows the identification of 14 major components in the EOs extract (Table 2.5.1.4 and Figure 2.5.1.4). Their (RIs) and their RT are reported in Table 2.5.1.4. with their molecular weight.

Mentha piperita oil was characterized by components of Trans-carveol, Carvone, Caryophyllene, Germacrene-D, and Cis-calamenene. They inhibited the corrosion effect on mild steel due to the presence of aromatic loops, sulfur, and nitrogen atoms and followed by some amounts of Heptasiloxane, 1,1,3,3,5,5,7,7,9,9,11,11,13,13-tetradecamethyl, Chlorpyrifos, Heptadecanoic acid, 9-methyl ester, Butanoic acid, 1a,2,5,5a,6,9,10,10a-octa, Hydro-5a-hydroxy-4-(hydroxymethyl) -1,1,7,9-tetramethyl-6,11-dioxo-1H-2, 8a methanocyclopenta[a]Cyclopropa [e]cyclodecan-5-yl esters. It acts as an inhibitor due to the presence of long-chain fatty acid, which can prevent corrosion attack, and π – *bonds* reveal that pi-bond and lone pair interact with the vacant d-orbital of Fe atoms (Okewale & Olaitan, 2017).

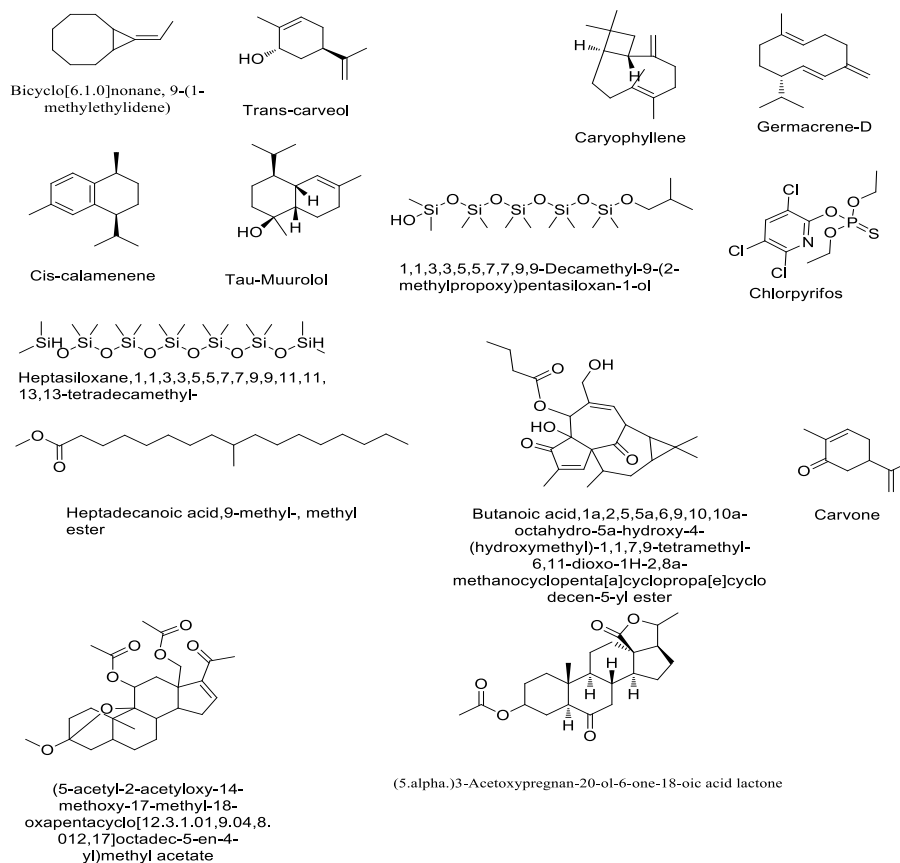


Figure 2.5.1.4: Main phytochemical constituents in MP extract

Table 2.5.1.5 Phytochemical constituents of extracted oils from garlic '*Allium Sativum* (AS)

S/No.	RT	RSI	Compound Name	Formula	MW	CAS
1	4.60	890	3H-1,2-Dithiole	C ₃ H ₄ S ₂	104	288-26-6
2	4.80	874	Dimethyl trisulfide	C ₂ H ₆ S ₃	126	3658-80-8
3	7.46	787	Diallyl disulfide	C ₆ H ₁₀ S ₂	146	2179-57-9
4	9.41	884	Trisulfide, methyl-2-propenyl	C ₄ H ₈ S ₃	152	34135-85-8
5	12.27	767	2-vinyl-4H-1,3-dithiine	C ₆ H ₈ S ₂	144	80028-57-5
6	15.37	904	Trisulfide, di-2-propenyl	C ₆ H ₁₀ S ₃	178	2050-87-5
7	19.56	480	Ethyl-iso-allocholate	C ₂₇ H ₄₄ O ₅	436	NA
8	23.07	590	Cycloheptasiloxane, tetradecamethyl-	C ₁₄ H ₄₂ O ₇ Si ₇	518	107-50-6
9	24.63	364	(5alpha)3-Acetoxypregnan-20-ol-6-one-18-oic acid lactone	C ₂₃ H ₃₂ O ₅	388	NA
10	29.17	657	2,5-Dihydroxybenzoic acid, 3TMS derivative	C ₁₆ H ₃₀ O ₄ Si ₃	370	3618-20-0
11	32.28	434	Stearic acid,3-(octadecyloxy)propyl ester	C ₃₉ H ₇₈ O ₃	594	17367-40-7
12	36.72	562	Carda-16,20(22)-dienolide,3-[(6-deoxy-3,4-O-methylenehexopyranos-2-ulos-1-yl)oxy]-5,11,14-trihydroxy-12-oxo-	C ₃₀ H ₃₈ O ₁₁	574	29428-87-3
13	40.14	781	Chlorpyrifos	C ₉ H ₁₁ Cl ₃ NO ₃ PS	349	2921-88-2

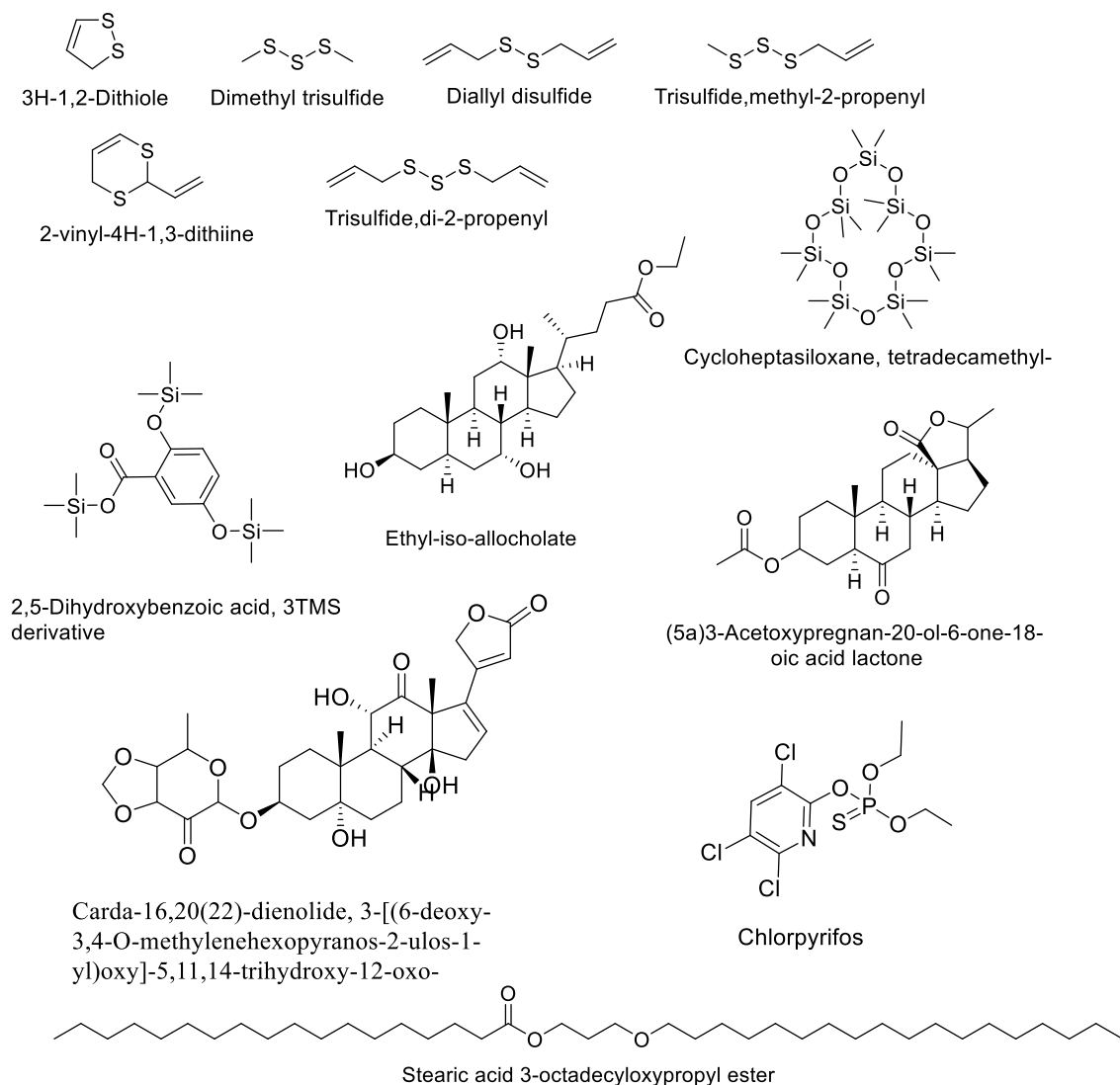


Figure 2.5.1.5 : Main phytochemical constituents in AS extract.

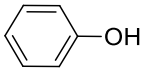
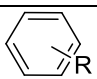
GC-MS analysis is a suitable method to identify the phytochemicals present in the given compound. *Allium Sativum* oils extracts are composed of different organic compounds with various molecular weights such as 3H-1,2-Dithiole, Dimethyl trisulfide, Diallyl disulfide, Trisulfide, methyl-2-propenyl, 2-vinyl-4H-1,3-dithiine, Allyl trisulfide, Ethyl-iso-allocholate and chlorpyrifos. Major component found in GC-MS analysis are given in Table 2.5.1.5 and Figure 2.5.1.5. Therefore, GC-MS analysis was used to more accurately examine the possible compounds in the '*Allium Sativum*' (Garlic bulb) extracted oils.

Therefore, it can be concluded that the oils extracted from '*Allium Sativum*' bulbs contain long-chain fatty acids. It can also confirm the presence of the organic compounds containing hetero-atoms containing sulfur and the presence of oxygen and aromatic loop. These compounds can be used as inhibitors in acidic media (Eddy et al., 2011).

2.5.2 FT-IR analysis of EOs extract

FTIR data showed (Figure 2.5.2.1) the resulting spectrum corresponds specifically to the chemical bonds that present in the molecules as found in GCMS. Therefore, in this study, the FTIR analyses were carried out to identify the major functional groups involved in the *Zingiber Mioga* oil (Table 2.5.2.1).

Table 2.5.2.1: FT-IR characterization of *ZingiberMioga* (ZM)

Functional group	Observed Wavelength (cm^{-1})	Vibration type
-O-H	3071.08	$\nu(\text{O-H})$
-COOH	2918.73	$\nu(\text{C=O})$
$\text{R}_2\text{C=NR/-C=NOH}$	1643.05	$\nu(\text{C=N})$
	1373.07	$\nu(\text{C-O})$
$-\text{C}_{\text{AR}}-\text{O}-\text{R}$	1258.32	$\nu(\text{C-O})$
$-\text{C}=\text{C}-$	876.488	$\nu(\text{C=C})$
	722.211	$\nu(\text{C-H})$

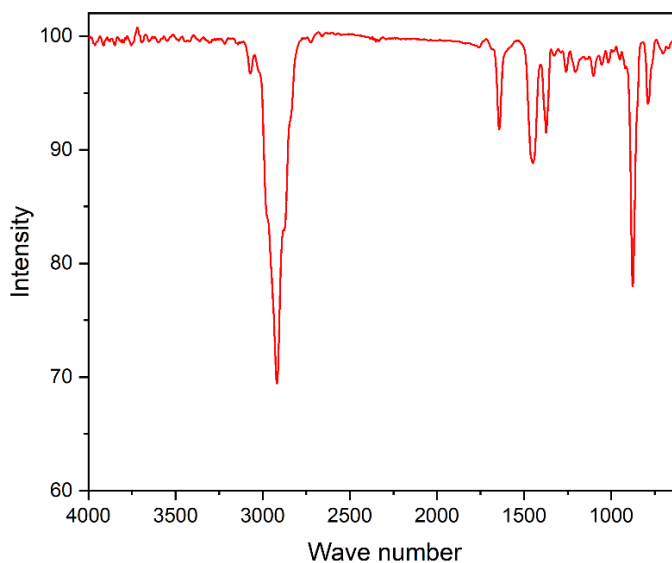


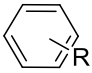
Figure 2.5.2.1: FTIR Spectra of ZM essential oils extract

The FTIR spectra of ZM essential oil illustrates the presence of an O-H group at wavenumber 3071.08 cm^{-1} , C=O of COOH group at wavenumber 2918.73 cm^{-1} . This broad band in oils extract results from intermolecular hydrogen bonding. Then, the bond of C=N appear at wavenumber of 1643.05 cm^{-1} . Meanwhile, the spectrum of possess to have C-O stretch group on the wavenumber of 1373.07 cm^{-1} . Another important vibrational mode associated to $C_{AR}\text{-O-R}$ groups is presented in the spectrum at 1258.32 cm^{-1} and the low intensity of C=C groups in the wavenumbers at 876.488 cm^{-1} . A CH group of aromatic ring vibration mode is in the wavenumbers at 722.211 cm^{-1} .

FTIR data of *Zingiber Officinale* showed the resulting spectrum corresponds specifically to the chemical bonds that present in the molecules as found in GCMS (Table 2.5.2.2).

Table 2.5.2.2: FT-IR characterization of Zingiber Officinale (ZO)

Functional group	Observed Wavelength (cm^{-1})	Vibration type
$-\text{C}_2\text{H}_6\text{O}$	3456.78	$\nu(\text{O-H})$
$-(\text{CH}_3)_2\text{NH}$	2956.34	$\nu(\text{N-H})$
$-\text{CH}_2=\text{CH}_2$	2921.63	$\nu(\text{C-H})$

-CO ₂	2334	$\nu(\text{O}=\text{C}=\text{O})$
-C ₆ H ₆	1673.91	$\nu(\text{C}-\text{H})$
-R-COOH	1440.35	$\nu(\text{C}=\text{O})$
-C ₆ H ₆ O	1377.35	$\nu(\text{O}-\text{H})$
-R-CO-OR	1176	$\nu(\text{C}-\text{O})$
-CH ₂ =CH ₂	880.345	$\nu(\text{C}=\text{C})$
	720	$\nu(\text{C}-\text{H})$
-C-Br	675.93	$\nu(\text{C}-\text{X})$

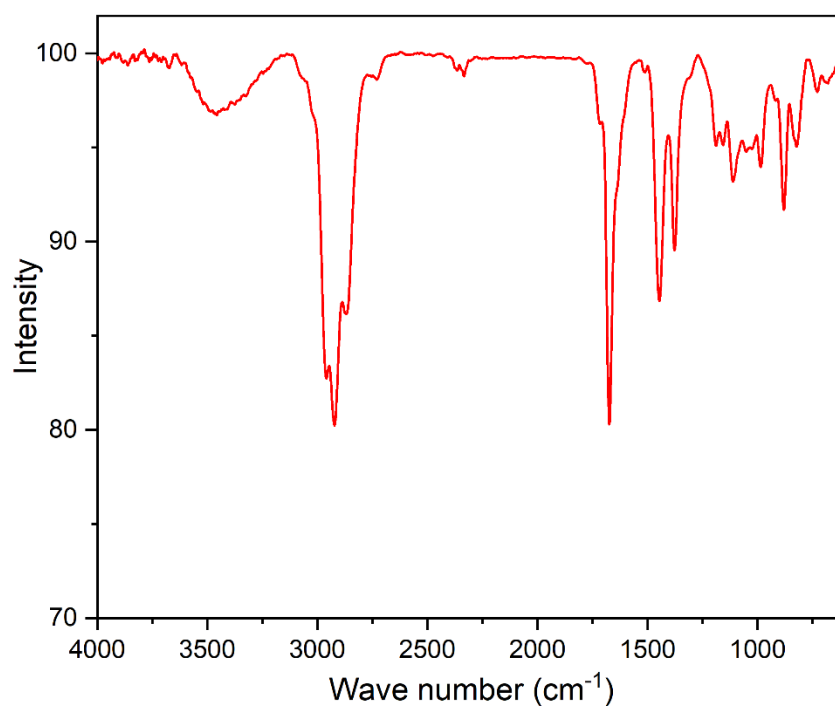


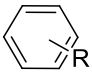
Figure 2.5.2.2 : FTIR Spectra of ZO essential oils extract

The FTIR spectra of ZO essential oil illustrates the presence of an O-H group at wavenumber 3456.78cm^{-1} , N-H of secondary amine of at wavenumber 2956.34 cm^{-1} , C-H of alkene at wavenumber 2921.63 cm^{-1} , O=C=O of CO₂ at wavenumber

2334 cm^{-1} . The C-H bending vibrations are present in the FTIR spectra at 1673.91 cm^{-1} , whereas the C=O and O-H stretching vibrations are shown at 1440.35 and 1377.35 cm^{-1} , respectively. The C-O and C=C stretching vibrations are shown at 1176 and 880.345 cm^{-1} , respectively. A CH group of aromatic ring vibration mode is in the wavenumbers at 720 cm^{-1} and C-X vibration mode is in the wavenumber at 675.93 cm^{-1} (Figure 2.5.2.2).

FTIR data of *Eryngium Foetidum* showed the resulting spectrum corresponds specifically to the chemical bonds that present in the molecules as found in GCMS (Table 2.5.2.3). FTIR analyses were carried out to identify the major functional groups involved in the *Eryngium Foetidum* oil.

Table 2.5.2.3: FT-IR characterization of *Eryngium Foetidum* (EF)

Functional group	Observed Wavelength (cm^{-1})	Vibration type
-O-H	3446	$\nu(\text{O-H})$
-NH ₂	2885.1	$\nu(\text{N-H})$
-CHO	2726.85	$\nu(\text{C-H})$
-RCONH ₂	1689	$\nu(\text{C=O})$
-(C=O)-	1671.98	$\nu(\text{C=O})$
R ₂ C=NR/-C=NOH	1644	$\nu(\text{C=N})$
-CH ₃	1459.85	$\nu(\text{C-H})$
R-O-R	1231.33	$\nu(\text{C-O})$
-C=C-	973.87	$\nu(\text{C=C})$
	722.211	$\nu(\text{C-H})$

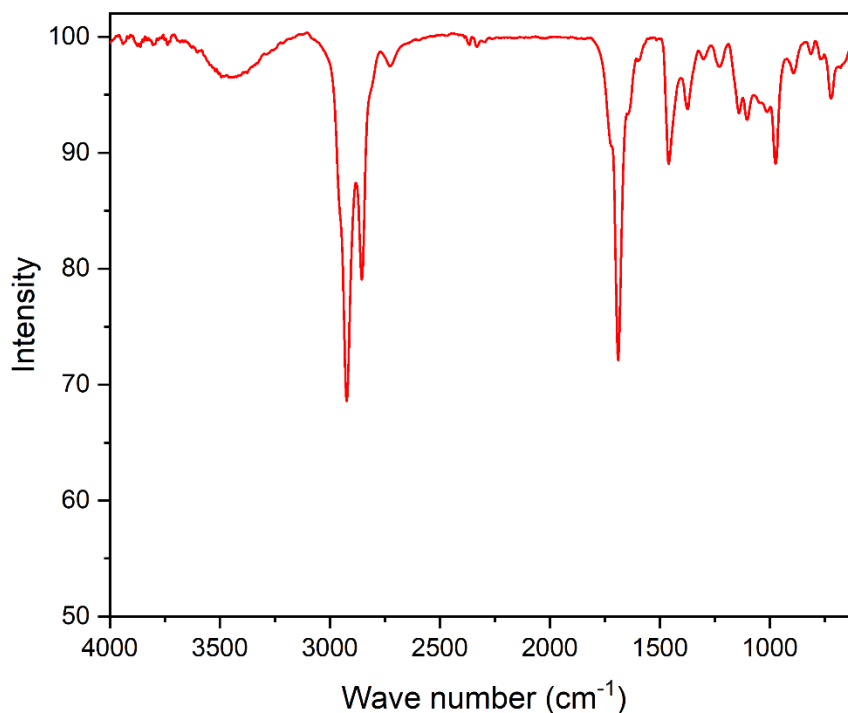
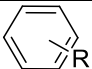


Figure 2.5.2.3: FTIR Spectra of EF essential oils extract

The FTIR spectra of EF essential oil illustrates the presence of an O-H group at wavenumber 3446 cm^{-1} , N-H of NH_2 group at wavenumber 2885.1 cm^{-1} , C-H of CHO group at wavenumber 2726.85 cm^{-1} , C=O of CONH_2 group at wavenumber 1689 cm^{-1} and C=O of ketone group at wavenumber 1671.98 cm^{-1} . This broad band in oils extract results from intermolecular hydrogen bonding. Then, the bond of C=N appear at wavenumber of 1644 cm^{-1} . Meanwhile, the spectrum of possess to have C-O stretch group on the wavenumber of 1231.33 cm^{-1} . Another important vibrational mode associated to C-H of CH_3 groups is presented in the spectrum at 1459.85 cm^{-1} and the low intensity of C=C groups in the wavenumbers at 973.87 cm^{-1} . A CH group of aromatic ring vibration mode is in the wavenumbers at 722.211 cm^{-1} (Figure 2.5.2.3).

FTIR data of *Mentha Piperita* showed the resulting spectrum corresponds specifically to the chemical bonds that present in the molecules as found in GCMS (Table 2.5.2.4). Therefore, in this study, the FTIR analyses were carried out to identify the major functional groups involved in the *Mentha Piperita* oil.

Table 2.5.2.4: FT-IR characterization of *Mentha Piperita* (MP)

Functional group	Observed Wavelength (cm ⁻¹)	Vibration type
-O-H	3494.38	v(O-H)
-COOH	3078.80	v(C=O)
-NH ₂	2954.52	v(N-H)
-(C=O)-	1671.98	v(C=O)
$\begin{array}{c} \text{O} \\ \\ -\text{S}-\text{NH}_2 \\ \\ \text{O} \end{array}$	1370.18	v(S=O)
-C-NH	1244.83	v(C-N)
-C-O-C-	1144.55	v(C-O)
-C=C	990.265	v(C=C)
	700.998	v(C-H)

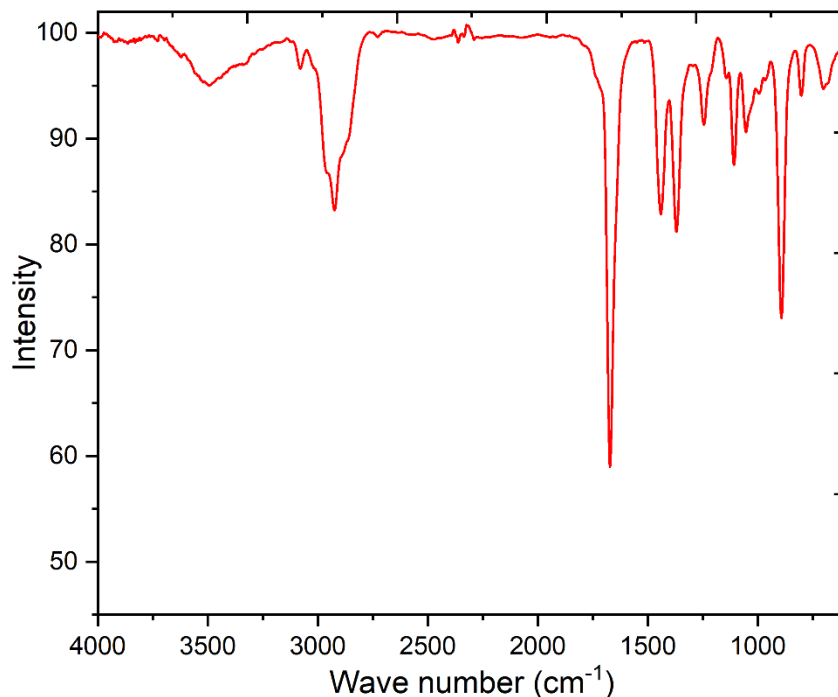
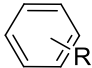


Figure 2.5.2.4: FTIR Spectra of MP essential oils extract

The FTIR spectra of MP essential oil illustrates the presence of an O-H group at wavenumber 3494.38 cm^{-1} , N-H of NH_2 group at wavenumber 2954.52 cm^{-1} , C=O of ketone group at wavenumber 1671.98 cm^{-1} . This broad band in oils extract results from intermolecular hydrogen bonding. Then, the bond of S=O appear at wavenumber of 1370.18 cm^{-1} . Meanwhile, the spectrum of possess to have C-N stretch group on the wavenumber of 1244.83 cm^{-1} . Another important vibrational mode associated to C-O-C groups is presented in the spectrum at 1144.55 cm^{-1} and the low intensity of C=C groups in the wavenumbers at 990.265 cm^{-1} . A CH group of aromatic ring vibration mode is in the wavenumbers at 700.998 cm^{-1} (Figure 2.5.2.4).

FTIR data of *Allium Sativum* showed the resulting spectrum corresponds specifically to the chemical bonds that present in the molecules as found in GCMS (Table 2.5.2.5). Therefore, in this study, the FTIR analyses were carried out to identify the major functional groups involved in the *Allium Sativum* oil.

Table 2.5.2.5: FT-IR characterization of *Allium Sativum* (AS)

Functional group	Observed Wavelength (cm^{-1})	Vibration type
-O-H	3498.23	$\nu(\text{O-H})$
R-NH ₂	3078.79	$\nu(\text{N-H})$
-(C=O)-	1719.23	$\nu(\text{C=O})$
-(C=O)-	1671.98	$\nu(\text{C=O})$
-C=C-	1636.30	$\nu(\text{C=C})$
C _{AR} -NH ₂	1304.61	$\nu(\text{C-N})$
-O(CH=CH ₂) ₂	1216.86	$\nu(\text{C-O})$
	722.211	$\nu(\text{C-H})$

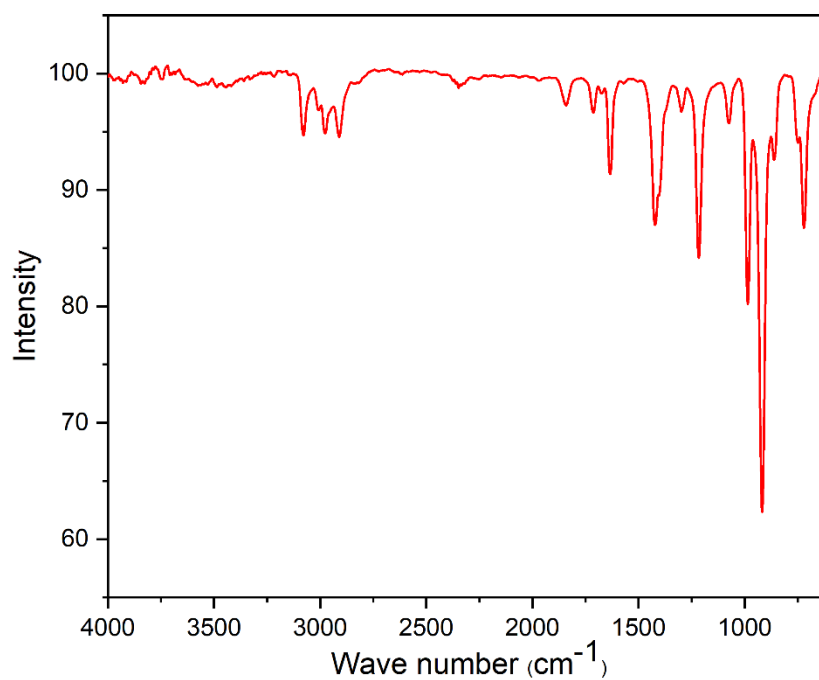


Figure 2.5.2.5: FTIR Spectra of AS essential oils extract

The FTIR spectra of AS essential oil illustrates the presence of an O-H group at wavenumber 3498.23 and 3078.79 cm^{-1} , C=O of ketone group at wavenumber 1719.23 and 1671.98 cm^{-1} . This broad band in oils extract results from intermolecular hydrogen bonding. Then, the bond of C=C appear at wavenumber of 1636.30 cm^{-1} . Meanwhile, the spectrum of possess to have C-N stretch of $\text{C}_{\text{AR}}\text{-NH}_2$ group on the wavenumber of 1304.61 cm^{-1} . Another important vibrational mode associated to C-O of $-\text{O}(\text{CH}=\text{CH}_2)_2$ groups is presented in the spectrum at 1216.86 cm^{-1} . A CH group of aromatic ring vibration mode is in the wavenumbers at 722.211 cm^{-1} (Figure 2.5.2.5).

STUDY OF CORROSION INHIBITION EFFICIENCY OF EXTRACT

3.1. Weight loss measurement

A weight loss/gravimetric measurement was done on the specimens of the rectangular shape that weighed mild steel of those mentioned in the methodology made with 2.59cm x 1.73cm x 0.28cm exposure area. In all the weight loss experiments, the specimens were suspended in a glass beaker containing 1M HCl of 100 ml in the absence and presence of inhibitors of oils extracted from plants at various concentrations at a working temperature of 30°C, which is controlled by a water bath. The mild steel specimens were taken out after six hours of immersion time. It was cleaned with double distilled water and then rinsed with acetone, dried in a hot oven at enough temperature for a few minutes, and carefully weighed the mild steel for getting an accurate result. All the experiments were repeated to ensure reproducibility, and mean values were reported.

Weight loss study of all the metal specimens was attained by taking their weights before and after immersion in 1M HCl of the solution and with EO extract at a different concentration at working temperature, calculation of the corrosion rates (C_R) by using standard method (Hosseini et al., 2010); (Khadom, 2013) of the following equation:

$$C_R (\text{mgcm}^{-2}\text{h}^{-1}) = \frac{\Delta W}{SXT} \quad (1)$$

where, ΔW = Weight Loss, S = Surface area of mild steel in cm^2 , T = Immersion time (6 h).

The corrosion inhibition efficiencies (%IE) were calculated by using the following relation:

$$\% \text{ IE} = \frac{C_{R0} - C_{Rinh}}{C_{R0}} \times 100 \quad (2)$$

Where C_{Ro} and C_{Rinh} are the corrosion rates in the absence and presence of inhibitor molecules, respectively. The surface area covered by the inhibitor molecules on the mild steel, θ is given as,

$$\theta = \frac{IE}{100} \quad (3)$$

3.1.1 *Zingiber mioga* (ZM)

Weight loss study of all the metal specimens was attained by taking their weights before and after immersion in 1M HCl of the solution and with EO extract of *Zingiber mioga* (ZM) at a different concentration at a working temperature of 30°C. The inhibition efficiency at various concentrations of essential oils extracted in an acidic medium was measured by gravimetric measurement. Weight loss parameters of corrosion rate (C_R), Inhibition efficiency (%IE), and surface coverage (θ) with inhibitor molecules extracted from EOs of various concentrations are shown in Table 3.1.1.

Table 3.1.1 Weight loss measurement for mild steel in 1M HCl without and with inhibitors in different concentrations of *Zingiber mioga* EO extract at 30°C.

Inhibitors Concentration (g/L)	Corrosion Rate (C_R) (mg/cm²h)	Inhibition Efficiency (%IE)	Surface Coverage (θ)
Blank	0.174	-	-
1	0.0409	76.49	0.7649
2	0.034	80.46	0.8046
3	0.0273	84.31	0.8431
4	0.019	89.08	0.8908
5	0.011	93.74	0.9374

The analysis of these results in Table 3.1.1 clearly shows a rapid decrease in corrosion rate (mg/cm²h). In contrast, the corrosion inhibitor concentration gradually increases and reaches the maximum concentration of 5g/L. The value of corrosion

efficiency was found to be 93.74%; by this performance, it can be identified the surface coverage θ increases at 30°C. More EOs extracted molecules are adsorbed over metal surfaces, and hence the formation of protective layers due to adsorption increases with increasing concentration of corrosion inhibitors, which protect mild steel surfaces from the destructive acidic corrosive medium (Thirupathi & Venkatraman, 2021). Therefore, it was analyzed by adding inhibitor molecules in the corrosive medium. The corrosion rate gradually decreased due to this thin film of protective layers formed on the surface of the mild steel surface (Khaled, 2010).

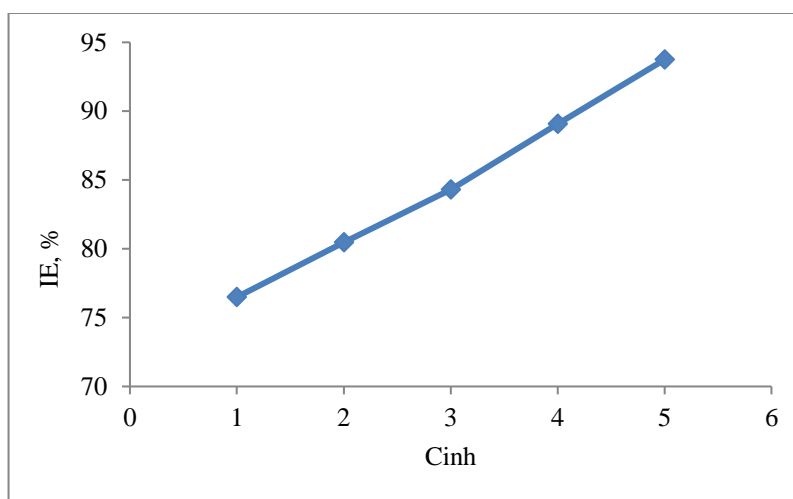


Fig. 3.1.1. Gravimetric plot of mild steel with and without inhibitor in various concentrations in 1M HCl solution of *Zingiber mioga* EO extract at a temperature of 30°C

Figure 3.1.1 (graph) shows that inhibition efficiency (%IE) linearly increases with increasing the concentration of EOs extract of *Zingiber mioga*. These results conclude that the essential oils of ZM extracts are a suitable corrosion inhibitor for mild steel in 1M HCl acidic solution at a moderate temperature.

3.1.2 *Zingiber officinale* (ZM)

Weight loss study of all the metal specimens was attained by taking their weights before and after immersion in 1M HCl of the solution and with EO extract of *Zingiber officinale* (ZO) at a different concentration at working temperature 30°C. Table 3.1.2 signifies the inhibition efficiency at various concentrations of essential oils extracted in an acidic medium using gravimetric measurement. Weight loss

parameters of corrosion rate (C_R), Inhibition efficiency (%IE), and surface coverage (θ) with inhibitor molecules extracted from EO of various concentrations are shown in Table 3.1.2.

Table 3.1.2 Weight loss measurement for mild steel in 1M HCl without and with inhibitors in different concentrations of *Zingiber officinale* EO extract at 30°C.

Inhibitors Concentration (g/L)	Corrosion Rate (C_R) (mg/cm²h)	Inhibition Efficiency (%IE)	Surface Coverage (θ)
Blank	0.157	-	-
1	0.035	77.71	0.7771
2	0.029	81.53	0.8153
3	0.022	85.98	0.8854
4	0.014	91.27	0.9127
5	0.009	94.27	0.9427

The analysis of these results in Table 3.1.2 clearly shows a rapid decrease in corrosion rate (mg/cm²h) (Abboud et al., 2009). In contrast, the corrosion inhibitor concentration gradually increases and reaches the maximum concentration of 5g/L. The value of corrosion efficiency was found to be 94.27%; by this performance, it can be identified the surface coverage θ increases at 30°C. More EOs extracted molecules are adsorbed over metal surfaces. Hence, the formation of protective layers due to adsorption increases with increasing concentration of corrosion inhibitors, which protect mild steel surfaces from the destructive acidic corrosive medium. Therefore, it was analyzed by adding inhibitor molecules in the corrosive medium, corrosion rate gradually decreased. Due to this, a thin film of protective layers formed on the surface of the mild steel surface (Khaled, 2010).

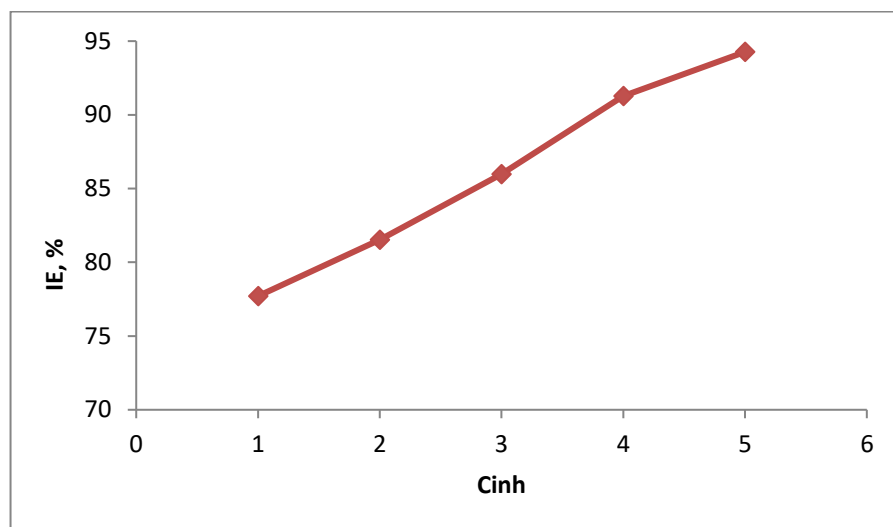


Fig.3.1.2. Gravimetric plot of mild steel with and without inhibitor in various concentrations in 1M HCl solution of EO (*Zingiber officinale*) extract at a temperature of 30°C

Figure 3.1.2 (graph) shows that inhibition efficiency (%IE) linearly increases with the concentration of EOs extract of *Zingiber officinale*. These results conclude that EO extracts of ZO are a suitable corrosion inhibitor for mild steel in 1M HCl acidic solution at a moderate temperature.

3.1.3 *Eryngium foetidum* (EF)

Weight loss study of all the metal specimens was attained by taking their weights before and after immersion in 1M HCl of the solution and with EO extract of *Eryngium foetidum* (EF) at a different concentration at a working temperature of 30°C. The inhibition efficiency at various concentrations of essential oils extracted in an acidic medium was measured using gravimetric measurement. Weight loss parameters of corrosion rate (C_R), Inhibition efficiency (%IE), and surface coverage (θ) with inhibitor molecules extracted from AOs of various concentrations are shown in Table 3.1.3.

Table 3.1.3. Weight loss measurement for mild steel in 1M HCl without and with inhibitors in different concentrations of *Eryngium foetidum* EO extract at 30°C.

Inhibitors Concentration (g/L)	Corrosion Rate (C_R) (mg/cm²h)	Inhibition Efficiency (%IE)	Surface Coverage (θ)
Blank	0.170	-	-
1	0.031	81.76	0.8176
2	0.024	85.88	0.8588
3	0.017	90.00	0.90
4	0.009	94.70	0.9470
5	0.005	97.06	0.9706

The analysis of these results, Table 3.1.3 clearly shows a rapid decrease in corrosion rate (mg/cm²h) (Bammou et al., 2014). In contrast, the corrosion inhibitor concentration gradually increases to the maximum concentration of 5g/L, and the value of corrosion efficiency was found to be 97.06%; by this performance, it can be identified the surface coverage θ increases at 30°C. More EOs extracted molecules are adsorbed over metal surfaces (Chaubey et al., 2017), and hence the formation of protective layers due to adsorption increases with increasing concentration of corrosion inhibitors, which protect mild steel surfaces from the destructive acidic corrosive medium (Abboud et al., 2009). Therefore, it was analyzed by adding inhibitor molecules in the corrosive medium. The corrosion rate gradually decreased due to this, and a thin film of protective layers formed on the surface of the mild steel surface (Khaled, 2010).

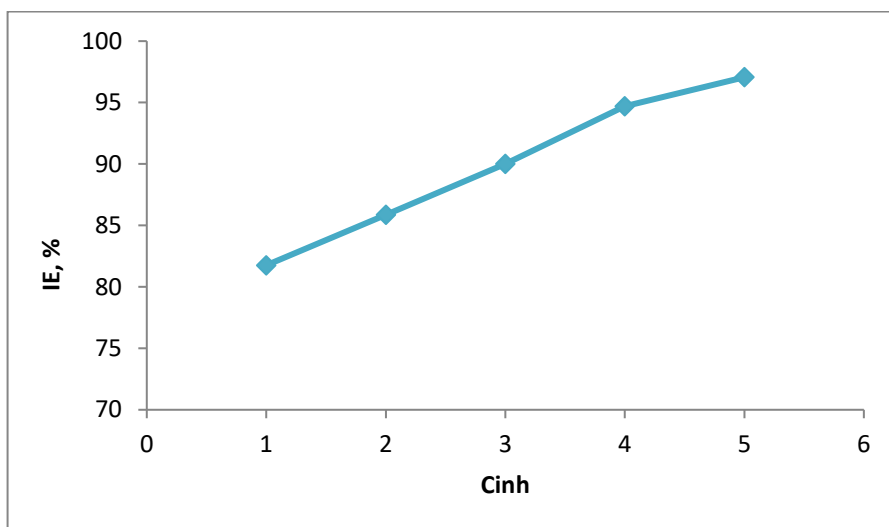


Fig.3.1.3. Gravimetric plot of mild steel with and without inhibitor in various concentrations in 1M HCl solution of *Eryngium foetidum* L. EO extract at temperature 30°C

Figure 3.1.3 (graph) shows that inhibition efficiency (%IE) linearly increases with the concentration of EOs extract of *Eryngium foetidum*. These results conclude that *Eryngium foetidum* EOs extracts are a suitable corrosion inhibitor for mild steel in 1M HCl acidic solution at a moderate temperature.

3.1.4 *Mentha. Piperita* (MP)

Weight loss study of all the metal specimens was attained by taking their weights before and after immersion in 1M HCl of the solution and with EO extract of *Mentha. Piperita* (MP) at a different concentration at a working temperature of 30°C. Table 3.1.4 signifies the inhibition efficiency at various concentrations of essential oils extracted in an acidic medium using gravimetric measurement. Weight loss parameters of corrosion rate (C_R), Inhibition efficiency (%IE), and surface coverage (θ) with inhibitor molecules extracted from EOs of various concentrations are shown in Table 3.1.4.

Table 3.1.4 Weight loss measurement for mild steel in 1M HCl without and with inhibitors in different concentrations of *M. Piperita* EO extract at 30°C.

Inhibitors Concentration (g/L)	Corrosion Rate (C_R) (mg/cm²h)	Inhibition Efficiency (%IE)	Surface Coverage (θ)
Blank	0.185	-	-
1	0.040	78.38	0.7838
2	0.033	82.16	0.80
3	0.025	86.49	0.8649
4	0.017	90.81	0.9081
5	0.010	94.59	0.9459

The analysis of these results, Table 3.1.4, clearly shows a rapid decrease in corrosion rate (mg/cm²h). In contrast, the corrosion inhibitor concentration gradually increased to the maximum concentration of 5 g/L, and the corrosion efficiency value was 94.59%. This performance can be identified by the surface coverage θ increasing at 30°C. More EOs extracted molecules are adsorbed over metal surfaces, and hence the formation of protective layers due to adsorption increases with increasing concentration of corrosion inhibitors, which protect mild steel surfaces from the destructive acidic corrosive medium (Abboud et al., 2009);(Khaled, 2010). Therefore, it was analyzed by adding inhibitor molecules in the corrosive medium. The corrosion rate gradually decreased; a thin film of protective layers formed on the surface of the mild steel surface.

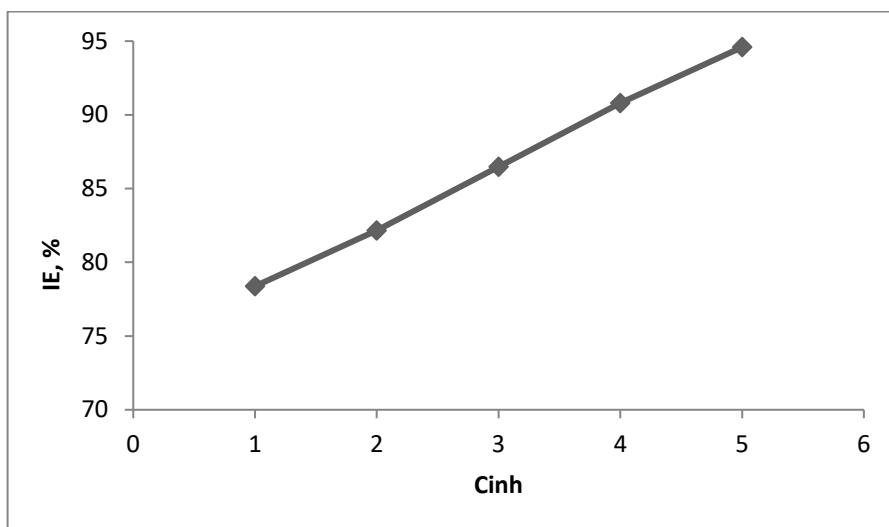


Fig.3.1. 4. Gravimetric plot of mild steel with and without inhibitor in various concentrations in 1M HCl solution of EOs (*M. Piperita*) extract at temperature 30°C

Figure 3.1.4. (graph) shows that inhibition efficiency (%IE) linearly increases with increasing the concentration of EOs extract of *Mentha piperita*. These results conclude that the EO of *Mentha piperita* extracts is a suitable corrosion inhibitor for mild steel in 1M HCl acidic solution at a moderate temperature.

3.1.5 Garlic (*Allium sativum*)

Weight loss study of all the metal specimens was attained by taking their weights before and after immersion in 1M HCl of the solution and with EO extract of *Allium sativum* at a different concentration at a working temperature of 30°C. The inhibition efficiency at various concentrations of essential oils extracted in an acidic medium was measured by gravimetric measurement (Khaled, 2010). Weight loss parameters of corrosion rate (C_R), Inhibition efficiency (%IE), and surface coverage (θ) with inhibitor molecules extracted from AOs of various concentrations are shown in Table 3.1.5.

Table 3.1.5 Gravimetric analysis for mild steel in an acidic medium with different temperatures in the absence and presence of various concentrations of *Allium sativum* EO extract at 30°C.

Inhibitors Concentration (g/L)	Corrosion Rate (C_R) (mg/cm²h)	Inhibition Efficiency (%IE)	Surface Coverage (θ)
Blank	0.154	-	0.812
1	0.050	67.53	1.301
2	0.038	75.32	1.420
3	0.027	82.47	1.569
4	0.015	90.26	1.823
5	0.008	94.81	2.097

The analysis of these results, Table 3.1.5, clearly shows a rapid decrease in corrosion rate (mg/cm²h). In contrast, the corrosion inhibitor concentration gradually increased to the maximum concentration of 5g/L, and the corrosion efficiency value was 94.81% at this concentration. This performance can be identified by the surface coverage θ increasing at 30°C. More EOs extracted molecules are adsorbed over metal surfaces, and hence the formation of protective layers due to adsorption increases with increasing concentration of corrosion inhibitors, which protect mild steel surfaces from the destructive acidic corrosive medium (Abboud et al., 2009). Therefore, it was analyzed by adding inhibitor molecules in the corrosive medium. The corrosion rate gradually decreased due to this thin film of protective layers formed on the surface of the mild steel surface.

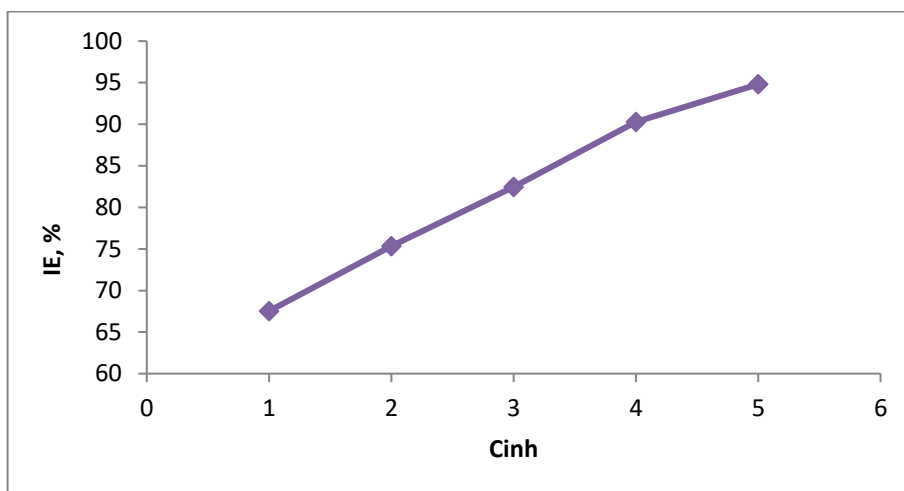


Fig.3.1.5 Gravimetric plot of mild steel with and without inhibitor in various concentrations in 1M HCl solution of *Allium sativum* EO extract at a temperature of 30°C.

Figure 3.1.5 (graph) shows that inhibition efficiency (%IE) linearly increases with increasing the concentration of EOs extract *Allium sativum*. It concludes that the EO of *Allium sativum* extracts is a suitable corrosion inhibitor for mild steel in 1M HCl acidic solution at a moderate temperature.

Among the various natural products, such as the extract of bamboo leaves extract (X. Li et al., 2012), such as the extract of *Eruca sativa* seed (Gadow & Fakeeh, 2022), *Paederiafoetida* leaves (Hossain et al., 2021) studied as a corrosion inhibitor. *Crataegus oxyacantha* leaves extract (Zehra et al., 2022) studied effective corrosion inhibitors for mild steel in a 1M HCl acidic medium. Maximum inhibition efficiencies of *Aquilaria subintergra* leaves extracts as sustainable mild steel corrosion inhibitors 93.28% (SIB), 91.82% (SIP), and 93.44% (SIC), respectively, were reported with 1500 ppm at 303 K in HCl solution (Sin et al., 2017). Similar results were reported for *Jatropha Leaf* Extract in a Hydrochloric Acid solution (Ikpeseni et al., 2021). The inhibition efficiency (%IE) linearly increases with the addition of EO extract of all five-plant extracts. Our results conclude that the EO of our selected species, *Allium sativum*, *Mentha piperita*, *Eryngium foetidum*, *Zingiber officinale*, and *Zingiber mioga* extracts are a suitable corrosion inhibitor for mild steel in 1M HCl acidic solution at a moderate temperature.

3.2 Electrochemical measurements

The electrochemical measurements were performed with an electrochemical instrument with CHI604c software assembled with three electrodes. Platinum rod and calomel electrode were used as counter and reference electrodes, respectively, and mild steel with an exposure area of 1 cm² was used as the working electrode. Before measurements of potentiodynamic polarization (PDP) and electrochemical impedance spectroscopy (EIS), the mild steel was mechanically scraped with different grades of emery papers from 80 to 1200, respectively, then placed into the corrosive medium at stable-state open circuit potentials (OCP) for one and half hours at 300 K to achieve the equilibrium state (Mai et al., 2016). Electrochemical Impedance Spectroscopy study was attained at Open Circuit Potential (OCP) using an ac voltage signal of small periodic (0.01V) amplitude with a wide-ranging frequency spectrum from 1 x 10⁵ Hertz to 0.01 Hertz. Nyquist plots were used for analyzing the impedance data. At least three similar results were measured in all the above values, and their mean values have been reported (Zhang & Hua, 2009). By recording the Tafel slopes at anodic and cathodic curves, the potentiodynamic polarization study was investigated without and with inhibitors of different concentrations by changing the working electrode potentials versus the corrosion potential (E_{corr}) from -0.80V to +0.25 V at a repeated sweep rate of 0.001V per second and sensitivity 0.001V. These Tafel slopes were assumed to determine the corrosion current densities (I_{corr}) for inhibited and uninhibited mild steel specimens.

The C_{rate} of MS specimen in 1M HCl solutions with and without different concentrations of oils extract was calculated by Tafel polarization data using the following equations:

$$C_{rate} = \frac{I_{corr} K \times Eq.Wt}{D}, \quad (4)$$

C_{rate} and I_{corr} are corrosion rate (mmpy) and corrosion current density (μAcm⁻²), respectively. Eq.Wt is the equivalent weight in a gram of mild steel, D is density in

gram/cm³, and K is constant (taken from the machine used)(Bommersbach et al., 2005).

The following equation can give the corrosion inhibition efficiency (% IE) of Tafel polarization from essential oils extract.

$$\%IE = \frac{I_{corr} - I_{corrinh}}{I_{corr}} \times 100 \quad (5)$$

Where, I_{corr} and $I_{corrinh}$ are the values of current-density of corrosion in the absence and presence of inhibitor, respectively.

The corrosion inhibition efficiency (% IE) of the corrosion inhibitor was calculated using the following impedance equation.

$$IE\% = \frac{R_{ct} - R_u}{R_{ct}} \times 100 \quad (6)$$

Where, R_{ct} and R_u are the charge transfer resistance of mild steel in 1M HCl in the presence and absence of inhibitors, respectively.

The impedance spectra were analyzed by fitting them to the equivalent circuit model built by the Z-view software. The following equation calculated the Cdl:

$$C_{dl} = \frac{1}{2\pi R_{ct} f_{max}} \quad (7)$$

Where f_{max} is the frequency at which the imaginary part of the Impedance is maximum. The Nyquist plots (impedance diagram) were obtained by measuring the AC impedance for mild steel in 1 M HCl solution in the absence and presence of various concentrations of plant extracts.

3.2.1 *Zingiber mioga* (ZM)

Potentiodynamic polarization study

The corrosion current densities versus corrosion potential in 1M HCl solution for metal surface in 1M HCl with additions of various concentrations of EO extract at 30°C are shown in Fig. 3.2.1.1 and Table 3.2.1.1. The metal surface was kept to the blank test solution of 1M HCl in the presence of a different concentration of

inhibitors for one and a half hours with an appropriate arrangement of electrodes for this investigation. Polarization parameters such as current density (I_{corr}), corrosion potential (E_{corr}), the slope of the cathodic curves (β_c) and slope of the anodic curves (β_a), and corresponding percentage inhibition efficiencies ($\eta\%$) were determined by the Tafel-extrapolation method (Aribo et al., 2017), and the result was recorded in Table 3.2.1.1.

Investigating the exposure impact of EOs extract by increasing the EOs extract decreases the corrosion current densities in 1M HCl solution given in Table 3.2.1.1. The extreme decrease was observed at 5g/L concentration at temperature 30 °C, the cathodic curves shifted towards lower current densities, and corrosion potential (E_{corr}) shifted markedly towards negative value in addition of oils extract as compared to the blank solution (Petek & Kovačič, 2014). The cathodic active corrosive surfaces might be due to the adsorption of EO inhibitors extract and decrease the corrosion rate. This phenomenon indicates that the presence of inhibitors in an acid medium affects the rate of cathodic hydrogen evolution without causing any significant decrease in the value of corrosion potential and the anodic rate of dissolution of mild steel.

Table 3.2.1.1 Values of potentiodynamic polarization obtained for mild steel in the absence and presence of several *Zingiber mioga* EO extract concentrations at 30°C.

Inhibitors Concentration g/L	-E_{corr} mV vs SCE	β_a mV/decade	-β_c mV/decade	I_{corr} $\mu\text{A cm}^{-2}$	Corrosio n Rate (mmpy)	%IE
Blank	579	88.77	99.5	386.9	4.64	-
1	563	86.09	98.5	248.0	2.3	35.96
2	655	100.1	92.6	97.15	1.2	74.87
3	644	100.6	102.3	84.11	0.9	78.24
4	642	100.4	94.1	76.07	0.7	80.32
5	631	89.27	99.7	58.14	0.6	84.98

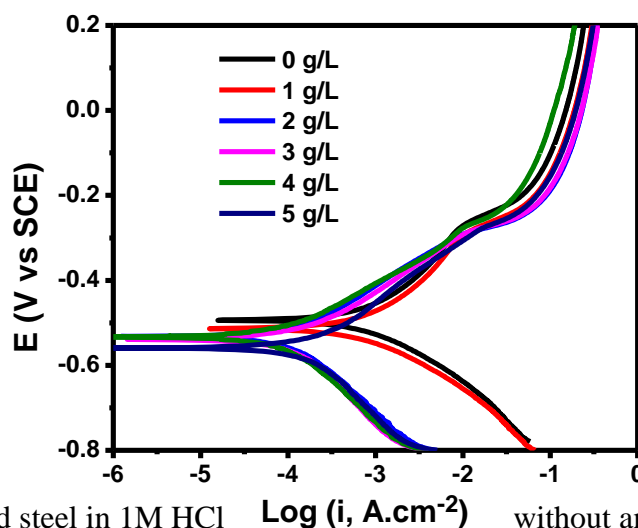


Fig 3.2.1.1 Tafel-polarisation curves for mild steel in 1M HCl without and with inhibitors of various concentrations of *Zingiber mioga* EO extract at 30°C.

However, there was no specific relation between corrosion potential and the inhibitors' concentrations, indicating that the EO inhibitors act as mixed-type inhibitors (X. Li, Deng, & Xie, 2014). These consequences are interrelated to the adsorption of the inhibitors compound on the electrode surface at the active sites, which slows down the corrosion reaction at the corrosive medium (Lebrini et al., 2010). Moreover, table 3.2.1.1 shows that increasing the inhibitor concentration moved the anodic curves towards lesser I_{corr} . The higher value of anodic slopes (β_a) is relatively more affected when compared to the lower values of cathodic slopes (β_c), indicating that the investigated functionalized EO extract predominantly acts as an anodic type (P. Singh et al., 2016).

Electrochemical impedance spectroscopy (EIS)

The impedance study was performed to determine the effect of inhibitors added to the corrosive media with a steady potential (Olasunkanmi et al., 2015). At moderate temperature, the metal surface represents Nyquist plots in Fig. 3.2.1.2 (a) containing 1M HCl solutions in the absence and presence of various concentrations of *Zingiber mioga* EO extract. The presence of an inhibitor causes changes in the shape and size of the impedance plots (Rajeswari et al., 2014). Additionally, we

tested a number of Electrical Circuit models, but only the R(QR)(QR) circuit provided the best fit. The first (QR) loop in this EC model, which can be attributed to a faradaic process, corresponds to charge transfer resistance (R_{ct}) and a frequency-dependent constant phase element instead of capacitance (Q_1). At low frequencies, the second QR loop may be the resistance of the adsorption and desorption process of the coated film (R_f) and a frequency-dependent constant phase element (Q_2). These loops are linked together in a series of connections. We can see from the impedance diagrams and impedance fitting diagram that the size of the capacitive loops expands as the concentration of *Zingiber mioga* EO extract increases. It suggested that *Zingiber mioga* EO extract reduced metal corrosion by increasing charge transfer resistance and creating a thin film or protective layer on the metal surface (Kakino et al., 2010);(Machnikova et al., 2008);(X. Li, Deng, Fu, et al., 2014); Afrokh et al., 2021) and (Jafari et al., 2022). A capacitive loop is produced due to the formation of a double layer and the storage of charge as a capacitor, which is released through a resistor. The diameter of the depressed semicircle becomes larger with increasing the inhibitor concentration, as obtained from Fig. 3.2.1.2, leading to the fall of corrosion rate using adsorption of inhibitor species like H^+ atoms on the surface of electrodes (Dinodi & Shetty, 2014);(Verma et al., 2014);(Mourya et al., 2014);(El Ouali et al., 2013);(Sabirneeza & Subhashini, 2014).

Table 3.2.1.2 Values of impedance parameters obtained from fitting EIS data with R(QR)(QR) equivalent circuit for Myoga Ginger (*Zingiber mioga* EO) extract in 1M HCl in the absence and presence of inhibitors of various concentrations at 30°C.

Sample conc.	$R_s (\Omega \text{ cm}^2)$	Q		$R_{ct} (\Omega \text{ cm}^2)$	Q_f		$R_f (\Omega \text{ cm}^2)$
		$Y_o (\times 10^{-5} \text{ S cm}^{-2})$	n		$Y_o (\times 10^{-5} \text{ S cm}^{-2})$	n	
0 g/L	1.261	49.95	0.8	66.1	43.35	0.8	6.513
1 g/L	1.293	120.9	0.6702	114.5	15.69	1	0.2247
2 g/L	1.146	33.48	0.7099	248.2	2.989	0.9656	16.29
3 g/L	1.043	28.07	0.732	271.4	381.3	0.9474	1.317

4 g/L	1.607	14.82	0.8	288.1	6.552	0.8	17.31
5 g/L	1.096	13.25	0.8668	313.94	0.7318	1	0.4349

Table 3.2.1.3 Inhibition efficiency and surface coverage obtained from R_{ct} with increasing inhibitor concentration.

Concentration of inhibitors (g/L)	R_{ct} Ωcm^2	%IE	Surface Coverage ϕ
Blank	66.1	-	-
1	114.5	42.27	0.4227
2	248.2	73.37	0.7337
3	271.4	75.64	0.7564
4	288.1	77.06	0.7706
5	313.94	78.94	0.7894

Investigation of Tables 3.2.1.2 and 3.2.1.3 reveals that the charge transfer resistance is directly proportional to the activity of inhibitor concentration and inversely proportional to the corrosion rate (Ahmad et al., 2010). The inhibition efficiency (%IE) reached the maximum percentage at the optimum inhibitor concentration.

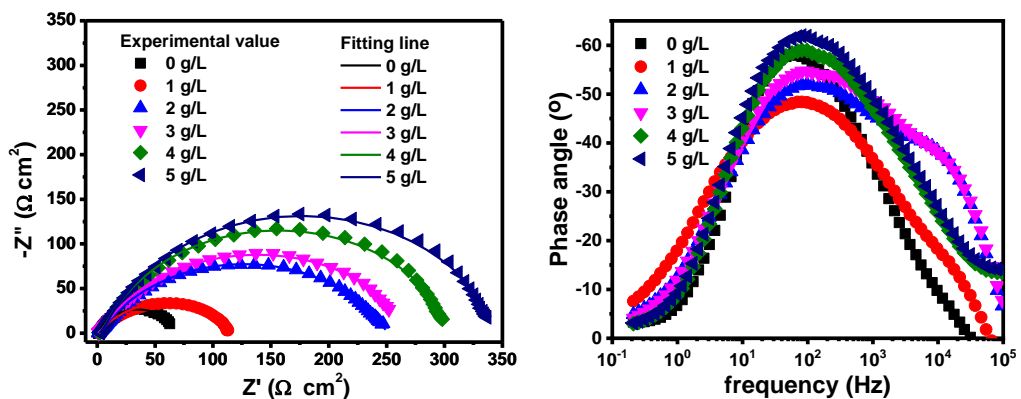


Fig. 3.2.1.2 (a) Nyquist plot for mild steel without and with different concentrations of *Zingiber mioga* EO extract in 1M HCl at 30°C and (b) bode plots for mild steel in 1M HCl with and without inhibitors of different concentrations in *Zingiber mioga* EO extract at 30°C.

Fig. 3.2.1.3 represents the Bode phase plot, the impedance modulus $|Z|$ versus frequency at various concentrations in 1M HCl in a corrosive medium. In the absence of an inhibitor, Impedance was found at $64 \Omega \text{ cm}^2$, and in the presence of extracted oils, by increasing the concentration of inhibitors, Impedance increased up to $350 \Omega \text{ cm}^2$. It specifies the development of a thin film or protecting layers on mild steel (Sabirneeza & Subhashini, 2014). The minor phase angle was seen without inhibitors in the graph between phase angle and frequency, as shown in Fig. 3.2.1.2(b). It demonstrates that, in contrast to various inhibitor concentrations, the corroded surface area increases in the corrosive media. It shows that the phase angle gradually increases and attains a low value on the corroding surface with inhibitor concentration. This result specifies that the extracted oils inhibitor particles adsorbed on a mild steel surface, which breakdown the interaction with a corrosive medium due to the improvement in interfacial impedance parameters with increasing the concentration of inhibitors (Ahamad et al., 2010).

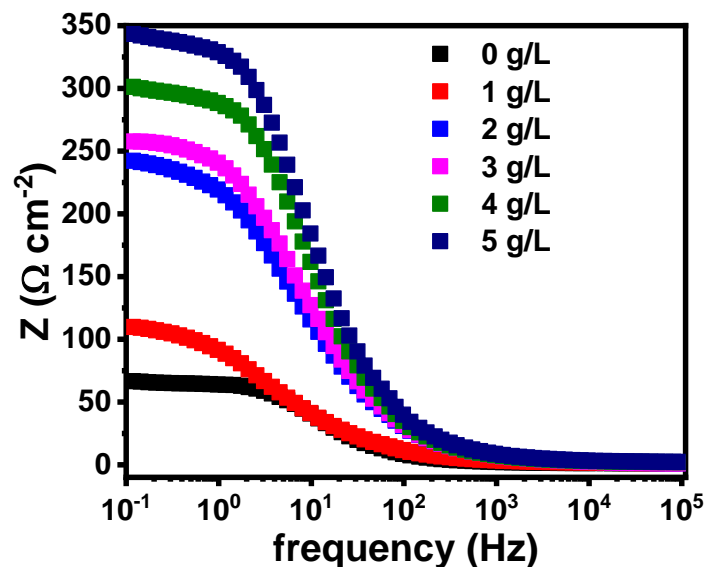


Fig.3.2.1.3 Impedance modulus vs. frequency of bode plots for mild steel in 1M HCl with and without inhibitors of different concentrations in *Zingiber mioga* EO extract at 30°C.

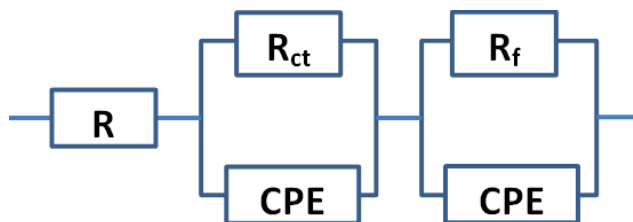


Fig. 3.2.1.4 Equivalent electrical circuit model for EIS measurement.

The corrosion Inhibition efficiency (% IE) of Myoga ginger extracted oils achieved from several experimental techniques is in Fig. 3.2.1.5. Results indicate that in all circumstances, the inhibition efficiency increases with increasing the concentration of inhibitor, and the curves from weight loss, Nyquist, Tafel has an appropriate agreement with each other (Bayol et al., 2008).

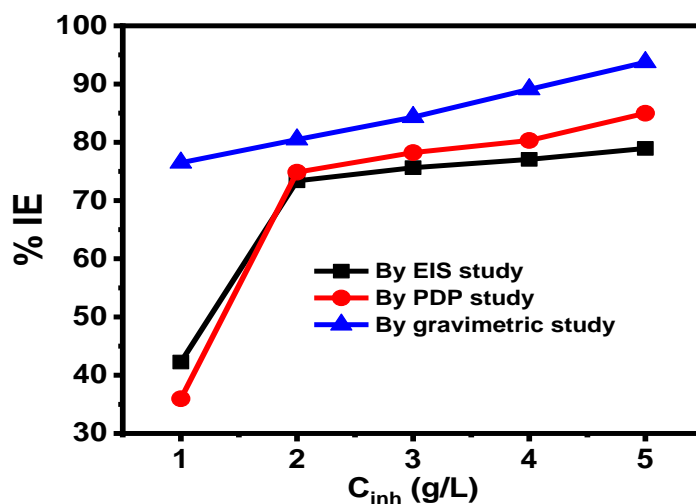


Fig. 3.2.1.5. Inhibition efficiency for mild steel in 1M HCl containing different concentrations of *Zingiber mioga* EO extracted by weight loss (Gravimetric analysis), Polarization curves, and the Nyquist plot.

3.2.2 Zingiber Officinale (ZO)

Potentiodynamic polarization study

The corrosion current densities versus corrosion-potential in 1M HCl solution for metal surface in 1M HCl with additions of various concentrations of EO extract at 30°C are shown in Fig. 3.2.2.1. The metal surface was kept to the blank test

solution of 1M HCl and presence of different concentration for one and half hour with appropriate arrangement of electrode for this investigates. Polarization parameters such as current density (I_{corr}), corrosion potential (E_{corr}), the slope of the cathodic curves (β_c) and slope of the anodic curves (β_a), and corresponding percentage inhibition efficiencies ($\eta\%$) were determined by the Tafel-extrapolation method (Kovács et al., 2014);(Hoseizadeh et al., 2014) and the result is in Table 3.2.2.1.

Table 3.2.2.1 Values of potentiodynamic polarization obtained for mild steel in the absence and presence of several concentrations of *Zingiber officinale* EO extract at 30°C.

Inhibitors Concentration g/L	-E _{corr} mV vs SCE	β_a mV/decade	$-\beta_c$ mV/decade	I_{corr} μAcm^{-2}	Corrosion Rate (mmpy)	Inhibition Efficiency %IE
Blank	479	78.77	112.5	426.7	5.18	-
1	463	76.09	128.5	148.0	1.39	65.31
2	539	85.1	92.6	97.15	0.94	77.23
3	544	94.6	102.3	84.11	0.75	80.29
4	542	100.4	94.5	76.07	0.47	82.17
5	531	100.27	98.9	64.17	0.28	84.96

I_{corr} and $I_{corrinh}$ are the current corrosion density in the absence and presence of an inhibitor, respectively. Investigation of the exposure effect of the extract by increasing the EOs extract exposure gradually decreases the corrosion current densities in 1M HCl solution in Table 3.2.2.1. The extreme decrease was observed at 5g/L concentration at a temperature of 30°C, the cathodic curves shifted towards lower current densities, and corrosion potential (E_{corr}) shifted markedly towards negative value in addition of oils extract as compared to the blank solution(Umoren et al., 2013). The cathodic active corrosive surfaces might be due to the adsorption of AOs inhibitors extract and decrease the corrosion rate. This phenomenon indicates that the presence of inhibitors in an acid medium affects the rate of cathodic hydrogen evolution without causing any significant decrease in the value of

corrosion potential and the anodic rate of dissolution of mild steel. However, there was not a specific relation between corrosion potential and the inhibitors' concentrations, indicating that the ZO inhibitors act as mixed-type inhibitors (X. Li, Deng, & Xie, 2014). These consequences are interrelated to the adsorption of the inhibitors compound on the electrode surface at the active sites, which slows down the corrosion reaction at the corrosive medium (Lebrini et al., 2010). Moreover, Table 3.2.2.1 shows that increasing the inhibitor concentration moved the anodic curves towards lesser I_{corr} . The higher value of anodic slopes (β_a) is relatively more affected when compared to the lower values of cathodic slopes (β_c), indicating that the investigated functionalized EOs extract predominantly acts as an anodic type (P. Singh et al., 2016).

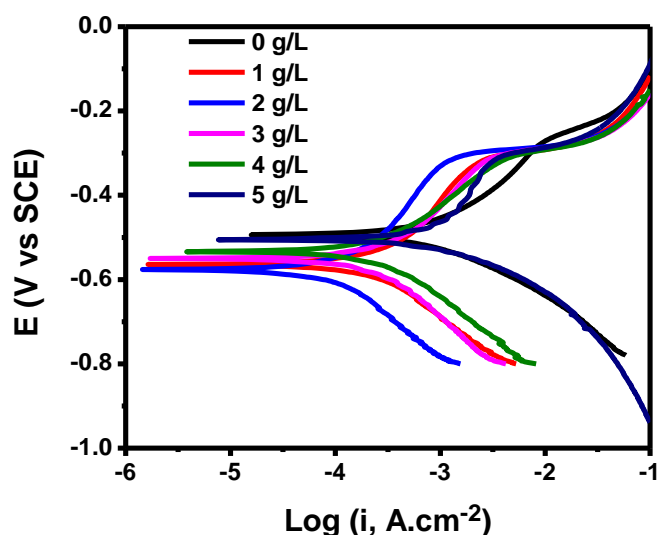


Fig 3.2.2.1 Tafel-polarisation curves for mild steel in 1M HCl without and with inhibitors of various concentrations of *Zingiber officinale* EO extract at 30°C.

Electrochemical impedance spectroscopy (EIS)

An impedance investigation was conducted to ascertain the impact of inhibitors added to the corrosive media with a stable voltage (Olasunkanmi et al., 2015). The metal surface depicts Nyquist plots of 1M HCl solutions in the absence and presence of varying amounts of *Zingiber officinale* EO extract at room temperature (see Fig. 3.2.2.2 (a)). The impedance plots' size and shape changed when an inhibitor was present (Rajeswari et al., 2014). Several electrical circuit models

were also examined, but only the R(QR)(QR) circuit offered the best fit. This EC model's first (QR) loop, which is related to a faradaic process, corresponds to charge transfer resistance (R_{ct}), not capacitance, and uses a frequency-dependent constant phase element (Q_1). The coating's adsorption and desorption process (R_f) resistance and a frequency-dependent constant phase element could make up the second QR loop at low frequencies (Q_2). In a series connection, these loops are joined. The impedance diagrams and the impedance fitting diagram show that as the concentration of *Zingiber officinale* EO extract rises, the size of the capacitive loops increases. Increasing charge transfer resistance and producing a thin film or protective coating on the metal surface, it was hypothesized, were two ways that *Zingiber officinale* EO extract allegedly decreased metal corrosion (Kakino et al., 2010); (Machnikova et al., 2008); (X. Li, Deng, Fu, et al., 2014); (Afrokh et al., 2021); (Jafari et al., 2022); (Dinodi & Shetty, 2014); (Verma et al., 2014); (El Ouali et al., 2013) and (Mourya et al., 2014a). Due to the development of a double layer and the storage of charge as a capacitor, which is then released through a resistor, a capacitive loop is produced. According to Fig. 3.2.2 (a), the width of the depressed semicircle grows as the inhibitor concentration rises, which lowers the corrosion rate by exploiting the adsorption of inhibitor species such as H^+ atoms on the surface of electrodes (Sabirneeza & Subhashini, 2014).

Table 3.2.2.2 Values of impedance parameters obtained from fitting EIS data with R(QR)(QR) equivalent circuit for *Zingiber officinale* EO extract in 1M HCl in the absence and presence of various concentrations of inhibitor at 30°C.

Sample conc.	R_s (Ω cm ²)	Q		R_{ct} (Ω cm ²)	Q_f		R_f (Ω cm ²)
		Y_o ($\times 10^{-5}$ S s ⁿ cm ⁻²)	n		Y_o ($\times 10^{-5}$ S s ⁿ cm ⁻²)	n	
0 g/L	1.261	0.0004771	0.8	64.63	55.07	0.8	7.992
1 g/L	0.8325	25.64	0.8	109.5	2.708	0.8	21.15
2 g/L	0.039	29.24	0.7983	137	54.63	0.5622	10.23
3 g/L	16.85	32.7	0.748	159.4	19.65	0.604	10.09

4 g/L	14.12	19.54	0.7185	268.3	3.933	0.7046	1000
5 g/L	2.652	12.56	0.8	340.2	0.3884	0.8	0.01

Table 3.2.2.3. Inhibition efficiency and surface coverage obtained from R_{ct} with increasing concentration of inhibitor.

Concentration of inhibitors (g/L)	R_{ct} $\Omega \text{ cm}^2$	Inhibition Efficiency %IE	Surface Coverage ϕ
Blank	64.63	-	-
1	109.5	40.97717	0.40977
2	137	52.82482	0.52825
3	159.4	59.4542	0.59454
4	268.3	75.91129	0.75911
5	340.2	81.00235	0.81002

$$IE\% = \frac{R_{ct} - R_u}{R_{ct}} \times 100$$

(11)

where, R_{ct} and R_u are the charge transfer resistance of mild steel in 1M HCl in the presence and absence of inhibitors, respectively.

Investigation of Tables 3.2.2.2 and 3.2.2.3 reveals that the charge transfer resistance is directly proportional to the activity of inhibitor concentration and inversely proportional to the corrosion rate (Ahamad et al., 2010). The inhibition efficiency (%IE) reached the maximum percentage at the optimum inhibitor concentration.

Fig. 3.2.2.3 represents the Bode phase plot, the impedance modulus $|Z|$ versus frequency at various concentrations in 1M HCl in a corrosive medium. In the absence of an inhibitor, Impedance was found at $64 \Omega \text{ cm}^2$, and in the presence of extracted oils, by increasing the concentration of inhibitors, Impedance increased up to $340 \Omega \text{ cm}^2$. It specifies the development of a thin film or protecting layers on mild

steel (Sabirneeza & Subhashini, 2014). The minor phase angle was seen without inhibitors in the graph between phase angle and frequency, as shown in Fig. 3.2.2.2(b). This demonstrates that, in contrast to various inhibitor concentrations, the corroded surface area increases in the corrosive media. It shows that the phase angle gradually increases and attains a low value on the corroding surface with inhibitor concentration. This result specifies that the extracted oils inhibitor particles adsorbed on a mild steel surface, which breakdown the interaction with a corrosive medium due to the improvement in interfacial impedance parameters with increasing the concentration of inhibitors (Ahamad et al., 2010).

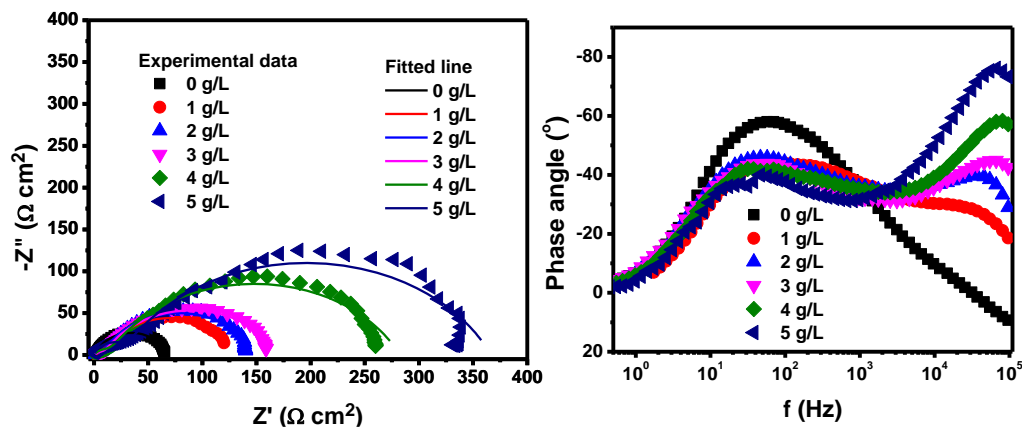


Fig. 3.2.2.2 Nyquist plot for mild steel without and with different concentrations of *Zingiber officinale* EO extract in 1M HCl at 30°C and (b) bode plots for mild steel in 1M HCl with and without inhibitors of different concentrations in *Zingiber officinale* EO extract at 30°C.

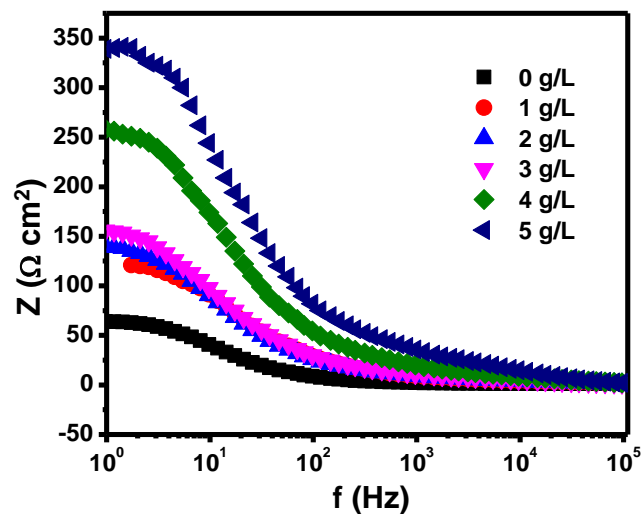


Fig. 3.2.2.3 Impedance modulus vs. frequency of bode plots for mild steel in 1M HCl with and without inhibitors of different concentrations in *Zingiber officinale* EO extract at 30°C.

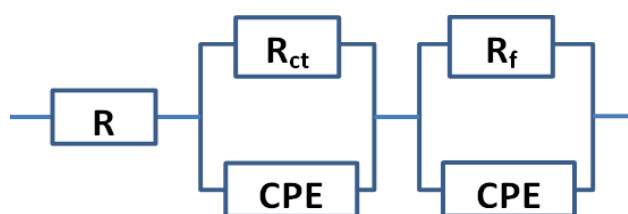


Fig. 3.2.2.4 Equivalent electrical circuit model for EIS measurement.

The corrosion Inhibition efficiency (% IE) of *Zingiber officinale* EO extract achieved from several experimental techniques can be seen in Fig 3.2.2.5, and we can say that in all circumstances, the inhibition efficiency increases with increasing the concentration of inhibitor and the curves from weight loss, Nyquist, Tafel has an appropriate arrangement with each other.

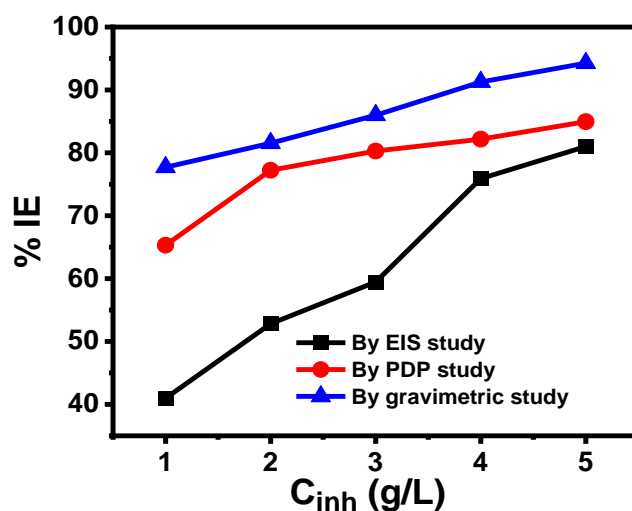


Fig 3.2.2.5 Inhibition efficiency for mild steel in 1M HCl containing different concentrations of *Zingiber officinale* EO extracted by weight loss (Gravimetric analysis), Polarization curves, and the Nyquist plot (Kumari et al., 2017).

3.2.3 Electrochemical measurements of EF *Eryngium foetidum* L

Potentiodynamic polarization study

The corrosion current densities versus corrosion-potential in 1M HCl solution for metal surface in 1M HCl with additions of various concentrations of EOs extract at 30°C are shown in Fig. 3.2.3.1. The metal surface was kept to the blank test solution of 1M HCl and presence of different concentration for one and half hour with appropriate arrangement of electrode for this investigates. Polarization parameters such as current density (I_{corr}), corrosion potential (E_{corr}), the slope of the cathodic curves (β_c) and slope of the anodic curves (β_a), and corresponding percentage inhibition efficiencies ($\eta\%$) were determined by the Tafel-

investigation of Table 3.2.3.1 suggests that increasing the EOs extract gradually decreases the corrosion current densities in 1M HCl solution.

Table 3.2.3.1 Values of potentiodynamic polarization obtained for mild steel in the absence and presence of several concentrations of *Eryngium foetidum* L. EO extract at 30°C.

Inhibitors Concentration g/L	-E_{corr} mV vs SCE	β_a mV/decade	-β_c mV/decade	I_{corr} μAcm⁻²	Corrosion Rate (mmpy)	%IE
Blank	396	68.77	117.5	418.5	5.62	-
1	424	65.04	98.5	137.3	2.44	67.19
2	412	67.12	92.6	86.14	1.27	79.42
3	407	69.65	112.3	74.12	0.92	82.29
4	319	93.47	94.1	56.07	0.73	86.60
5	327	78.27	99.7	42.16	0.55	89.92

The extreme decrease was observed at 5g/L concentration at a temperature of 30°C, the cathodic curves shifted towards lower current densities, and corrosion potential (E_{corr}) shifted markedly towards negative value in addition to oils extract as compared to blank solution. The cathodic active corrosive surfaces might be due to the adsorption of EOs inhibitors extract and decrease the corrosion rate (Yousefi et al., 2015). This phenomenon indicates that the presence of inhibitors in an acid medium affects the rate of cathodic hydrogen evolution without causing any large decrease in the value of corrosion potential and the anodic rate of dissolution of mild steel. However, there was not a specific relation between corrosion potential and concentrations of the inhibitors indicating that the inhibitors of AOs act as mixed-type inhibitors (X. Li, Deng, & Xie, 2014). These consequences are interrelated to the adsorption of the inhibitors compound on the electrode surface at the active sites, which slows down the corrosion reaction at the corrosive medium. Moreover, Table 3.2.3.1 shows that with increasing the concentration of the inhibitors, the anodic curves moved towards lesser I_{corr} . The higher value of anodic slopes (β_a) is relatively more affected when compared to the lower values of cathodic slopes (β_c), indicating

that the investigated functionalized EOs extract predominantly acts as an anodic type (P. Singh et al., 2016).

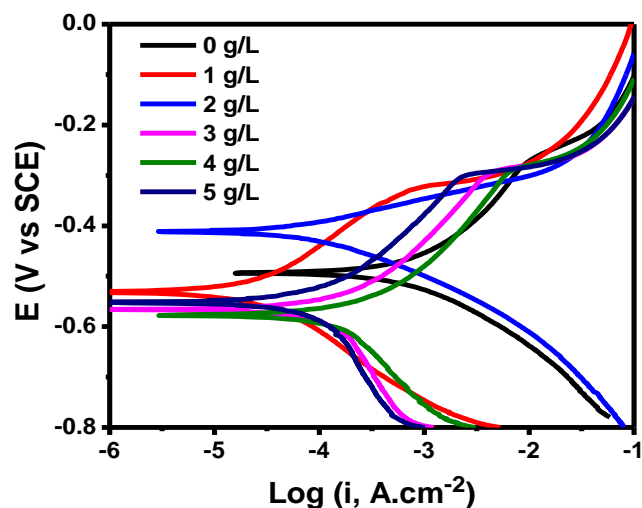


Fig. 3.2.3.1 Tafel-polarisation curves for mild steel in 1M HCl without and with inhibitors of various concentrations of *Eryngium foetidum* L. EO extract at 30°C.

Electrochemical impedance spectroscopy (EIS)

The impedance study was performed to determine the effect of inhibitors added to the corrosive media with a steady potential. At moderate temperature, the metal surface represents Nyquist plots in Fig. 3.2.3.2 (a) containing 1M HCl solutions in the absence and presence of various concentrations of *Eryngium foetidum* L. EO extract. The presence of an inhibitor caused changes in the shape and size of the impedance plots (Olasunkanmi et al., 2015);(Rajeswari et al., 2014). Additionally, we tested a number of Electrical Circuit models, but only the R(QR)(QR) circuit provided the best fit. The first (QR) loop in this EC model, which can be attributed to a faradaic process, corresponds to charge transfer resistance (R_{ct}) and a frequency-dependent constant phase element instead of capacitance (Q_1). At low frequencies, the second QR loop may be the resistance of the adsorption and desorption process of the coated film (R_f) and a frequency-dependent constant phase element (Q_2). These loops are linked together in a series of connections. We can see from the impedance diagrams and impedance fitting diagram that the size of the capacitive loops expands as the concentration of *Eryngium foetidum* L. EO extract

increases. It suggested that *Eryngium foetidum* L. EO extract reduced metal corrosion by increasing charge transfer resistance and creating a thin film or protective layer on the metal surface (Machnikova et al., 2008);(Kakino et al., 2010); (X. Li, Deng, Fu, et al., 2014); (Afrokh et al., 2021);(Jafari et al., 2022). A capacitive loop is produced due to the formation of a double layer and the storage of charge as a capacitor, which is released through a resistor. The diameter of the depressed semicircle becomes larger with increasing the inhibitor concentration, as obtained from Fig. 3.2.3.2(a), leading to the fall of corrosion rate using adsorption of inhibitor species like H⁺ atoms on the surface of electrodes (Dinodi & Shetty, 2014);(Verma et al., 2014);(Mourya et al., 2014);(El Ouali et al., 2013);(Sabirneeza & Subhashini, 2014).

Investigation of Table 3.2.3.2 reveals that the charge transfer resistance is directly proportional to the activity of inhibitor concentration and inversely proportional to the corrosion rate (Ahamad et al., 2010). The inhibition efficiency (%IE) reached the maximum percentage at the optimum inhibitor concentration.

Table 3.2.3.2. Values of impedance parameters obtained from *Eryngium foetidum* L. EO extract in 1M HCl in the absence and presence of inhibitors of various concentrations at 30°C.

Sample conc.	R _s (Ω cm ²)	Q		R _{ct} (Ω cm ²)	Q _f		R _f (Ω cm ²)
		Y _o (× 10 ⁻⁵ S s ⁿ cm ⁻²)	n		Y _o (× 10 ⁻⁵ S s ⁿ cm ⁻²)	n	
0 g/L	1.261	49.95	0.8	66.1	43.35	0.8	6.513
1 g/L	0.06606	35.43	0.7215	221.7	9.195	0.6743	17.78
2 g/L	1.302	20.45	0.8	318.1	1.876	0.7248	13.07
3 g/L	0.01	16.88	0.7037	386.9	129.5	1	17.13
4 g/L	1.42	6.892	0.8	801.1	1.754	0.8	8.038
5 g/L	1.765	5.983	0.8	1002	5.507	0.8	5.845

Table 3.2.3.3. Inhibition efficiency and surface coverage obtained from R_{ct} with increasing concentration of inhibitor.

The concentration of inhibitors (g/L)	R_{ct} Ωcm^2	Inhibition Efficiency %IE	Surface Coverage θ
Blank	66.1	-	-
1	221.7	70.18	0.70185
2	318.1	79.22	0.7922
3	386.9	82.92	0.82915
4	801.1	91.75	0.91749
5	1002	93.40	0.93403

Fig. 3.2.3.3 represents the Bode phase plot, the impedance modulus $|Z|$ versus frequency at various concentrations in 1M HCl in a corrosive medium. In the absence of an inhibitor, Impedance was found at $64 \Omega \text{ cm}^2$, and in the presence of extracted oils, by increasing the concentration of inhibitors, Impedance increased up to $1002 \Omega \text{ cm}^2$. It specifies the development of a thin film or protecting layers on mild steel (Sabirneeza & Subhashini, 2014). The minor phase angle was seen without inhibitors in the graph between phase angle and frequency, as shown in Fig. 3.2.3.2(b). This demonstrates that, in contrast to various inhibitor concentrations, the corroded surface area increases in the corrosive media. It shows that the phase angle gradually increases and attains a low value on the corroding surface with inhibitor concentration. This result specifies that the extracted oils inhibitor particles adsorbed on a mild steel surface, which breakdown the interaction with a corrosive medium due to the improvement in interfacial impedance parameters with increasing the concentration of inhibitors (Ahamad et al., 2010).

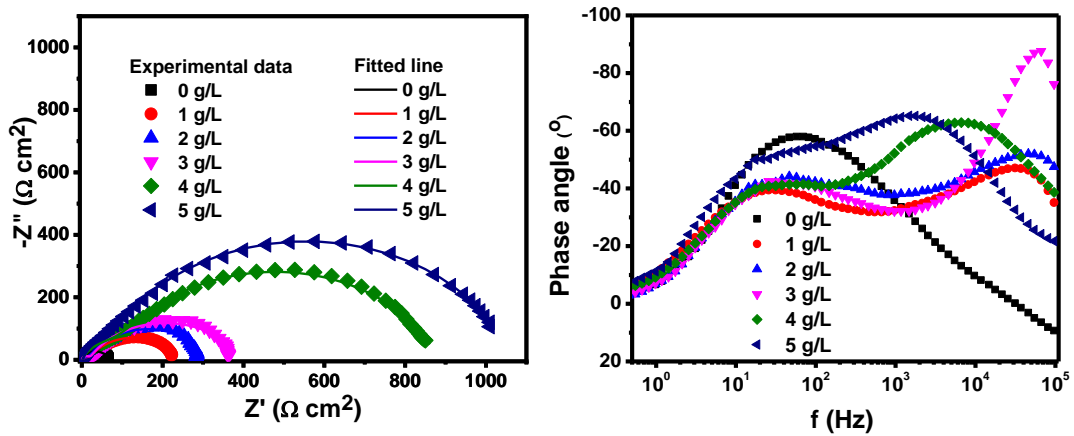


Fig. 3.2.3.2 Impedance of Nyquist plot for mild steel without and with inhibitors of various concentrations of *Eryngium foetidum* L. EO extract in 1M HCl at 30°C. (b) bode plots for mild steel in 1M HCl with and without inhibitors of different concentrations in *Eryngium foetidum* L. EO extract at 30°C.

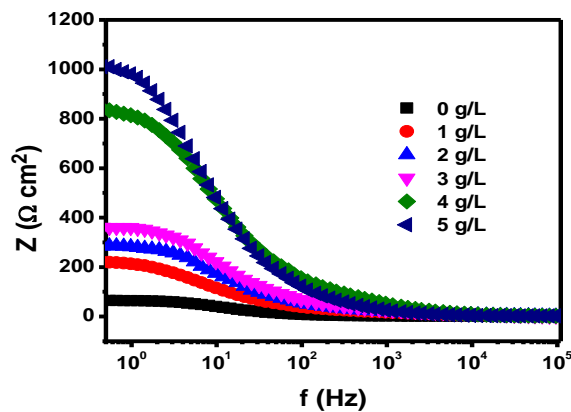


Fig.3.2.3.3. Impedance modulus vs. frequency of bode plots for mild steel in 1M HCl with and without inhibitors of different concentrations in *Eryngium foetidum* L. EO extract at 30°C.

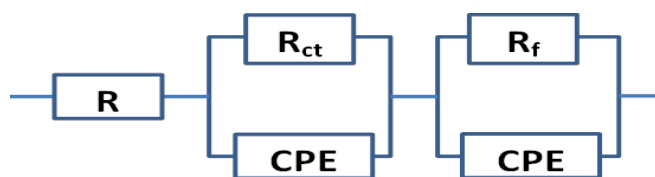


Fig. 3.2.3.4. Equivalent electrical circuit model for EIS measurement.

The corrosion Inhibition efficiency (% IE) of *Eryngium foetidum* L. EO extract achieved from several experimental techniques can be seen in Fig. 3.2.3.5, and we can say that in all circumstances, the inhibition efficiency increases with increasing the concentration of inhibitor and the curves from weight loss, Nyquist, Tafel has an appropriate arrangement with each other.

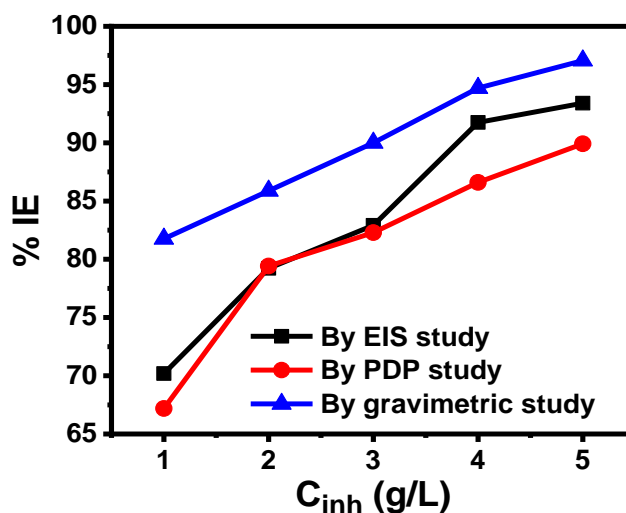


Fig. 3.2.3.5 Inhibition efficiency for mild steel in 1M HCl containing different concentrations of *Eryngium Foetidum* essential oils extracted by weight loss (Gravimetric analysis), Polarization curves, and the Nyquist plot (Zhang & Hua, 2009).

3.2.4 Electrochemical measurements of *Mentha Piperita* (MP)

Potentiodynamic polarization study

The corrosion current densities versus corrosion-potential in 1M HCl solution for metal surface in 1M HCl with additions of various concentrations of EOs extract at 30°C are shown in Fig. 3.2.4.1. The metal surface was kept to the blank test solution of 1M HCl and presence of different concentration for one and half hour with appropriate arrangement of electrode for this investigates. Polarization parameters such as current density (I_{corr}), corrosion potential (E_{corr}), the slope of the cathodic curves (β_c) and slope of the anodic curves (β_a), and corresponding

percentage inhibition efficiencies ($\eta\%$) were determined by the Tafel-extrapolation method, and the result was recorded in Table 3.2.4.1.

Investigation of Table 3.2.4.1 exposes that increasing the EOs extract gradually decreases the corrosion current densities in 1M HCl solution (J. Li et al., 2016).

Table 3.2.4.1. Values of potentiodynamic polarization were obtained for mild steel in the absence and presence of several concentrations of *M. Piperita* EO extract at 30°C.

Inhibitors Concentration g/L	-E_{corr} mV vs SCE	β_a mV/decade	$-\beta_c$ mV/decade	I_{corr} μAcm^{-2}	Corrosion Rate (mmpy)	%IE
Blank	427	78.90	120.4	406.7	6.02	-
1	453	86.05	128.5	148.4	3.34	63.51
2	525	97.1	122.6	102.9	1.25	74.66
3	549	93.6	142.3	85.17	0.84	79.06
4	553	100.4	100.1	70.07	0.72	82.73
5	571	79.27	105.7	46.14	0.59	88.65

The extreme decrease was observed at 5 g/L concentration at a temperature of 30°C, the cathodic curves shifted towards lower current densities, and corrosion potential (E_{corr}) shifted markedly towards negative value in addition to oils extract as compared to the blank solution. The cathodic active corrosive surfaces might be due to the adsorption of EOs inhibitors extract and decrease the corrosion rate (Gupta et al., 2017). This phenomenon indicates that the presence of inhibitors in an acid medium affects the rate of cathodic hydrogen evolution without causing any large decrease in the value of corrosion potential and the anodic rate of dissolution of mild steel. However, there was not a specific relation between corrosion potential and concentrations of the inhibitors indicating that the inhibitors of EOs act as mixed-type inhibitors (X. Li, Deng, & Xie, 2014). These consequences are interrelated to the adsorption of the inhibitors compound on the electrode surface at the active sites,

which slows down the corrosion reaction at the corrosive medium (Lebrini et al., 2010). Moreover, table 3.2.4.1 shows that with increasing the concentration of the inhibitors, the anodic curves moved towards lesser I_{corr} . The higher value of anodic slopes (β_a) is relatively more affected when compared to the lower values of cathodic slopes (β_c), indicating that the investigated functionalized EOs extract predominantly acts as an anodic type (P. Singh et al., 2016).

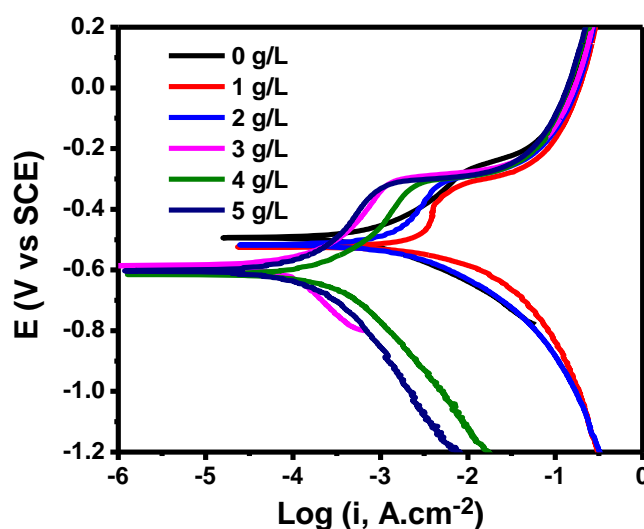


Fig 3.2.4.1 Tafel-polarisation curves for mild steel in 1M HCl without and with inhibitors of various concentrations of *M. Piperita* EO extract 30°C.

Electrochemical impedance spectroscopy (EIS)

The impedance investigation was carried out to ascertain the impact of inhibitors applied to the steady-potential corrosive media. Nyquist plots of 1M HCl solutions without and with various concentrations of *M. Piperita* EO extract on the metal surface at room temperature are shown in Fig. 3.2.4.2 (a). The size and contour of impedance graphs shifted when an inhibitor was present (Olasunkanmi et al., 2015); (Rajeswari et al., 2014). Furthermore, we tried a variety of Electrical Circuit models; however, the best fit was found with the R(QR)(QR) circuit. The first (QR) loop is associated with a faradaic process in this EC model. It represents charge transfer resistance (R_{ct}) and a frequency-dependent constant phase element in place of capacitance (Q_1). The second QR loop at low frequencies could be the frequency-dependent constant phase element and the resistance of the coated film's adsorption

and desorption process, R_f (Q_2). A series of connections are made between these loops. The impedance diagrams and impedance fitting diagram show that the capacitive loops grow in size as the concentration of *M. Piperita* EO extract increases. According to these findings, a thin film or protective layer was formed on the metal's surface after *M. Piperita* EO extract was applied (Kakino et al., 2010);(Machnikova et al., 2008);(X. Li, Deng, Fu, et al., 2014); (Afrokh et al., 2021) and (Jafari et al., 2022). A capacitive loop is generated when a double layer forms, storing charge as a capacitor before discharging it through a resistor. As seen in Fig. 3.2.4.2 (a), the corrosion rate can be reduced by adsorbing inhibitor species such as H^+ atoms onto the surface of electrodes. As the concentration of inhibitors is increased, the diameter of the depressed semicircle grows (Dinodi & Shetty, 2014);(Verma et al., 2014);(Mourya et al., 2014).

Investigation of Tables 3.2.4.3 and 3.2.4.4 reveals that the charge transfer resistance is directly proportional to the activity of inhibitor concentration and inversely proportional to the corrosion rate (Ahamad et al., 2010). The inhibition efficiency (%IE) reached the maximum percentage at the optimum inhibitor concentration.

Table 3.2.4.2. Values of impedance parameters obtained from *M. Piperita* EO extract in 1M HCl in the absence and presence of inhibitors of various concentrations at 30°C.

Sample conc	R_s (Ω cm^2)	Q		R_{ct} (Ω cm^2)	Q_f		R_f (Ω cm^2)
		Y_o ($\times 10^{-5} S s^n cm^{-2}$)	n		Y_o ($\times 10^{-5} S s^n cm^{-2}$)	n	
0 g/L	1.261	49.95	0.8	66.1	43.35	0.8	6.513
1 g/L	0.01	45.88	0.844	68.19	2032	0.2383	65.48
2 g/L	0.01097	759.4	0.8	101.5	29.83	0.8	1.216
3 g/L	0.1892	17.48	0.7596	286.9	1.233	0.6409	19.9
4 g/L	0.7008	20.15	0.8	328.1	1.886	0.8	21
5 g/L	0.71	20.81	0.8	334	1.806	0.8	20.56

Table 3.2.4.3. Inhibition efficiency and surface coverage obtained from R_{ct} with increasing concentration of inhibitor.

Concentration of inhibitors (g/L)	R_{ct} $\Omega \text{ cm}^2$	%IE	θ
Blank	66.1	-	-
1	68.19	3.06	0.03065
2	101.5	34.88	0.34877
3	286.9	76.96	0.76961
4	328.1	79.85	0.79854
5	334	80.20958	0.8021

Fig. 3.2.4.3 represents the Bode phase plot, the impedance modulus versus frequency at various concentrations in 1M HCl in a corrosive medium. In the absence of an inhibitor, Impedance was found at $64 \Omega \text{ cm}^2$, and in the presence of extracted oils, by increasing the concentration of inhibitors, Impedance increased up to $334 \Omega \text{ cm}^2$. It specifies the development of a thin film or protecting layers on mild steel (Sabirneeza & Subhashini, 2014). The minor phase angle was seen without inhibitors in the graph between phase angle and frequency, as shown in Fig. 3.2.4.2(b). This demonstrates that, in contrast to various inhibitor concentrations, the corroded surface area increases in the corrosive media. It shows that the phase angle gradually increases and attains a low value on the corroding surface with inhibitor concentration. This result specifies that the extracted oils inhibitor particles adsorbed on a mild steel surface, which breakdown the interaction with a corrosive medium due to the improvement in interfacial impedance parameters with increasing the concentration of inhibitors (Ahamad et al., 2010).

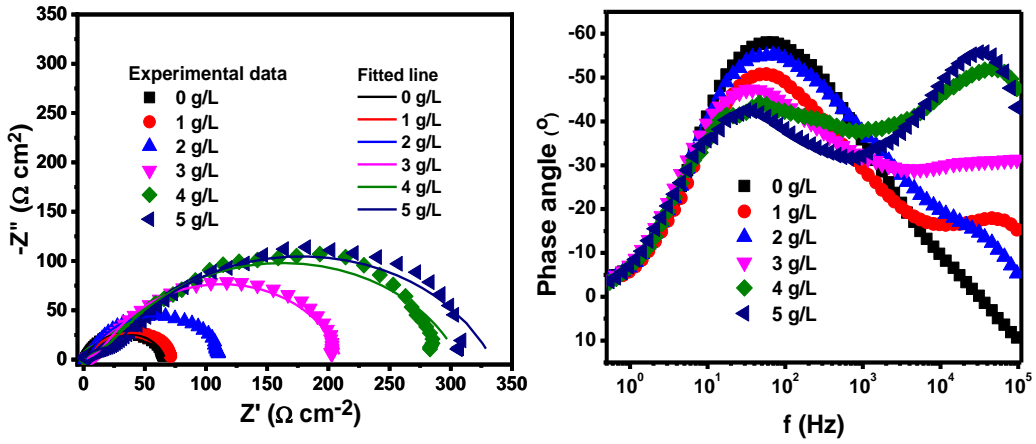


Fig. 3.2.4.2 (a) Nyquist plot for mild steel without and with inhibitors of various concentrations of *M. Piperita* EO extract in 1M HCl at 30°C. (b) bode plots for mild steel in 1M HCl with and without inhibitors of different concentrations in *M. Piperita* EO extract at 30°C.

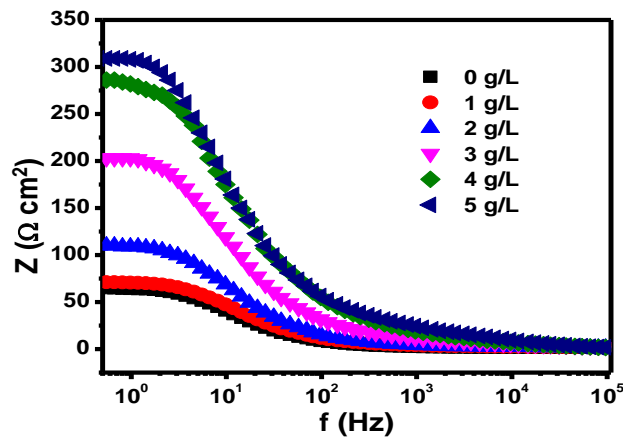


Fig. 3.2.4.3 Impedance modulus vs. frequency of bode plots for mild steel in 1M HCl with and without inhibitors of different concentrations in *M. Piperita* EO extract at 30°C.

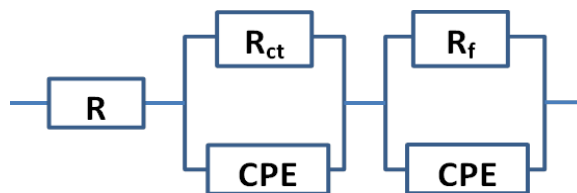


Fig. 3.2.4.4 Equivalent electrical circuit model for EIS measurement.

The corrosion Inhibition efficiency (% IE) of *M. Piperita* EO extract achieved from several experimental techniques can be seen in Fig. 3.4.5, and we can say that in all circumstances, the inhibition efficiency increases with increasing the concentration of inhibitor and the curves from weight loss, Nyquist, Tafel has an appropriate arrangement with each other.

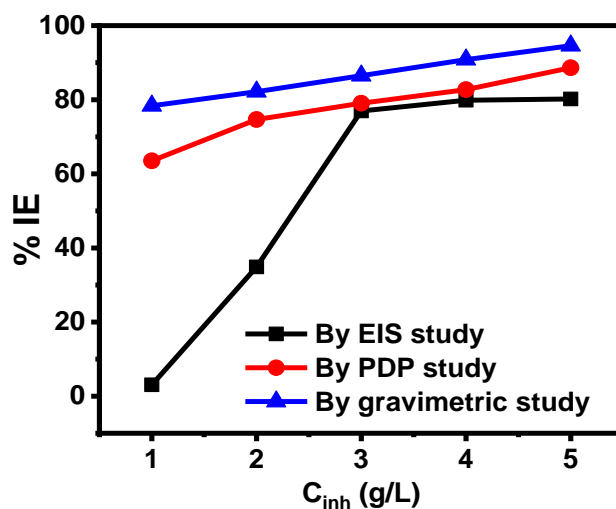


Fig 3.2.4.5 Inhibition efficiency for mild steel in 1M HCl containing different concentrations of *M. Piperita* EO extract by weight loss (Gravimetric analysis), Polarization curves, and the Nyquist plot.

Electrochemical measurements of *Allium Sativum* (AS)

Potentiodynamic polarization study.

Table 3.2.5.1. Values of potentiodynamic polarization were obtained for mild steel in the absence and presence of several concentrations of *Allium sativum* EO extract at 30°C.

Inhibitors Concentration g/L	-E _{corr} mV vs SCE	β_a mV/decade	- β_c mV/decade	I _{corr} μAcm^{-2}	Corrosion Rate (mmpy)	%IE
Blank	377	65.727	119.5	486.9	5.64	-
1	393	61.09	115.6	175.0	2.37	64.06
2	4245	61.23	102.7	107.16	1.28	77.99

3	448	67.51	108.3	98.11	0.92	79.85
4	659	71.4	104.1	82.07	0.54	83.14
5	470	89.27	95.7	53.14	0.26	89.09

The corrosion current densities versus corrosion-potential in 1M HCl solution for metal surface in 1M HCl with additions of various concentrations of EOs extract at 30°C are shown in Fig. 3.2.5.1 The metal surface was kept to the blank test solution of 1M HCl and presence of different concentration for one and half hour with appropriate arrangement of electrode for this investigates. Polarization parameters such as current density (I_{corr}), corrosion potential (E_{corr}), the slope of the cathodic curves (β_c), the slope of the anodic curves (β_a), and corresponding percentage inhibition efficiencies ($\eta\%$) were determined by the Tafel-extrapolation method.

The investigation of Table 3.2.5.1 suggests that increasing the EOs extract gradually decreases the corrosion current densities in 1M HCl solution. The extreme decrease was observed at 5g/L concentration at a temperature of 30°C, the cathodic curves shifted towards lower current densities, and corrosion potential (E_{corr}) shifted markedly towards negative value in addition to oils extract as compared to the blank solution. The cathodic active corrosive surfaces might be due to the adsorption of EOs inhibitors extract and decrease the corrosion rate. This phenomenon indicates that the presence of inhibitors in an acid medium affects the rate of cathodic hydrogen evolution without causing any large decrease in the value of corrosion potential and the anodic rate of dissolution of mild steel. However, there was not a specific relation between corrosion potential and concentrations of the inhibitors indicating that the inhibitors of EOs act as mixed-type inhibitors (X. Li, Deng, & Xie, 2014). These consequences are interrelated to the adsorption of the inhibitors compound on the electrode surface at the active sites, which slows down the corrosion reaction at the corrosive medium (Lebrini et al., 2010). Moreover, Table 3.2.5.1 shows that with increasing the concentration of the inhibitors, the anodic curves moved towards lesser I_{corr} . The higher value of anodic slopes (β_a) is relatively more affected when compared to the lower values of cathodic slopes (β_c), indicating

that the investigated functionalized EOs extract predominantly acts as an anodic type (P. Singh et al., 2016).

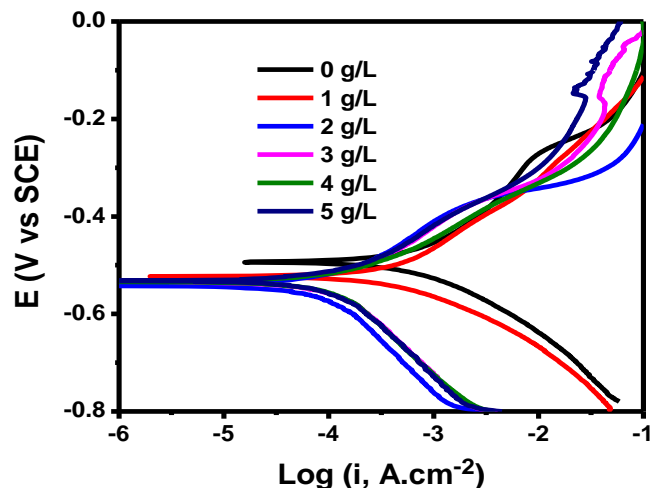


Fig 3.2.5.1 Tafel-polarisation curves for mild steel in 1M HCl without and with inhibitors of various concentrations of *Allium sativum* EO extract at 30°C.

Electrochemical impedance spectroscopy (EIS)

With a steady potential, the impedance study was done to see what would happen if inhibitors were added to the corrosive medium. At a moderate temperature, the surface of the metal looks like the Nyquist plots in Fig. 3.2.5.2 (a), which show 1M HCl solutions with and without different amounts of *Allium sativum* EO extract. The shape and size of the impedance plots changed when an inhibitor was present (Olasunkanmi et al., 2015). Also, we tried out several Electrical Circuit models, but the best fit was with the R (QR)(QR) circuit. The first (QR) loop in this EC model, which can be attributed to a faradaic process, is made up of charge transfer resistance (R_{ct}) and a frequency-dependent constant phase element instead of capacitance (Q_1). At low frequencies, the second QR loop could be the resistance of the adsorption and desorption process of the coated film (R_f) and a frequency-dependent constant phase element (Q_2). A series of connections links these loops together. From the impedance diagrams and the impedance fitting diagram, we can see that as the amount of *Allium sativum* EO extract increases, the capacitive loops get bigger. It showed that *Allium sativum* EO extract stopped metal from rusting by lowering charge transfer resistance and putting a thin film or protective layer on the surface of the metal (Rajeswari et

al., 2014). (Kakino et al., 2010), (Machnikova et al., 2008). (X. Li, Deng, Fu, et al., 2014); (Afrokh et al., 2021);(Jafari et al., 2022). A capacitive loop is made when a double layer forms and charge is stored in a capacitor. The charge is then released through a resistor. As shown in Fig. 3.2.5.2(a), as the inhibitor concentration goes up, the diameter of the depressed semicircle gets bigger. It means that the corrosion rate goes down when inhibitor species like H^+ atoms stick to the surface of electrodes (Dinodi & Shetty, 2014);(Verma et al., 2014) ;(Mourya et al., 2014).

Table 3.2.5.2. Values of impedance parameters obtained from *Allium sativum* EO extract in 1M HCl in the absence and presence of inhibitors of various concentrations at 30°C by fitting with R(QR)(QR) equivalent circuit.

Sample conc.	R_s (Ω cm^2)	Q		R_{ct} (Ω cm^2)	Q_f		R_f (Ω cm^2)
		Y_o ($\times 10^{-5}$ S s^n cm^{-2})	n		Y_o ($\times 10^{-5}$ S s^n cm^{-2})	n	
0 g/L	1.261	47.71	0.8	64.63	55.07	0.8	7.992
1 g/L	1.251	28.13	0.8	135.9	94.20	0.8	7.866
2 g/L	0.01	23.23	0.7622	197.5	6715	0.4116	6.276
3 g/L	1.392	152.5	0.4864	213	0.9414	0.9561	3.633
4 g/L	1.079	21.64	0.7727	232.1	666.3	0.8512	2.248
5 g/L	1.04	26.4	0.7429	261.1	6.243	0.8956	0.162

Table 3.2.5.3. Inhibition efficiency and surface coverage obtained from R_{ct} with increasing concentration of inhibitor.

The concentration of inhibitors (g/L)	R_{ct} Ωcm^2	%IE	θ
Blank	64.63	0	-
1	135.9	52.44297	0.52443
2	197.5	67.27595	0.67276
3	213	69.65728	0.69657

4	232.1	72.15424	0.72154
5	261.1	75.24703	0.75247

Tables 3.2.5.2 and 3.2.5.3 show that the charge transfer resistance is directly related to the activity of the inhibitor concentration and inversely related to the corrosion rate (Ahmad et al., 2010). The inhibition efficiency (%IE) was at its highest at the best inhibitor concentration.

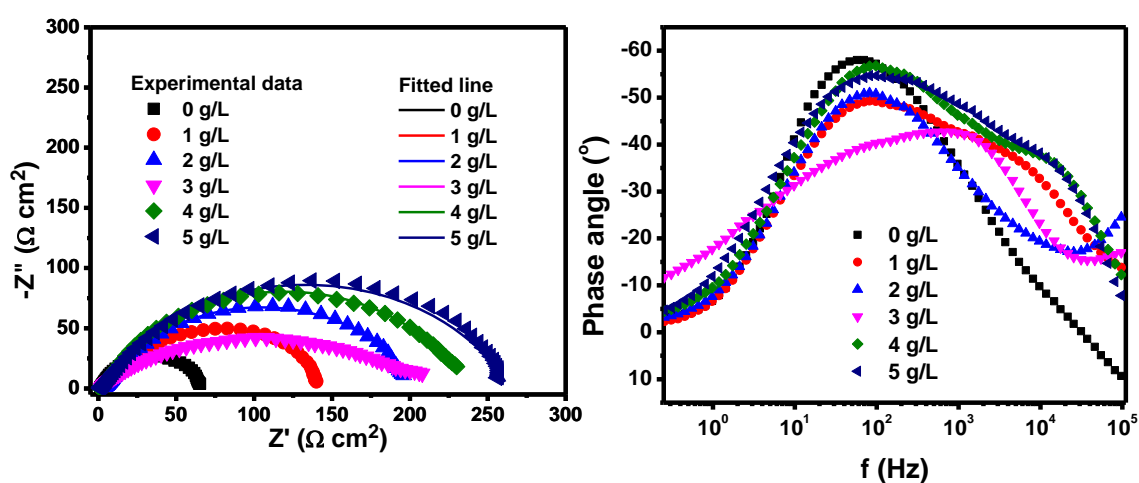


Fig. 3.2.5.2 (a) Nyquist plot for mild steel without and with inhibitors of various concentrations of *Allium sativum* EO extract in 1M HCl at 30°C. (b) Bode plots for mild steel in 1M HCl with and without inhibitors of different concentrations in *Allium sativum* EO extract at 30°C.

Figure 3.2.5.3 shows the Bode phase plot, which shows the impedance modulus versus frequency for different concentrations of 1M HCl in a corrosive medium. Without an inhibitor, the Impedance was found to be 64 $\Omega \text{ cm}^2$. When extracted oils were added, and the concentration of inhibitors was increased, the Impedance went up to 261 $\Omega \text{ cm}^2$. It says how a thin film or layer of protection should form on mild steel Sabirneeza & Subhashini, 2014). Without inhibitors, the graph between phase angle and frequency (shown in Fig. 3.5.2(b)) showed the minor phase angle. It shows that, unlike with different concentrations of inhibitors, the corroded surface area grows in corrosive media. It shows that as the inhibitor concentration increases, the phase angle slowly increases until it reaches a low value

at the corroding surface. This result indicates that the extracted oils' inhibitor particles stuck to the surface of mild steel, breaking down the interaction with the corrosive medium by improving the interfacial impedance parameters (Ahamad et al., 2010).

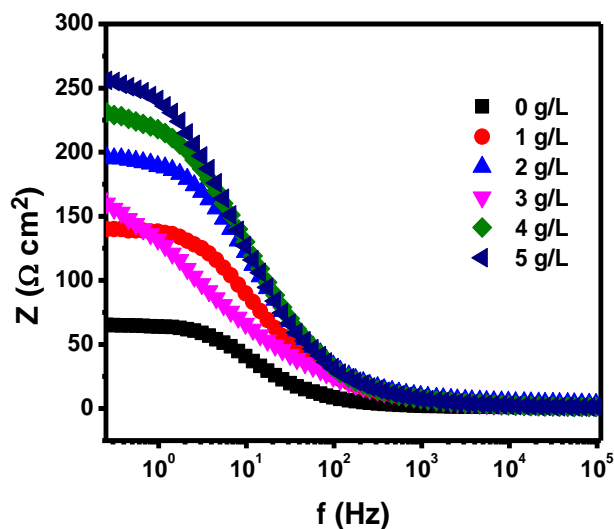


Fig. 3.2.5.3 Impedance modulus vs. frequency of bode plots for mild steel in 1M HCl with and without inhibitors of different concentrations in *Allium sativum* EO extract at 30°C.

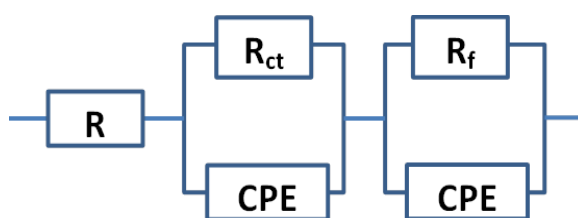


Fig. 3.2.5.4 Equivalent electrical circuit model for EIS measurement.

The corrosion Inhibition efficiency (% IE) of *Allium sativum* EO extract achieved from several experimental techniques can be seen in Fig. 3.5.5, and we can say that in all circumstances, the inhibition efficiency increases with increasing the concentration of inhibitor and the curves from weight loss, Nyquist, Tafel has an appropriate arrangement with each other.

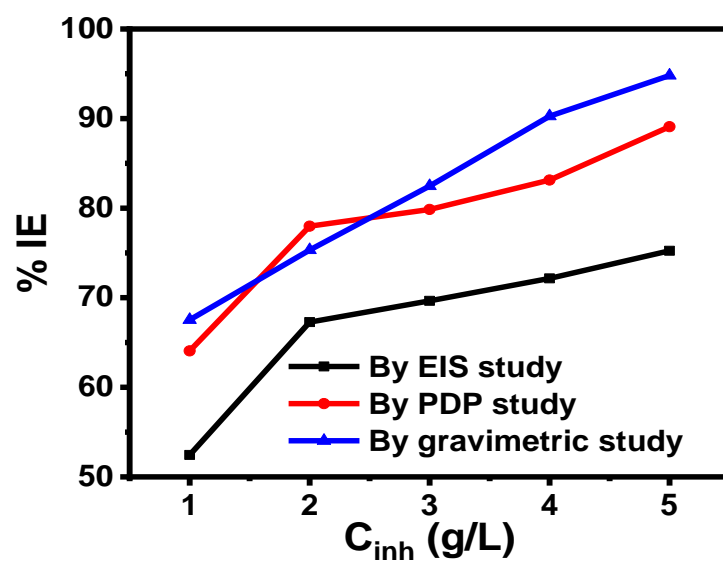


Fig 3.2.5.5 Inhibition efficiency for mild steel in 1M HCl containing different concentrations of *Allium sativum* EO extracted by weight loss (Gravimetric analysis), Polarization curves, and the Nyquist plot.

4. STUDY ON SURFACE MORPHOLOGY OF CORROSION INHIBITION

The nature of the reaction of the EOs extract adsorbed on the surface of the mild steel with the metal surface can be analyzed by understanding the adsorption isothermal process of the extract on the metal surface. This study provides the adsorption mechanism of the behavior of EOs extract adsorbed on the metal surface (Lukovits, 2001; Sastri & Perumareddi, 1997).

Adsorption isotherm and Thermodynamics parameters

A correlation between θ and C_{inh} under Langmuir adsorption isotherm can be given as:

$$C_{inh}/\theta = 1/K_{ads} + C_{inh} \quad (1)$$

$$\text{Where } \theta = IE/100 \quad (2)$$

C_{inh} is inhibitor concentration, K_{ads} is adsorption equilibrium constant, and θ is the degree of surface coverage, respectively.

For the determination of the type of adsorption of Gibb's free energy by the relation of the following equation,

$$\Delta G^{\circ}_{ads} = - RT \ln C_{solvent} \times K_{ads} \quad (3)$$

Where ΔG°_{ads} are the standard Gibb's free energy, K_{ads} is the adsorption equilibrium constant, and $C_{solvent}$ is the concentration of the initial solution. R is the universal gas constant, and T is the absolute temperature.

The activation energy (E_a) for adsorption of inhibitor on mild steel surface is calculated by the well-known Arrhenius equation as follows,

$$\log C_R = \ln A - \frac{E_a}{RT} \quad (4)$$

A graph between $\ln C_R$ vs. $1/T$ provides slope = E_a/R

E_a , R , and A are activation energy, universal gas constant, and Arrhenius pre-exponential factor, respectively.

The standard entropy of adsorption (ΔS°) and standard enthalpy of adsorption (ΔH°) for corrosion inhibition reaction is determined through the following calculation:

$$\ln C_R/T = \{\ln (R/Nh) + \Delta S^\circ/R\} - \Delta H^\circ/RT$$

(5)

A graph between $\ln C_R/T$ vs $1/T$ provide slope = $-\Delta H^\circ/R$ and intercept = $\{\ln (R/Nh) + \Delta S^\circ/R\}$

Here, N , ΔH° , and ΔS° are Avogadro's numbers, enthalpy changes, and entropy of the activation corrosion energies for the transition state complex compound. R is the perfect gas constant, and h is the Plank's constant.

4.1 Effect of Temperature on inhibition efficiency, Adsorption Isotherm, and Thermodynamic Parameters of *Zingiber mioga* (ZM) EO extract

The temperature effect on the inhibition efficiency at different temperatures in the absence and presence of oil extracts is shown in Table 4.1.1. It is observed that the rate of surface corrosion of the metal in 1M HCl solution increases steadily with an increase in temperature. It indicates that *Zingiber mioga* (ZM) adsorption on MS is physical in nature. Similar results were reported for *Punica granatum* peel extract in corrosion behavior (Behpour et al., 2012). In recent times, among the various natural products, such as the extract of *Retama retam* extracts (Ouahrani et al., 2014), *Mangifera indica* and *Citrus sinensis* fruit peel extracts (Da Rocha et al., 2010), *Chlorophytum borivilianum* root extract are, *Anacyclus pyrethrum* extracts (Benali et al., 2014) and *Chlorophytum borivilianum* root extract (Ji et al., 2013) are found to be effective corrosion inhibitors for steel in various corrosive solutions. Therefore, the surface area of mild steel exposed to a corrosive medium becomes more significant, and the inhibition efficiency decreases.

Table 4.1.1 Values of Corrosion rate and Inhibition efficiency without and with inhibitors (concentration = 5g/L) at various temperatures in the *Zingiber mioga* EO extracts.

Temperature (K)	Uninhibited (C_{Ro})	Inhibited (C_{Rinh})	Inhibition efficiency (%IE)
303	0.174	0.011	93.67
313	0.293	0.034	88.39
323	0.313	0.058	81.47
333	0.402	0.089	77.86

Thermodynamics and kinetic studies on the adsorption process

Thermodynamic parameters are computed to determine the type of adsorption on the surface of mild steel. The behavior of the adsorption process of inhibitor over the surface of mild steel can provide basic information regarding inhibitor-metal surface interaction and the influence of the nature of the inhibitor/metal and the condition of the environment on the adsorption process. At various concentrations of the Corrosion inhibitors (C_{inh}), the degree of surface coverage (θ) of ZM oils extracts is investigated by the weight loss method. At the same time, adsorption-isotherm has also been determined to prove that EO's adsorption occurs on the metal's surface (Li et al., 2014).

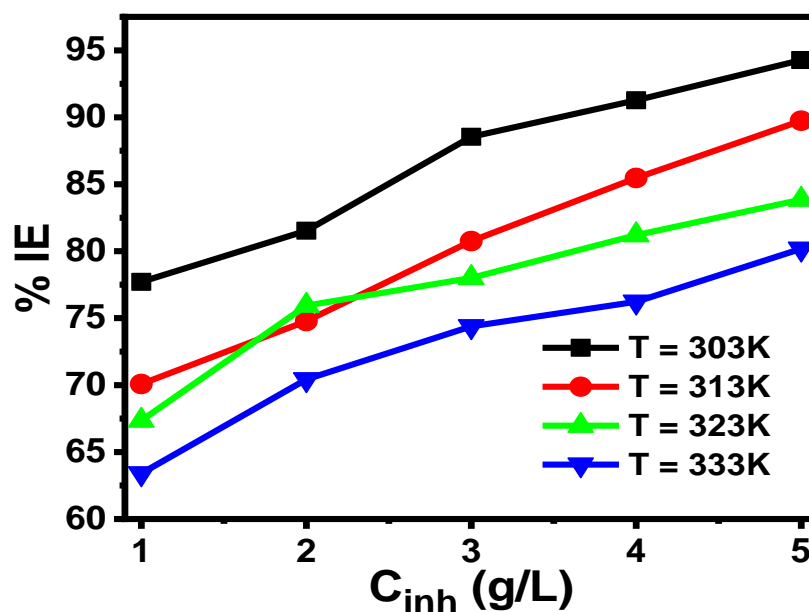


Fig. 4.1.1 Inhibitor efficiency with various concentrations of ZM extracted oils at different temperatures.

Table 4.1.2 Thermodynamic parameters for mild steel in 1M HCl acidic medium in various concentrations of *Zingiber mioga* EO extract at a temperature range (303K - 333K)

Inhibitors concentration(g/L)	E_a (kJ/mol)	ΔH° (kJ/mol)	$-\Delta S^\circ$ (J/molK)
Blank	21.77	19.12	195.73
1	29.54	26.90	182.54
2	32.72	30.07	173.51
3	37.04	34.40	160.96
4	44.62	41.98	138.65
5	57.45	54.80	100.26

Table 4.1.3 Thermodynamics parameters of *Zingiber mioga* EO for mild steel in the acidic medium at different temperatures.

Temperature(K)	$1/K_{ads}$	K_{ads}	ΔG°_{ads} (kJ/mol)
303	0.4178	2.39346	-12.32
313	0.4970	2.01212	-12.27
323	0.5673	1.76272	-12.30
333	0.2305	4.33846	-15.18

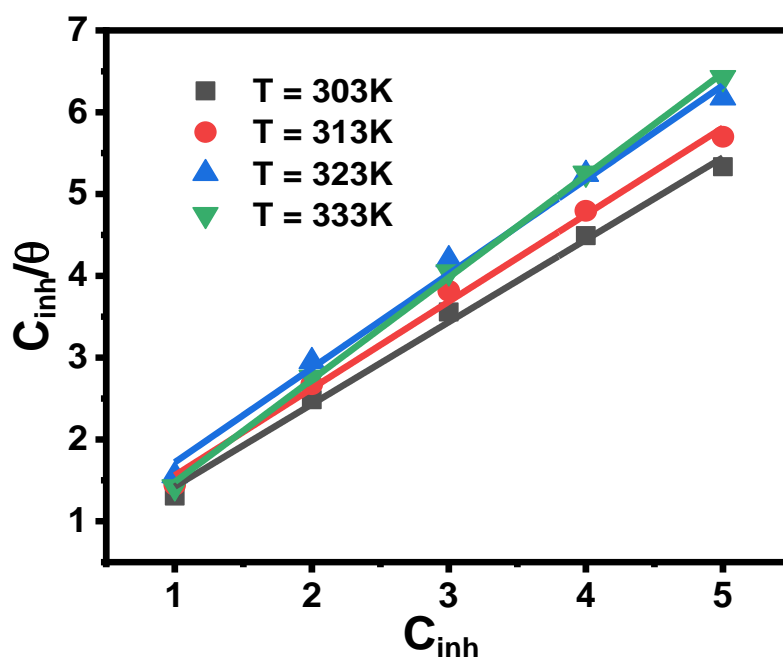


Fig. 4.1.2 Langmuir adsorption isotherm for inhibitor extracted from *Zingiber mioga* EO at various temperatures.

A graph between C_{inh}/θ and C_{inh} provides an intercept ($1/K_{ads}$). The surface coverage at various concentrations of corrosion inhibitor and various temperatures was determined to study the adsorption isotherm. Fig. 4.1.2 shows C_{inh}/θ is at an entire temperature high R^2 correlation coefficient and the graph plot gives a straight line revealing that inhibitors obey the Langmuir-adsorption isotherm. Hence, we can

conclude that the absorption of inhibitor molecules on the metal surface is a single-layer, not interaction with neighboring molecules (Akinbulumo et al., 2020). The adsorption equilibrium constant (K_{ads}) values are taken from isotherm lines of the plotted curves from y-intercepts.

In Table 4.1.3, The corresponding value of Gibb's free energy (ΔG°_{ads}) is found from $-12.32 \text{ kJmol}^{-1}$ to $-15.18 \text{ kJmol}^{-1}$, which reveals that the adsorption of ZM oils extract on mild steel surface is feasible. The presence of electrostatic interactions between charge ions of the mild steel surface and the inhibitors can be determined (Kosari et al., 2014). Moreover, the negative sign of Gibb's free adsorption energy indicates that the adsorption is spontaneous. The small value of K_{ads} indicates the inhibitor molecule and the charge ions held together by weak interaction on the metal surface. It is assumed that the inhibition process is exposed by physical adsorption. The value of the adsorption equilibrium constant is studied with gradually increasing temperature. Hence, the interaction of the inhibitor molecules with a mild steel surface is favorable at low temperatures. Due to the increased desorption process on the metal surface at higher temperatures (Kumar & Mohana, 2014) and solubility of the protective film formed rapidly on the metal surface (Kavitha et al., 2014).

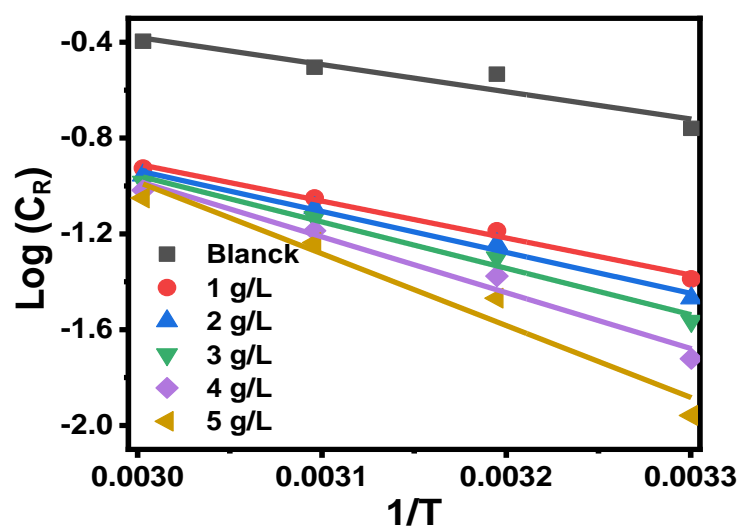


Fig.4.1.3 Arrhenius plots for corrosion rates ($\log C_R$ versus $1/T$) on the mild steel in 1M HCl solution without and with inhibitors of *Zingiber mioga* EO extract at different concentrations at 30°C.

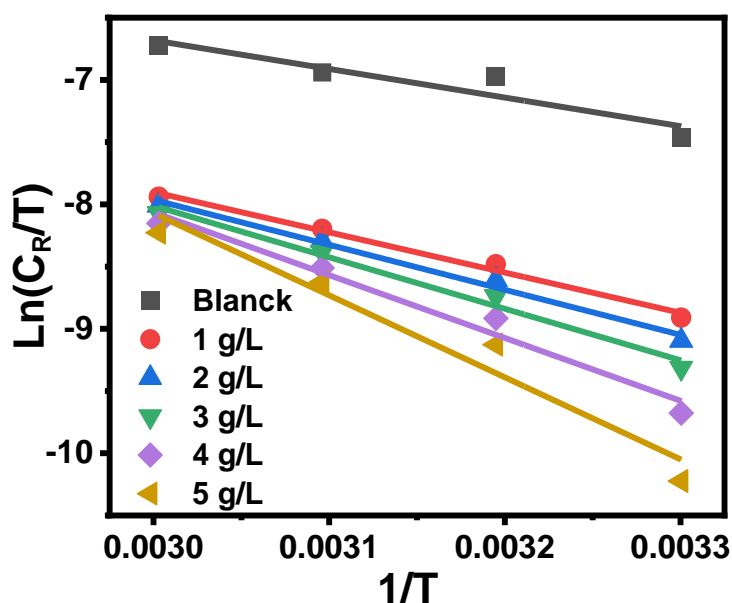


Fig.4.1.4 Transition state plots for corrosion rates ($\ln (C_R/T)$ versus $1/T$) on the mild steel in 1M HCl solution without and with inhibitors *Zingiber mioga* EO extract at different concentrations at 30°C.

From Fig.4.1.3, Plotting the graph between $\log C_R$ against $1/T$ in the absence and presence of inhibitors straight lines were found as shown in Table 4.1.2. Greater activation energy (E_a) values in the presence of essential oil extract from *Zingiber mioga* are found to generate an active inhibition by physisorption between the surface of the metal and the corrosive acidic medium (Florez-Frias et al., 2021). The standard entropy of adsorption (ΔS°) and standard enthalpy of adsorption (ΔH°) for corrosion inhibition reaction is determined through the following calculation.

As seen in fig. 4.1.3 The E_a (activation energy) was analyzed from the slopes of $\ln I_{corr}$ against the $1/T$ graph. Fig. 4.1.4 display a plot of $\ln (I_{corr} /T)$ against $1/T$ of extracted essential oil, the linear graph obtained with a slope of $(-\Delta H^\circ/R)$, and an intercept of $(\ln$ plots of $\log C_R/T$ against $1/T$ in the absence of inhibitors and for

containing various concentrations of essential oils extract provided straight lines. The values of ΔH° and ΔS° of gives straight lines were considered slopes and intercept. These outcomes are also seen in Table 4.1.2. The negative sign is found between the values of ΔS° and in the corrosive medium of the concentration of inhibitor, showing that the extraction of *Zingiber mioga* EO forms a protective layer on the surface of the metal (Fawzy & Toghhan, 2021);(Fouda & Haleem, 2020) while the positive sign of ΔH° which indicates that the corrosion development is endothermic. The process of dissolution of steel is slow in the presence of a corrosion inhibitor. A negative sign and a large value of entropy (ΔS°) indicate an intermediate state forming an activated complex in the rate-limiting step. It represents that the association step is more than the dissociation step; it means an increase in arrangement during the intermediate state takes place on working from reactant to the product. Due to less adsorption of inhibitor particles at a lower temperature, the surface area of metal arises in contact with a destructive environment, resulting in decreased C_R (Corrosion rates) (Mahmou et al., 2021). Table 4.1.2 data analysis indicates that the thermodynamic parameter (ΔH°) increases in the addition of inhibitors. ΔH° is found at 54.80 kJ/mol in the presence of *Zingiber mioga* EO at the highest concentration of extract 5g/L than in the absence of inhibitors 19.12 kJ/mol for dissolution reaction of mild steel in 1M HCl solution.

4.2 Effect of Temperature on inhibition efficiency, Adsorption Isotherm, and Thermodynamic Parameters of *Zingiber officinale* (ZO) EO extract

The temperature effect on the inhibition efficiency at different temperatures in the absence and presence of oil extracts is shown in Table 4.1.2. It is observed that the corrosion rate of the corrosion surface of the metal in 1M HCl solution rises with an increase in temperature from 303K to 333K (Abdel-Gaber et al., 2009). The rise in C_R is due to lowering the adsorptions of *Zingiber officinale* EO extract on the surface of the metal with a steady increase in temperature. The inhibitor particles disperse into 1M HCl solution from the surface of the metal with the temperature rise; therefore, the surface area of mild steel exposed to a corrosive medium becomes more prominent, then the inhibition efficiency decreases. During the adsorption and desorption processes, an equilibrium state may be attained in the presence of

corrosion inhibitors. To confirm the adsorption-desorption of corrosion inhibitors on the metal surface (Fouda et al., 2021).

Table 4.2.1 Variations of corrosion rate and inhibition efficiency with different temperatures in the presence of *Zingiber officinale* EO and without inhibitor.

Temperature(K)	(C _R) uninhibited	(C _R) inhibited	%IE
303	0.157	0.009	94.27
313	0.234	0.024	89.74
323	0.291	0.047	83.85
333	0.328	0.065	80.18

Thermodynamics and kinetic studies on the adsorption process

Thermodynamic parameters are computed to determine the type of adsorption on the surface of mild steel. The behavior of the adsorption process of inhibitor over the surface of mild steel can provide basic information regarding inhibitor-metal surface interaction and the active mechanism influenced by the nature of the inhibitor and metal and the condition of the environment (Mourya et al., 2014). At various concentrations, the degree of surface coverage (θ) of *Zingiber officinale* EO extract, Corrosion inhibitors (C_{inh}) investigated by weight loss method and adsorption-isotherm has been determined to prove the adsorption of EO happens on the surface of the metal (Prabhu et al., 2021).

To analyze the adsorption isotherm, the surface coverage level by corrosion inhibitor was determined at various concentrations of inhibitors with respect to variations in temperature. Fig. 4.2.1 shows C_{inh}/θ is at the entire temperature, a high R^2 correlation coefficient and the graph plot gives a straight line revealing that inhibitors obey the Langmuir-adsorption isotherm. Hence, we can conclude that the absorption of inhibitor molecules on the metal surface is a single layer, not interacting with neighboring molecules. The adsorption equilibrium constant (K_{ads}) values are taken from isotherm lines of the plotted curves from y-intercepts.

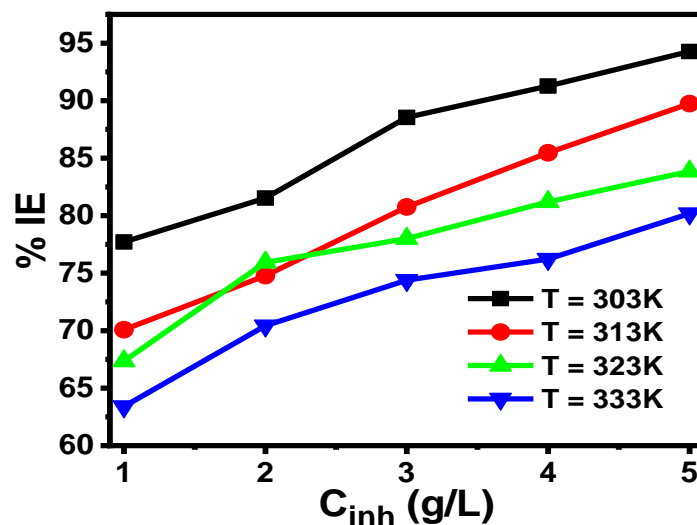


Fig. 4.2.1 Inhibitor efficiency with various concentrations of ginger extracted oils at different temperatures.

In table 4.2.3, the value of Gibb's free energy (ΔG°_{ads}) is found from -12.59 kJmol^{-1} to -13.22 kJmol^{-1} , which reveals that the adsorption of *Zingiber officinale* EO extract on mild steel surface is feasible. The presence of electrostatic interactions between charge ions of the mild steel surface and the inhibitors can be determined (Kosari et al., 2014). Moreover, the negative sign of Gibb's free adsorption energy indicates that the adsorption is spontaneous. The small value of K_{ads} indicates the inhibitor molecule and the charge ions held together by weak interaction on the metal surface. It is assumed that the inhibition process is exposed by physical adsorption. The value of the adsorption equilibrium constant is studied with gradually increasing temperature. Hence, the interaction of the inhibitor molecules with a mild steel surface is favorable at low temperatures. Due to the increased desorption process on the metal surface at higher temperatures (Kumar & Mohana, 2014) and solubility of the protective film is formed rapidly on the metal surface (Kavitha et al., 2014).

Table 4.2.2 Thermodynamics parameters for mild steel in the acidic medium in various concentrations of *Zingiber officinale* EO at temperature ranges between 303–333 K.

Inhibitor concentration (g/L)	E_a (kJ/mol)	ΔH° (kJ/mol)	-ΔS° (J/molK)
0	21.765	17.867	200.93
1	29.543	31.155	169.14
2	32.723	29.368	176.59
3	37.043	39.400	147.05
4	44.626	44.216	133.28
5	57.445	53.069	107.93

Table 4.2.3 Thermodynamics parameters for mild steel in an acidic medium of *Zingiber officinale* EO extract at different temperatures.

Temperature	1/K_{ads}	K_{ads}	ΔG°_{ads} (kJ/mol)
303	0.374	2.675	-12.596
313	0.525	1.904	-12.128
323	0.395	2.525	-13.274
333	0.469	2.133	-13.217

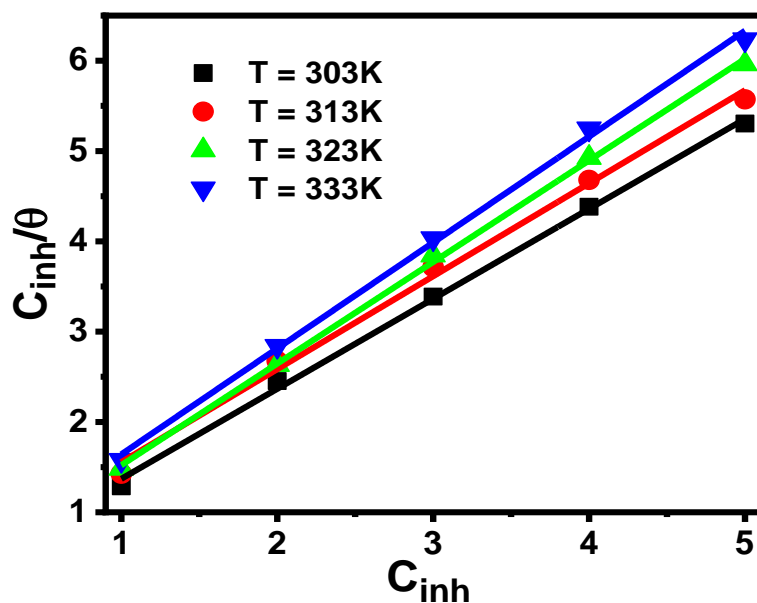


Fig. 4.2.2 Langmuir adsorption isotherm for inhibitor of various concentrations extracted from *Zingiber officinale* EO at different temperatures.

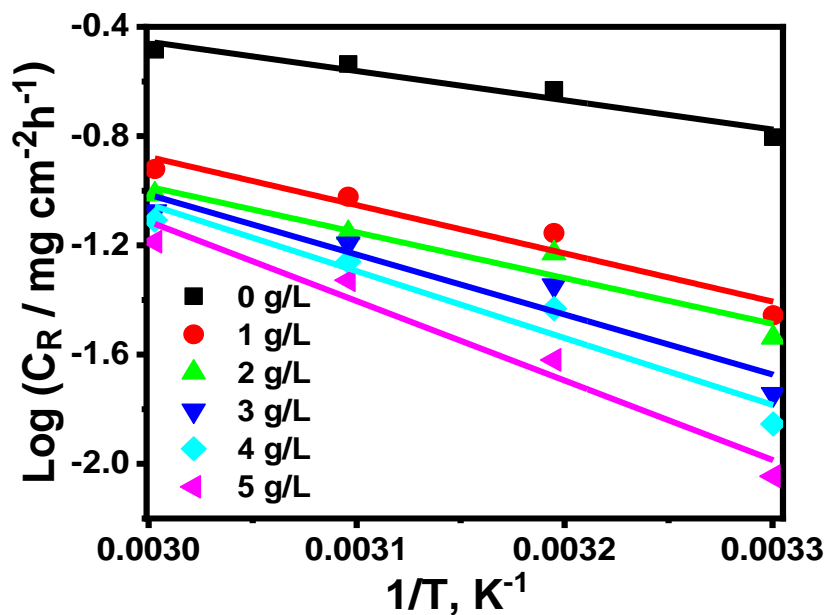


Fig.4.2.3 Arrhenius plots for Mild steel corrosion rates log CR versus $1/T$ in acidic in the absence and presence of *Zingiber officinale* EO.

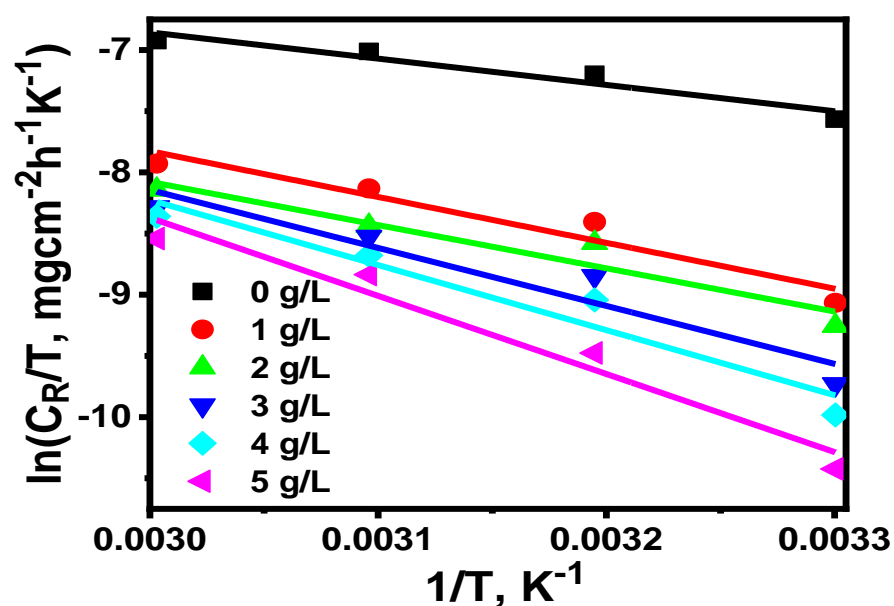


Fig.4.2.4 Transition ($\log (C_R/T)$ versus $1/T$) plots for Mild steel corrosion in the acidic medium in the absence and presence of *Zingiber officinale* EO.

As discussed in the case of ZM, the energy of activation can be obtained from the slope of the graph between $\ln C_R$ vs $1/T$. Plotting the graph between $\log C_R$ against $1/T$ in the absence and presence of inhibitors, straight lines were found as shown in Fig 4.2.3, and obtained E_a is provided in Table 4.2.2. Greater activation energy (E_a) values in the presence of essential oil extract from ginger indicate that it becomes an active inhibitor by physisorption between the surface of the metal and the corrosive acidic medium (Florez-Frias et al., 2021).

Fig. 4.2.4. display a plot of $\ln (I_{corr} /T)$ against $1/T$ of extracted essential oil, the linear graph obtained with a slope $(-\Delta H^\circ/R)$, and an intercept $(\ln (R/Nh)+\Delta S^\circ/R)$ has been obtained in the absence as well as present of various concentrations of essential oils extracts. Hence, values of ΔH° and ΔS° resulted by considering slopes and intercepts. These outcomes are also seen in Table 4.2.2. The negative sign of ΔS° in the corrosive medium suggests that *Zingiber officinale* EO extract forms a protective layer on the surface of the metal, while the positive sign of ΔH° indicates that the corrosion process is endothermic. An increase in the value of ΔH° with an

increase in the concentration of inhibitor suggests that process of dissolution of steel decrease with increasing concentration of inhibitor (Al-Senani, 2016). A negative sign and a large value of entropy (ΔS°) indicate an intermediate state forming an activated complex in the rate-limiting step. It represents an association step is more favorable than the dissociation step; it means an increase in arrangement during the intermediate state takes place on working from reactant to the product. Due to less adsorption of inhibitor particles at a lower temperature, the active surface area of metal available for corrosion arises, resulting in decreased C_R (Corrosion rates) (Mahmou et al., 2021). Table 4.2.2 investigated these. The data indicate that the thermodynamic parameter (ΔH°) increases in the presence of extracted *Zingiber officinale* EO inhibitors and found 53.07 kJ/mol at the highest concentration 5g/L than in the absence of inhibitors 17.87 kJ/mol for dissolution reaction of mild steel in 1M HCl solution.

4.3 Effect of Temperature on inhibition efficiency, Adsorption Isotherm, and Thermodynamic Parameters of *Eryngium foetidum* (EF) EO extract

The temperature effect on the inhibition efficiency at different temperatures in the absence and presence of oil extracts is shown in Table 4.3.1. It was observed that the corrosion reaction of the corrosion surface of the metal in 1M HCl solution increases with an increase in temperature from 303K to 333K. The rise in C_R is due to lowering the adsorptions of *Eryngium foetidum* EO extract on the surface of the metal with a steady increase in temperature. Similar trends were found in the inhibition effect of the Seaweed extract on the corrosion of MS in saline solution reported by Deyab et al., 2017.

An adsorption and desorption equilibrium state may be attained in the presence of corrosion inhibitors which is confirmed by studying the thermodynamic and kinetic parameters related to corrosion.

Table 4.3.1 Variation of corrosion rate and inhibition efficiency in *Eryngium foetidum* EO at different temperatures and without inhibitor.

Temperature(K)	(C_R) uninhibited	(C_R) inhibited	%IE
----------------	-----------------------	---------------------	-----

303	0.170	0.005	97.06
313	0.290	0.017	94.14
323	0.350	0.029	91.71
333	0.420	0.044	89.52

Thermodynamic and kinetic studies on the adsorption process

Thermodynamic parameters are computed to determine the type of adsorption on the surface of mild steel. The behavior of the adsorption process of inhibitor over the surface of mild steel can provide basic information regarding inhibitor-metal surface interaction and the active mechanism influenced by the nature of inhibitor and metal and the condition of the environment. At various concentrations, the degree of surface coverage (θ) of *Eryngium foetidum* EO extract, Corrosion inhibitors (C_{inh}) investigated by weight loss method and adsorption-isotherm has been determined to prove the adsorption of EO happens on the surface of the metal (Prabhu et al., 2021).

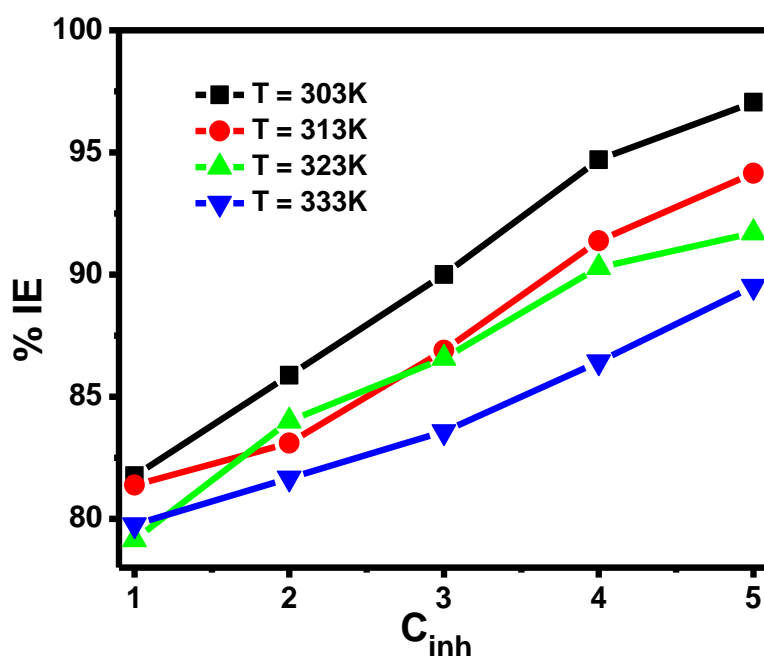


Fig. 4.3.1 Inhibitor efficiency with various concentrations of ginger extracted oils at different temperatures.

Table 4.3.2 Thermodynamics parameters for mild steel in the acidic medium in various concentration of *Eryngium foetidum* EO at a temperature ranges between (303 – 333) K.

Inhibitors concentration(g/L)	E_a (kJ/mol)	ΔH° (kJ/mol)	-ΔS° (J/molK)
0	24.52	21.87	186.81
1	28.11	25.47	189.10
2	30.66	28.01	182.58
3	37.25	34.60	163.67
4	49.28	46.63	129.05
5	59.61	56.96	99.42

Table 4.3.3 Thermodynamics parameters for mild steel in the acidic medium in *Eryngium foetidum* EO at different temperatures.

Temperature	1/K_{ads}	K_{ads}	ΔG°_{ads} (kJ/mol)
303	0.327	3.062	-12.94
313	0.315	3.178	-13.46
323	0.271	3.695	-14.29
333	0.248	4.025	-14.97

C_{inh} is inhibitor concentration, K_{ads} is the adsorption equilibrium constant, and θ is the degree of surface coverage, respectively. To examine the adsorption isotherm, the surface coverage level by corrosion inhibitor was determined at various concentrations of inhibitors with respect to variations in temperature. Fig.4.3.2 shows C_{inh}/θ is at an all-time high R^2 correlation coefficient and the graph plot gives a straight line revealing that inhibitors obey the Langmuir-adsorption isotherm. Hence, we can conclude that the absorption of inhibitor molecules on the metal surface is a single-layer, not interaction with neighboring molecules. The adsorption equilibrium

constant (K_{ads}) values are taken from isotherm lines of the plotted curves from y-intercepts.

In table 4.3.3, The corresponding value of Gibb's free energy (ΔG°_{ads}) is found from $-12.94 \text{ kJ mol}^{-1}$ to $-14.97 \text{ kJ mol}^{-1}$, which reveals the adsorption of *Eryngium foetidum* EO extract on mild steel surface is feasible. The presence of electrostatic interactions between charge ions of the mild steel surface and the inhibitors can be determined (Kosari et al., 2014). Moreover, the negative sign of Gibb's free adsorption energy indicates that the adsorption is spontaneous. The small value of K_{ads} indicates the inhibitor molecule and the charge ions held together by weak interaction on the metal surface. It is assumed that the inhibition process is exposed by physical adsorption. The value of the adsorption equilibrium constant is studied with gradually increasing temperature. Hence, the interaction of the inhibitor molecules with a mild steel surface is favorable at low temperatures. Due to the increased desorption process on the metal surface at higher temperatures (Kumar & Mohana, 2014), the solubility of the protective film formed rapidly on the metal surface (Kavitha et al., 2014).

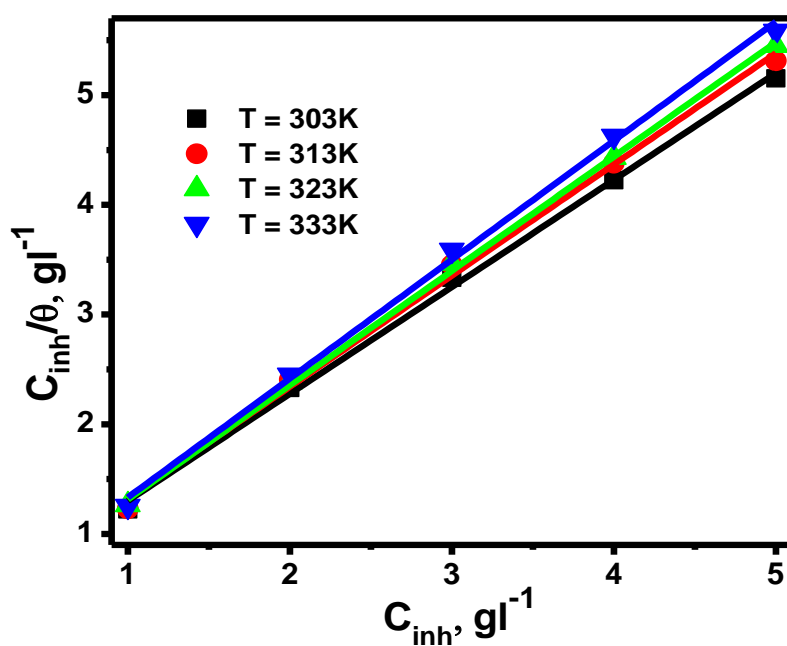


Fig. 4.3.2 Langmuir adsorption isotherm for inhibitor of various concentrations extracted from *Eryngium foetidum* EO at different temperatures.

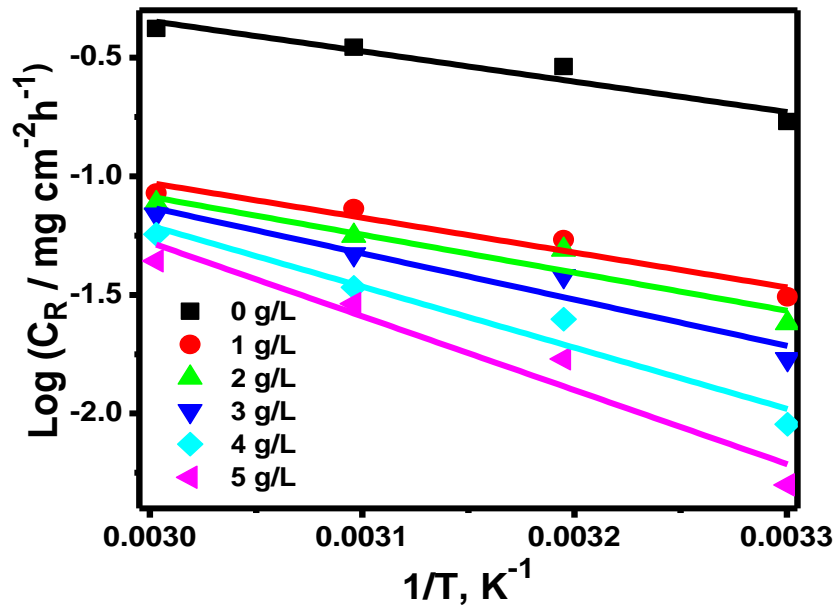


Fig.4.3.3. Arrhenius plots for Mild steel corrosion rates $\log C_R$ versus $1/T$ in acidic in the absence and presence of *Eryngium foetidum* EO.

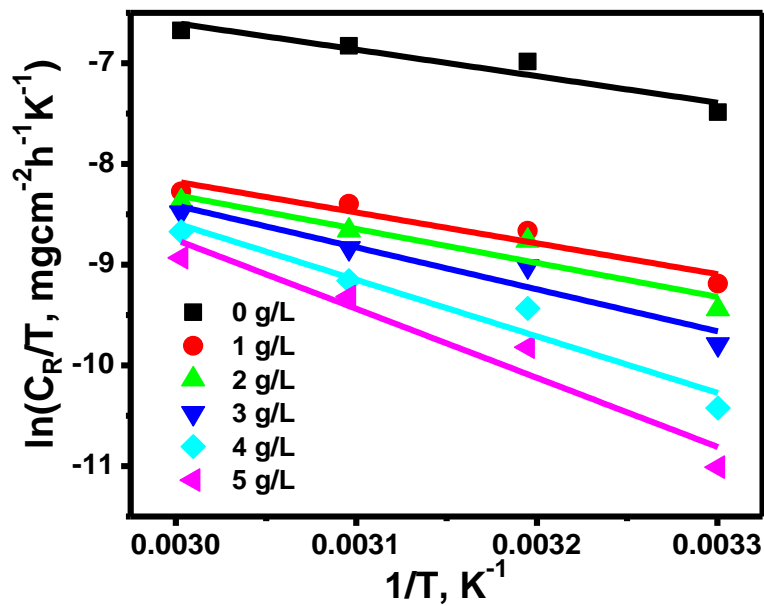


Fig.4.3.4 Transition ($\log(C_R/T)$ versus $1/T$) plots for Mild steel corrosion in the acidic medium in the absence and presence of *Eryngium foetidum* EO.

From Fig.4.3.3, Plotting the graph between $\log C_R$ against $1/T$ in the absence and presence of inhibitors straight lines were found as shown in Table 4.3.2. Greater activation energy (E_a) values in the presence of essential oil extract from ginger indicate that it becomes an active inhibitor by physisorption between the surface of the metal and the corrosive acidic medium (Florez-Frias et al., 2021).

A graph between $\ln C_R/T$ vs $1/T$ provide slope = $-\Delta H^\circ/R$ and intercept = $\{\ln (R/Nh) + \Delta S^\circ/R\}$.

As seen in fig. 4.3.3 the E_a (activation energy) was analyzed from the slopes of $\ln I_{\text{corr}}$ against the $1/T$ graph. Fig. 4.3.4 display a plot of $\ln (I_{\text{corr}} /T)$ against $1/T$ of extracted essential oil, the linear graph obtained with a slope of $(-\Delta H^\circ/R)$, and an intercept of $(\ln \text{ plots of } \log C_R/T \text{ against } 1/T \text{ in the absence of inhibitors and for containing various concentrations of essential oils extract provided straight lines. The values of } \Delta H^\circ \text{ and } \Delta S^\circ \text{ of gives straight lines were considered slopes and intercepts. These outcomes are also seen in Table 4.3.2. The negative sign is found between the values of } \Delta S^\circ \text{ and in the corrosive medium of the concentration of inhibitor, showing that the extraction of } Eryngium foetidum \text{ EO forms a protective layer on the surface of the metal (Al-Senani, 2016), while the positive sign of } \Delta H^\circ \text{ which indicates that the corrosion development is endothermic. The process of dissolution of steel is slow in the presence of a corrosion inhibitor. A negative sign and a large value of entropy (} \Delta S^\circ \text{) indicate that an intermediate state forms an activated complex in the rate-limiting step. It represents an association step more than the dissociation step, meaning an increase in arrangement during the intermediate state occurs on working from the reactant to the product. Due to less adsorption of inhibitor particles at a lower temperature, the surface area of metal arises in contact with a destructive environment, resulting in decreased } C_R \text{ (Corrosion rates) (Mahmou et al., 2021). Table 4.3.2 investigated these; the data suggested that the thermodynamic parameter (} \Delta H^\circ \text{) increases in the presence of extracted } Eryngium foetidum \text{ EO inhibitors 56.96 kJ/mol at the highest concentration 5g/L than that in the absence of inhibitors 21.87 kJ/mol for dissolution reaction of mild steel in 1M HCl solution.}$

4.4 Effect of Temperature on inhibition efficiency, Adsorption Isotherm, and Thermodynamic Parameters of *Mentha piperita* (MP) EO extract

The temperature effect on the inhibition efficiency at different temperatures in the absence and presence of oil extracts is shown in Table 4.4.1. It was observed that the corrosion rate of the corrosion surface of the metal in 1M HCl solution rises with an increase in temperature from 303K to 333K. The inhibitor particles disperse into 1M HCl solution from the surface of the metal with the temperature rise; therefore, the surface area of mild steel exposed to a corrosive medium becomes more prominent, then the inhibition efficiency decreases (Turcio-Ortega et al., 2007). During the adsorption and desorption process, an equilibrium state may be attained in the presence of corrosion inhibitors. To confirm the adsorption-desorption of corrosion inhibitors on the metal surface.

Table 4.4.1 Variation of corrosion rate and inhibition efficiency with different temperatures in the presence of 5g/L of *Mentha piperita* EO extract and without inhibitor.

Temperature(K)	(CR) uninhibited	(CR) inhibited	%IE
303	0.185	0.010	94.59
313	0.289	0.034	88.23
323	0.323	0.071	78.02
333	0.402	0.089	77.86

Thermodynamic parameters are computed to determine the type of adsorption on the surface of mild steel. The behavior of the adsorption process of inhibitor over the surface of mild steel can provide basic information regarding inhibitor-metal surface interaction and the active mechanism influenced by the nature of inhibitor and metal and the condition of the environment. At various concentrations, the degree of surface coverage (θ) of *Mentha piperita* EO extract, Corrosion inhibitors (C_{inh}) investigated by weight loss method and adsorption-isotherm has been determined to prove the adsorption of EO happens on the surface of the metal (Prabhu et al., 2021).

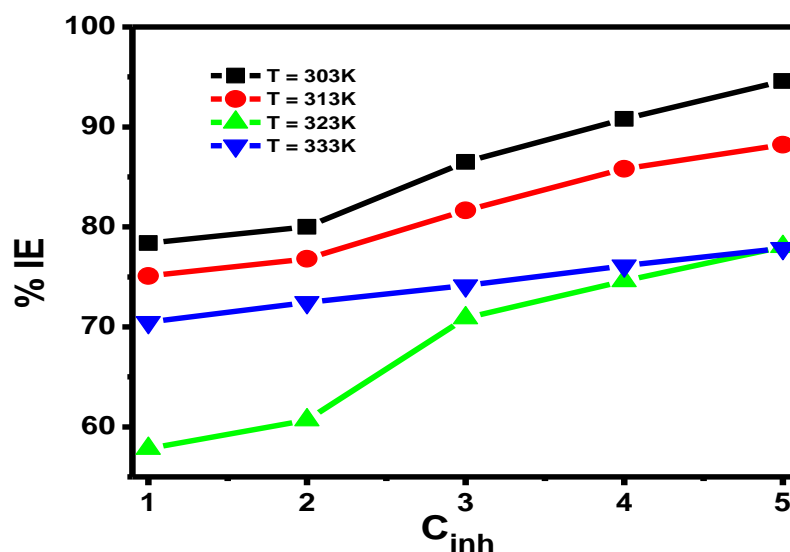


Fig. 4.4.1 Inhibitor efficiency with various concentrations of peppermint extracted oils at different temperatures.

C_{inh} is inhibitor concentration, K_{ads} is the adsorption equilibrium constant, and θ is the degree of surface coverage, respectively. To examine the adsorption isotherm, the surface coverage level by corrosion inhibitor was determined at various concentrations of inhibitors with respect to variations in temperature. Straight lines are observed in the graph between C_{inh}/θ vs C_{inh} at different temperatures. It is a clear indication that corrosion inhibitor adsorbed on the metal surface following Langmuir-adsorption isotherm (Fig.4.4.2). And adsorption of inhibitor molecules on the metal surface is a single-layer and without interaction between neighboring molecules. The adsorption equilibrium constant (K_{ads}) values are taken from isotherm lines of the plotted curves from y-intercepts.

In table 4.4.3, The corresponding value of Gibb's free energy (ΔG°_{ads}) is found from $-12.37 \text{ kJmol}^{-1}$ to $-15.18 \text{ kJmol}^{-1}$, which reveals that the adsorption of *Mentha piperita* EO extract on mild steel surface is feasible. The presence of electrostatic interactions between charge ions of the mild steel surface and the inhibitors can be determined (Kosari et al., 2014). Moreover, the negative sign of Gibb's free adsorption energy indicates that the adsorption is spontaneous. The small value of K_{ads} indicates the inhibitor molecule and the charge ions held together by

weak interaction on the metal surface. It is assumed that the inhibition process is exposed by physical adsorption. The value of the adsorption equilibrium constant is studied with gradually increasing temperature. Hence, the interaction of the inhibitor molecules with a mild steel surface is favorable at low temperatures. Due to the increased desorption process on the metal surface at higher temperatures [35] and solubility of the protective film formed rapidly on the metal surface (Kavitha et al., 2014); (Kumar & Mohana, 2014)

Table 4.4.2 Thermodynamics parameters for mild steel in the acidic medium in various concentrations of *Mentha piperita* EO extract at a temperature range between (303 – 333) K

Inhibitors concentration(g/L)	E_a (kJ/mol)	ΔH° (kJ/mol)	-ΔS° (J/molK)
0	20.58	17.94	200.94
1	32.86	30.22	169.14
2	33.16	30.51	176.59
3	41.01	38.36	147.04
4	49.74	47.09	133.28
5	61.69	59.04	107.93

Table 4.4.3 Thermodynamics parameters of *Mentha piperita* for mild steel in the acidic medium at different temperatures.

Temperature	1/K_{ads}	K_{ads}	ΔG°_{ads} (kJ/mol)
303	0.40952	2.44187	-12.37
313	0.36908	2.70944	-13.05
323	0.77793	1.28546	-11.46
333	0.2305	4.33846	-15.18

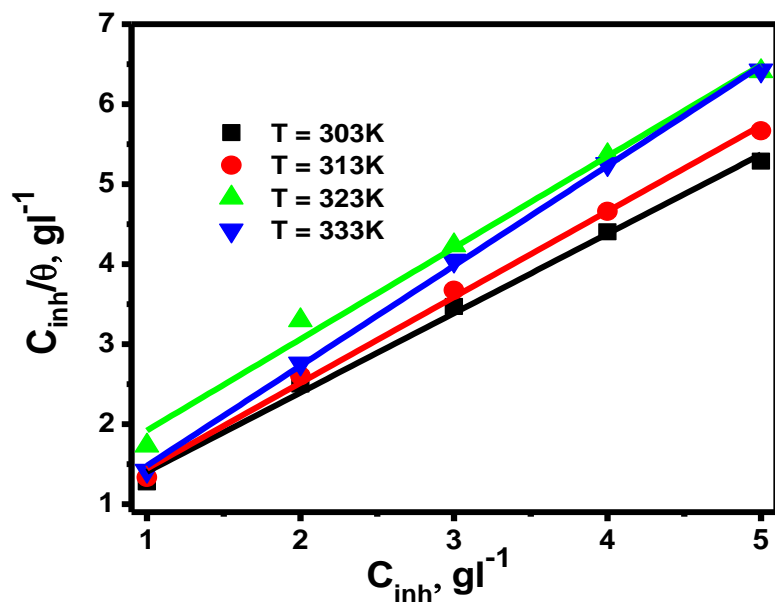


Fig. 4.4.2 Langmuir adsorption isotherm for inhibitor of various concentrations extracted from *Mentha piperita* EO at different temperatures.

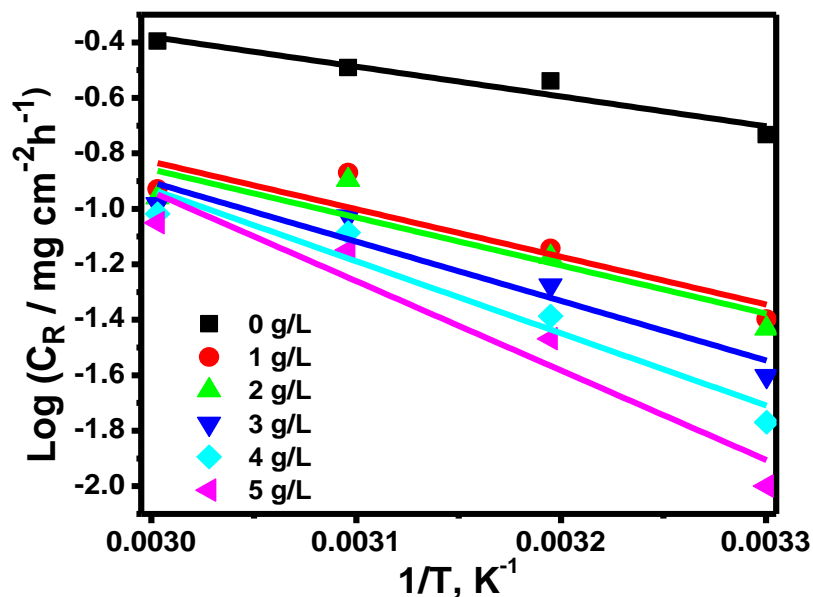


Fig.4.4.3 Arrhenius plots for Mild steel corrosion rates $\log C_R$ versus $1/T$ in acidic in the absence and presence of peppermint extracted oils.

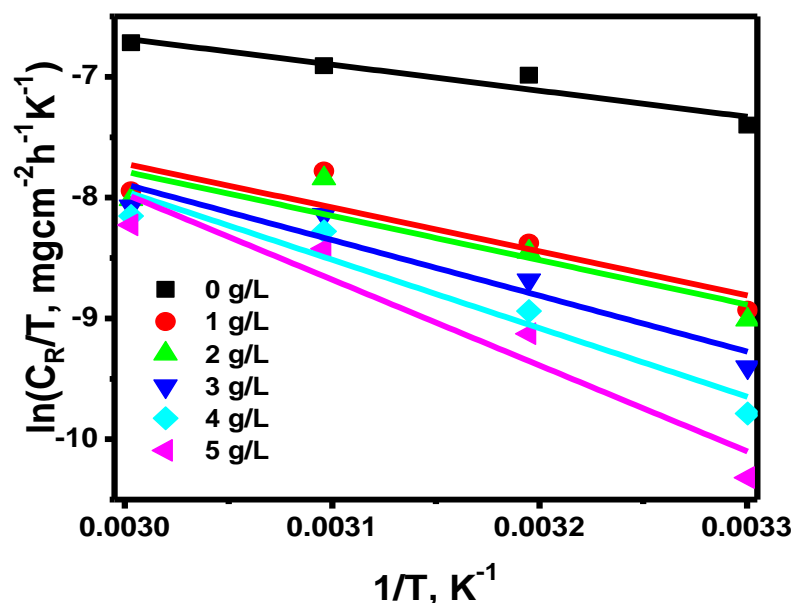


Fig.4.4.4 Transition state plots for Mild steel corrosion rates $\log (C_R/T)$ versus $1/T$ in acidic in the absence and presence of *Mentha piperita* extracted oils.

From Fig.4.4.3, Plotting the graph between $\log C_R$ against $1/T$ in the absence and presence of inhibitors straight lines were found as shown in Table 4.4.2. Greater activation energy (E_a) values in the presence of essential oil extract from ginger indicate that it forms an active inhibitor by physisorption between the surface of the metal and the corrosive acidic medium (Florez-Frias et al., 2021).

As seen in fig. 4.4.3 The E_a (activation energy) is analyzed from the slopes of $\ln I_{\text{corr}}$ against the $1/T$ graph. Fig. 4.4.4 display a plot of $\ln (I_{\text{corr}} /T)$ against $1/T$ of extracted essential oil, the linear graph obtained with a slope of $(-\Delta H^\circ/R)$, and an intercept of $(\ln \text{ plots of } \log C_R/T \text{ against } 1/T \text{ in the absence of inhibitors and for containing various concentrations of essential oils extract provided straight lines. The values of } \Delta H^\circ \text{ and } \Delta S^\circ \text{ were obtained from slopes and intercepts of fitted straight lines in the graph of } \ln (I_{\text{corr}} /T) \text{ vs } 1/T. \text{ These outcomes are also seen in Table 4.4.2. The negative sign is found between the values of } \Delta S^\circ \text{ and in the corrosive medium of the concentration of inhibitor, showing that the extraction of } \textit{Mentha piperita} \text{ EO forms a protective layer on the surface of the metal (Al-Senani, 2016), while the positive sign of } \Delta H^\circ \text{ which indicates that the corrosion development is endothermic.}$

The process of dissolution of steel is slow in the presence of a corrosion inhibitor. A negative sign and a large value of entropy (ΔS°) indicate an intermediate state forming an activated complex in the rate-limiting step. It represents an association step is more than the dissociation step; it means an increase in arrangement during the intermediate state takes place on working from reactant to the product (Mahmou et al., 2021). Due to less adsorption of inhibitor particles at a lower temperature, the surface area of metal arises in contact with a destructive environment, resulting in decreased C_R (Corrosion rates). Table 4.4.2 investigated these; the data suggested that the thermodynamic parameter (ΔH°) increases in the presence of extracted *Mentha piperita* EO inhibitors 59.04 kJ/mol at the highest concentration 5g/L than that in the absence of inhibitors 17.94 kJ/mol for dissolution reaction of mild steel in 1M HCl solution.

4.5 Effect of Temperature on inhibition efficiency, Adsorption Isotherm, and Thermodynamic Parameters of *Allium sativum* (AS) EO extract

The temperature effect on the inhibition efficiency at different temperatures in the absence and presence of oil extracts is shown in Table 4.5.1. It was observed that the corrosion rate of the corrosion surface of the metal in 1M HCl solution rises with an increase in temperature (Loto & Solomon, 2022). The rise in C_R is due to lowering the adsorptions of *Allium sativum* EO extract on the surface of the metal with a steady increase in temperature. The inhibitor particles disperse into 1M HCl solution from the surface of the metal with the temperature rise; therefore, the surface area of mild steel exposed to a corrosive medium becomes more prominent, then the inhibition efficiency decreases. During the adsorption and desorption process, an equilibrium state may be attained in the presence of corrosion inhibitors. To confirm the adsorption-desorption of corrosion inhibitors on the metal surface.

Table 4.5.1. Variation of corrosion rate and inhibition efficiency with different temperatures in the presence of 5g/L of *Allium sativum* oils extract and without inhibitor.

Temperature(K)	(CR) uninhibited	(CR) inhibited	%IE
303	0.154	0.008	94.80
313	0.265	0.027	89.81
323	0.348	0.052	85.06
333	0.427	0.072	83.14

Thermodynamic parameters are computed to determine the type of adsorption on the surface of mild steel. The behavior of the adsorption process of inhibitor over the surface of mild steel can provide basic information regarding inhibitor-metal surface interaction and the active mechanism influenced by the nature of inhibitor and metal and the condition of the environment. At various concentrations, the degree of surface coverage (θ) of *Allium sativum* EO extract, Corrosion inhibitors (C_{inh}) investigated by weight loss method and adsorption-isotherm has been determined to prove the adsorption of EO happens on the surface of the metal (Prabhu et al., 2021).

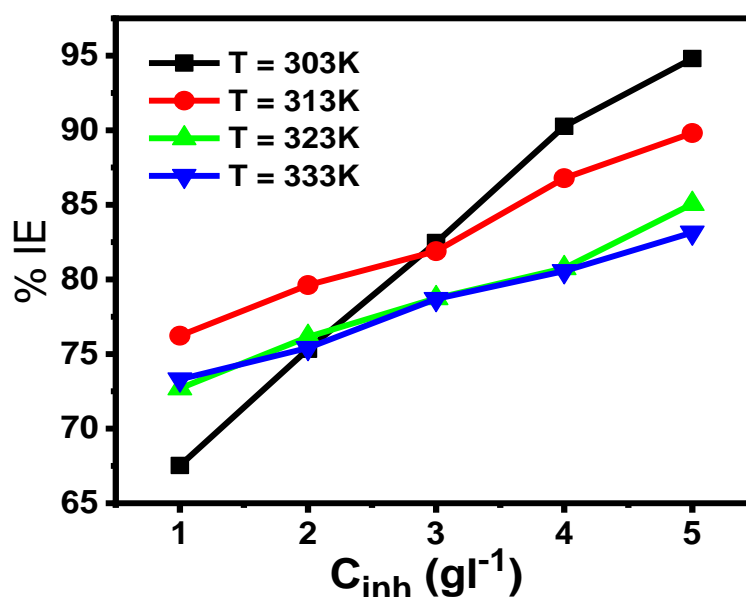


Fig. 4.5.1 Inhibitor efficiency at various concentrations of garlic extracted oils at different temperatures.

Table 4.5.2. Thermodynamics parameters for mild steel in the acidic medium in various concentrations of *Allium sativum* oils extract at a temperature range between (303 – 333) K

Inhibitors concentration(g/L)	E _a , (kJ/mol)	ΔH° (kJ/mol)	-ΔS° (J/molK)
0	28.12	25.47	175.84
1	24.20	21.56	198.95
2	29.23	26.59	184.45
3	34.39	31.74	169.70878
4	48.81	46.17	126.57352
5	61.24	58.59	90.12545

C_{inh} is inhibitor concentration, K_{ads} is the adsorption equilibrium constant, and θ is the degree of surface coverage, respectively. To examine the adsorption isotherm, the surface coverage level by corrosion inhibitor was determined at various concentrations of inhibitors with respect to variations in temperature. Fig.4.5.2 shows C_{inh}/θ is at an entire temperature high R^2 correlation coefficient and the graph plot gives a straight line revealing that inhibitors obey the Langmuir-adsorption isotherm. Hence, we can conclude that the absorption of inhibitor molecules on the metal surface is a single-layer, not interaction with neighboring molecules. The adsorption equilibrium constant (K_{ads}) values are taken from isotherm lines of the plotted curves from y-intercepts.

In fig. 4.5.4, The corresponding value of Gibb's free energy (ΔG°_{ads}) is found from $-11.07 \text{ kJmol}^{-1}$ to $-14.67 \text{ kJmol}^{-1}$, which reveals that the adsorption of ginger EO extract on mild steel surface is feasible. The presence of electrostatic interactions between charge ions of the mild steel surface and the inhibitors can be determined (Kosari et al., 2014). Moreover, the negative sign of Gibb's free adsorption energy indicates that the adsorption is spontaneous. The small value of K_{ads} indicates the

inhibitor molecule and the charge ions held together by weak interaction on the metal surface. It is assumed that the inhibition process is exposed by physical adsorption. The value of the adsorption equilibrium constant is studied with gradually increasing temperature. Hence, the interaction of the inhibitor molecules with a mild steel surface is favorable at low temperatures (Kumar & Mohana, 2014);(Kavitha et al., 2014). Due to the increased desorption process on the metal surface at higher temperatures and solubility of the protective film formed rapidly on the metal surface.

Table 4.5.3 Thermodynamics parameters of *Allium sativum* for mild steel in the acidic medium at different temperatures.

Temperature	1/K _{ads}	K _{ads}	ΔG° _{ads} (kJ/mol)
303	0.687	1.455	-11.06
313	0.350	2.854	-13.18
323	0.328	3.039	-13.77
333	0.278	3.599	-14.66

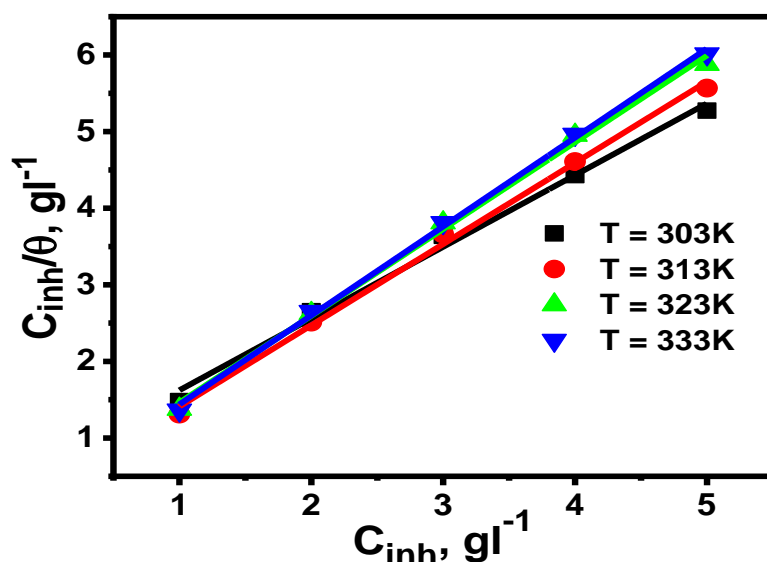


Fig. 4.5.2 Langmuir adsorption isotherm for inhibitor of various concentrations extracted from *Allium sativum* EO at different temperatures.

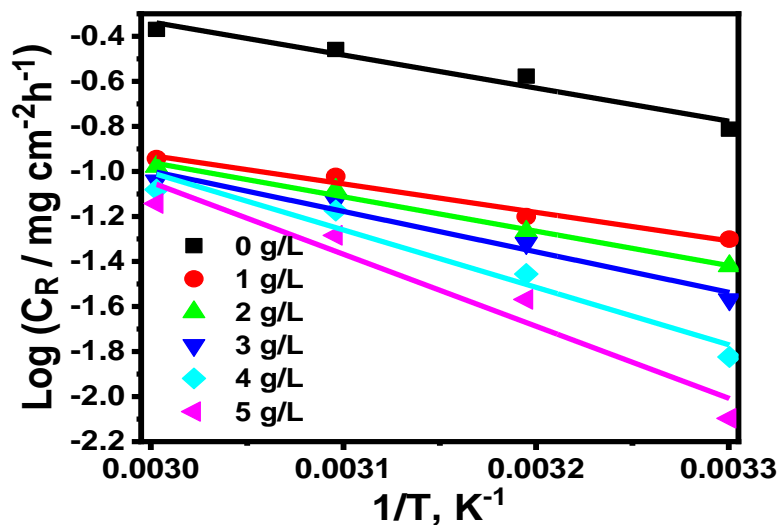


Fig.4.5.3 Arrhenius plots for Mild steel corrosion rates $\log C_R$ versus $1/T$ in acidic in the absence and presence of *Allium sativum* extracted oils.

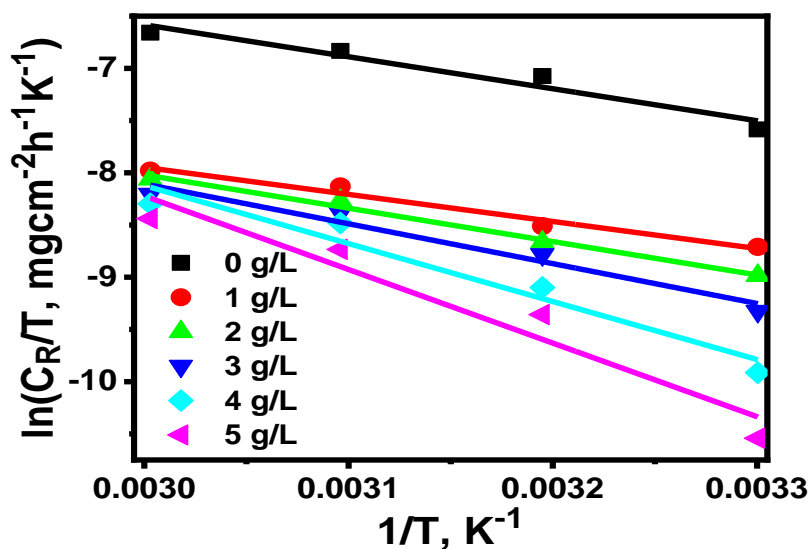


Fig.4.5.4 Transition state plots for Mild steel corrosion rates $\log (C_R/T)$ versus $1/T$ in acidic in the absence and presence of *Allium sativum* extracted oils.

From Fig.4.5.3, Plotting the graph between $\log C_R$ against $1/T$ in the absence and presence of inhibitors straight lines were found as shown in Table 4.5.2. Greater activation energy (E_a) values in the presence of essential oil extract from ginger

indicate that it forms an active inhibitor by physisorption between the surface of the metal and the corrosive acidic medium (Florez-Frias et al., 2021).

As seen in fig. 4.5.3 The E_a (activation energy) is analyzed from the slopes of $\ln I_{\text{corr}}$ against the $1/T$ graph. Fig. 4.5.4 display a plot of $\ln (I_{\text{corr}} / T)$ against $1/T$ of extracted essential oil, the linear graph obtained with a slope of $(-\Delta H^\circ/R)$, and an intercept of $(\ln \text{ plots of } \log C_R/T \text{ against } 1/T \text{ in the absence of inhibitors and for containing various concentrations of essential oils extract provided straight lines. The values of } \Delta H^\circ \text{ and } \Delta S^\circ \text{ of gives straight lines were considered slopes and intercept. These outcomes are also seen in Table 4.5.2. A negative sign is found between the values of } \Delta S^\circ \text{ and in the corrosive medium of the concentration of inhibitor, indicating that the extraction of } Allium sativum \text{ EO forms a protective layer on the surface of the metal (Al-Senani, 2016). While the positive sign of } \Delta H^\circ \text{ which indicates that the corrosion development is endothermic. The process of dissolution of steel is slow in the presence of a corrosion inhibitor. A negative sign and a large value of entropy (} \Delta S^\circ \text{) indicate an intermediate state forming an activated complex in the rate-limiting step. It represents an association step more than the dissociation step, meaning an increase in arrangement during the intermediate state occurs on working from the reactant to the product (Mahmou et al., 2021). Due to less adsorption of inhibitor particles at a lower temperature, the surface area of metal arises in contact with a destructive environment, resulting in decreased } C_R \text{ (Corrosion rates). Table 4.5.2 investigated these; the data suggested that the thermodynamic parameter (} \Delta H^\circ \text{) increases in the presence of extracted } Allium sativum \text{ EO inhibitors 58.59 kJ/mol at the highest concentration 5g/L than that of in the absence of inhibitors 25.47 kJ/mol for dissolution reaction of mild steel in 1M HCl solution.}$

4.6 Fourier Transform infrared spectroscopy (FTIR spectroscopy) Study

4.6.1 *Zingiber mioga*

The information about different functional groups contained in the substance is provided by FTIR analysis through their distinctive signature at various spectral

positions. FTIR analysis is carried out for pure extract and metal surfaces coated with various oils to analyze the establishment of a protective layer (Fockaert et al., 2020) on the metal substrate. (See Figures 4.6.1 - 4.6.5) Pure *Zingiber mioga* oil's FTIR spectra contain peaks at broad bands at 2918 cm^{-1} due to $-\text{CH}_2$ symmetric and anti-symmetric stretch of methyl group mainly from lipids (See chapter 2 for phytochemical analysis) (Park et al., 2021).

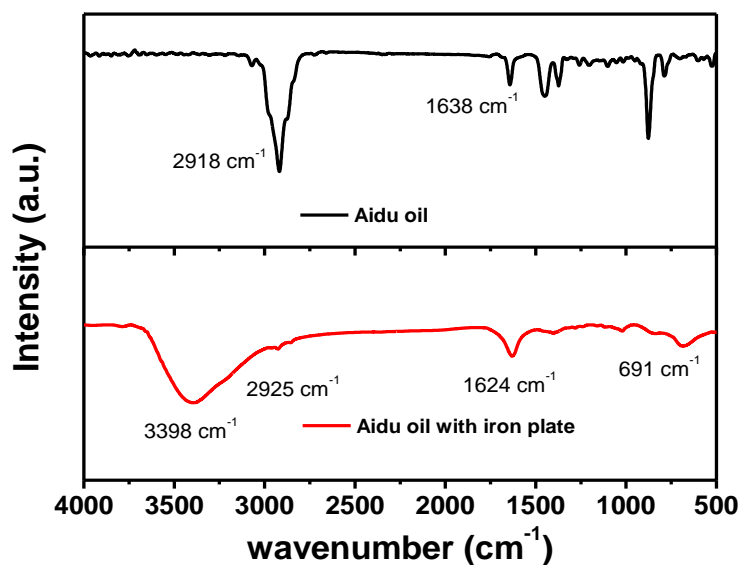


Fig.4.6.1 FT-IR spectra of (a) Pure *Zingiber mioga* (Aidu oils) and (b) protective layer developed on MSS after immersion for 6 h in 1 M HCl containing 5 g/L *Zingiber mioga* (Aidu oil)

The vibration spectra bands in the range from 1800 to 800 cm^{-1} accurately reflected the chemical contents of *Zingiber mioga* oil extracts, particularly lipids, proteins, polysaccharides, and polyphenols.

The primary bands in the infrared spectra of metal surfaces coated with *Zingiber mioga* oils correspond to the hydroxyl and carbonyl groups. When compared to the pure extract, the carbonyl band's intensity rose with a slight shift in position (1624 cm^{-1}). Additionally, a broad peak at 3398 cm^{-1} is attributable to the hydroxyl group. In comparison to pure oil, the combined intensities of the individual peaks are extremely low, clearly suggesting the creation of a thin layer on the metal surface. Although *Zingiber mioga* oil extract primarily included aliphatic

phytochemicals, it is evident from FTIR studies that only phytochemicals having hydroxyl/carbonyl groups of alcohol/acid/ester/aldehyde/ketonic group were able to form a protective layer on metal surfaces.

4.6.2 *Zingiber officinale*

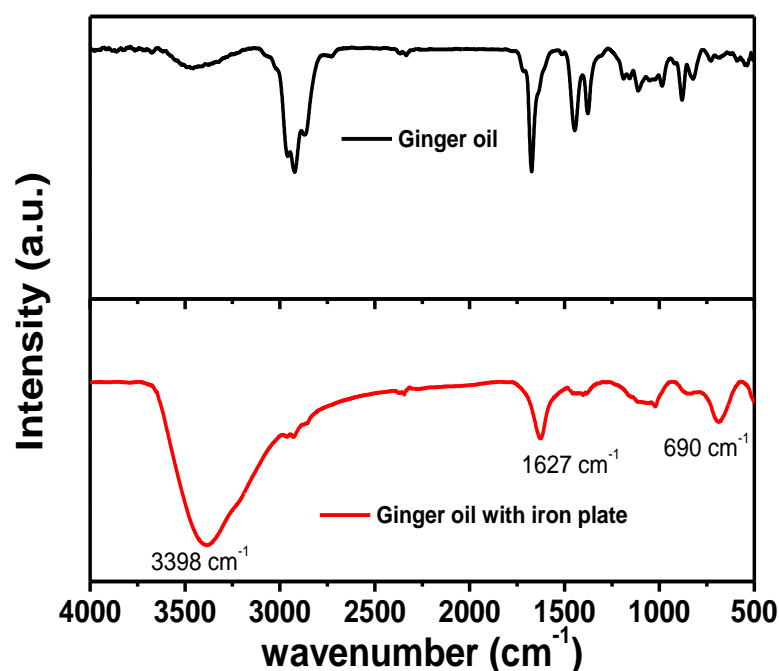


Fig. 4.6.2 FT-IR spectra of (a) pure *Zingiber officinale* (Ginger oil) and (b) protective layer developed on MSS after immersion for 6 h in 1 M HCl containing 5 g/L *Zingiber officinale* (Ginger oil).

The ginger oil also exhibits the band corresponding to aliphatic groups of proteins and lipids, which are major constituents (Hussein et al., 2017). Intriguingly, FTIR analysis of plant extracts coated on MSS surface shows that, due to the interaction of the polar functional group to the metal surface, the constituents connected on the metal surface largely comprise -OH and carbonyl functional group.

4.6.3 *Eryngium foetidum*

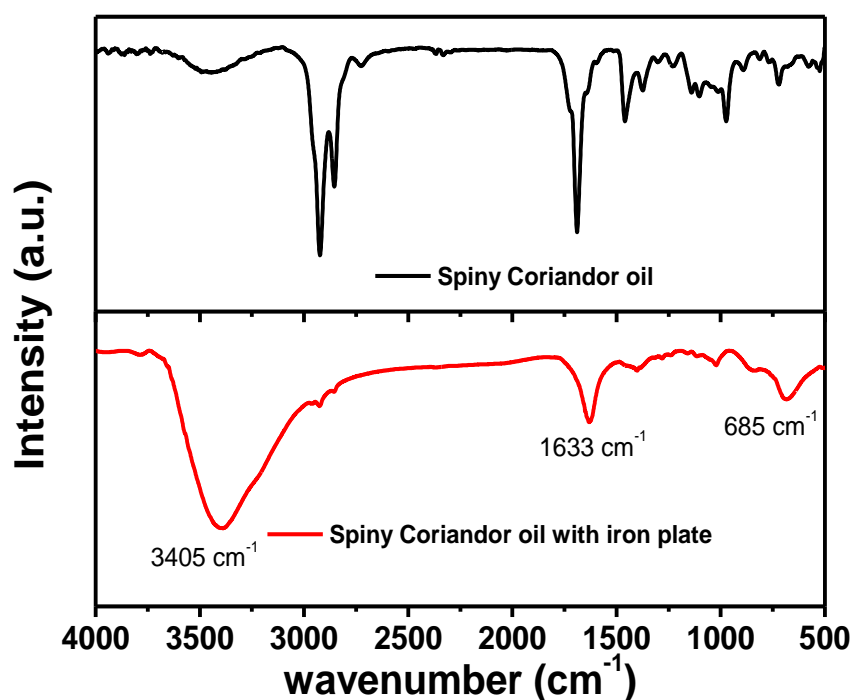


Fig. 4.6.3 FT-IR spectra of (a) pure *Eryngium foetidum* (Spiny coriander oil) and (b) protective layer developed on MSS after immersion for 6 h in 1 M HCl containing 5 g/L *Eryngium foetidum* (spiny coriander oil).

FTIR spectra of *Eryngium foetidum* oil show the presence of aliphatic C-H in plant extract (See chapter 2 for phytochemical analysis) as a major constituent (Acharya et al., 2021). Low-intensity peaks with slight shifts (2-5 cm⁻¹) are observed when the plant extracts are coated on the MSS surface, indicating the formation of a thin layer on the metal surface. In most cases, a broad IR band is observed at 3398 cm⁻¹ due to the OH group forming on the surface of MSS by atmospheric oxidation. In addition, peaks observed at 685 cm⁻¹ is due to the formation of the metal-oxygen (functional group) bond. The peak at ~1633 cm⁻¹ is due to carbonyl groups of acid/ester and ketonic group present in phytochemicals of *Eryngium foetidum* oil.

Hence, IR spectroscopic studies suggest that in different plant oils, mainly lipids and proteins are present. However, carbonyl and hydroxyl groups containing phytochemicals are mainly attached to the surface of the metal and protect the metal from corrosion.

4.6.4 *Mentha Piperita*

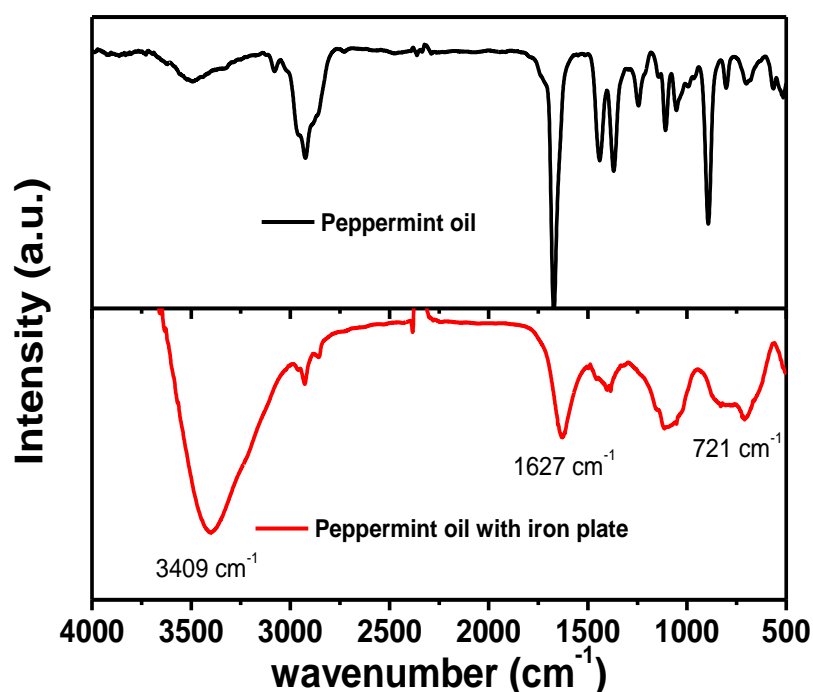


Fig. 4.6.4 FT-IR spectra of (a) pure Peppermint oil and (b) protective layer developed on MSS after immersion for 6 h in 1 M HCl containing 5 g/L *Mentha Piperita* (Peppermint oil).

FTIR spectra of peppermint oil match well with the reported literature (Lopedota et al., 2021). Oils coating on the metal surface reveals peak corresponding to hydroxyl and carbonyl groups of proteins and lipids. In addition, peaks observed at 721 cm⁻¹ is due to the formation of the metal-oxygen (functional group) bond. The peak at ~1627 cm⁻¹ is due to carbonyl groups of acid/ester and ketonic group present in phytochemicals of MP

4.6.5 *Allium sativum*

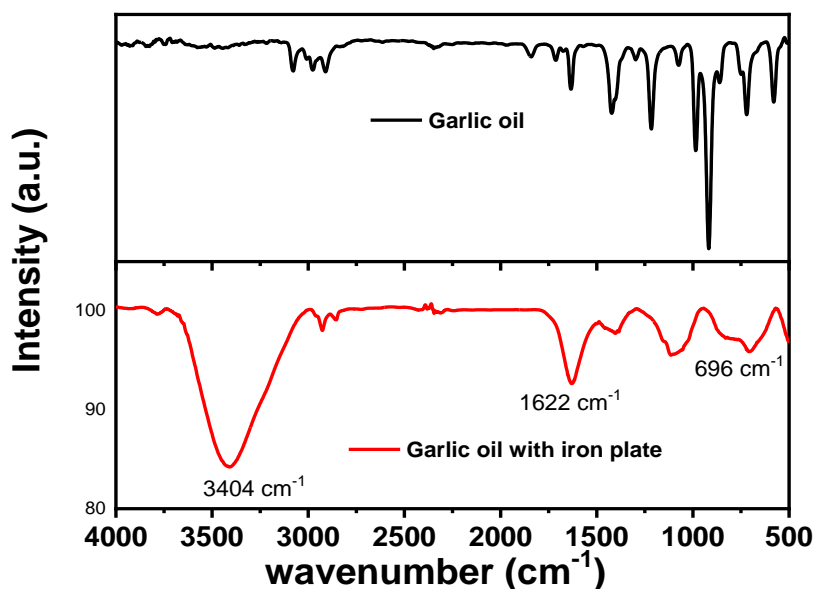


Fig. 4.6.5 FT-IR spectra of (a) pure *Allium sativum* (Garlic oil) and (b) protective layer developed on MSS after immersion for 6h in 1 M HCl containing 5 g/L *Allium sativum* (Garlic oil).

Similarly, the FTIR spectrum of garlic oil shows the presence of aliphatic C-H as the primary ingredient (See chapter 2 for phytochemical analysis). When plant extracts are coated on MSS, broad peaks are observed at 3404 and 1622 cm⁻¹ due to carbonyl groups of acid/ester and ketonic groups present in the phytochemicals of garlic oil (Divya et al., 2017).

The C=C stretching vibration of the allyl group is responsible for the intense peak found at 1638 cm⁻¹. It was caused by the *Allium sativum* oil and was identified as belonging to the conjugated double bond of the Diallyldisulphide. Symmetric CH₃ bending modes of the methyl groups of proteins may be detected at ~1400

4.7 Scanning Electron Microscope (SEM) analysis

SEM pictures of the metal surface before and after three hours of immersion in 1 N HCl with and without plant extract oils such as *Zingiber mioga*, *Zingiber*

officinale, *Mentha piperita*, *Eryngium foetidum*, and *Allium sativum* are recorded at 5 μm resolution, and 10000 or 15000 magnifications has been recorded.

4.7.1 *Zingiber mioga*

The metal surface was imaged using a scanning electron microscope (SEM) before and after three hours of immersion in 1 N HCl with and without *ZM*-extracted oils. The images were taken at a resolution of 5 μm , and 10000 magnifications for Fig. 4.7.1(c) and 15000 for both Fig. 4.7.1(a) & (b) have been recorded. In the absence of plant oils, MSS disintegration in a corrosive media causes the substrate surface to become rough and damaged (Miralrio & Espinoza Vázquez, 2020). However, adding 5 g L^{-1} of plant extracts causes a noticeable shift in the surface chemistry of MSS. The creation of a protective film on the metal surface prevents the metal from dissolving in a corrosive liquid and gives the surface a smooth appearance, making it easy to compare with the unpolished surface.

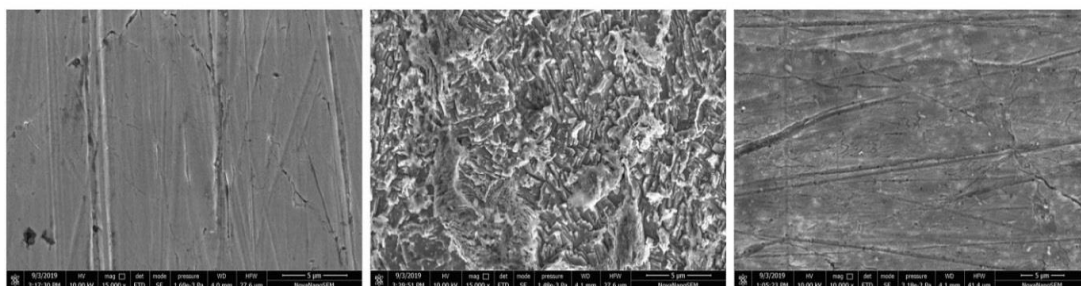


Fig. 4.7.1: SEM images of MSS: (a) before immersion in corrosive solution; (b) after immersion in 1 M HCl for 6 h; (c) after immersion in 1M HCl solution containing 5 g/L *Zingiber mioga* extracted oils for 6 h.

4.7.2 *Zingiber officinale*

SEM images of the metal surface before and after three hours of immersion in 1 N HCl with and without *ZO* were captured at 5 μm resolution and 10000 magnifications for Fig. 4.7.2 (c) and 15000 for both Figs. 4.7.2 (a) and (b) Without plant oils, the substrate surface becomes rough and deteriorates as a result of MSS disintegration in corrosive media (Loto & Solomon, 2022). But the surface chemistry of MSS changes noticeably when 5 g L^{-1} of plant extracts are added. The formation of a protective film on the metal surface keeps the metal from dissolving in a corrosive

liquid and gives a smoother surface, making it simple to compare with an unpolished surface.

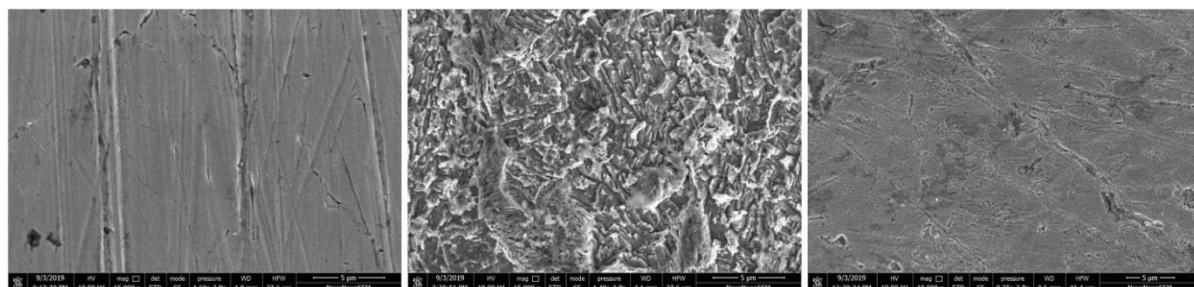


Fig. 4.7.2: SEM images of MSS: (a) before immersion in corrosive solution; (b) after immersion in 1 M HCl for 6 h; (c) after immersion in 1M HCl solution containing 5 g/L *Zingiber officinale* extracted oils for 6 h.

4.7.3 *Mentha piperita*

Figure 4.7.3 shows SEM images of the metal surface before and after three hours of immersion in 1M HCl with and without *Mentha piperita* oil. The images were captured at a resolution of 5 μm and a magnification of 15000. The substrate surface becomes badly affected and rough due to MSS disintegration in corrosive media without plant oils (Salleh et al., 2021). On the other hand, adding 5 g L⁻¹ of plant extracts results in a noticeable change in the surface chemistry of MSS. The formation of a protective film on the metal surface keeps the metal from dissolving in corrosive liquids and gives the surface a smooth finish that is easy to compare to an unpolished surface.

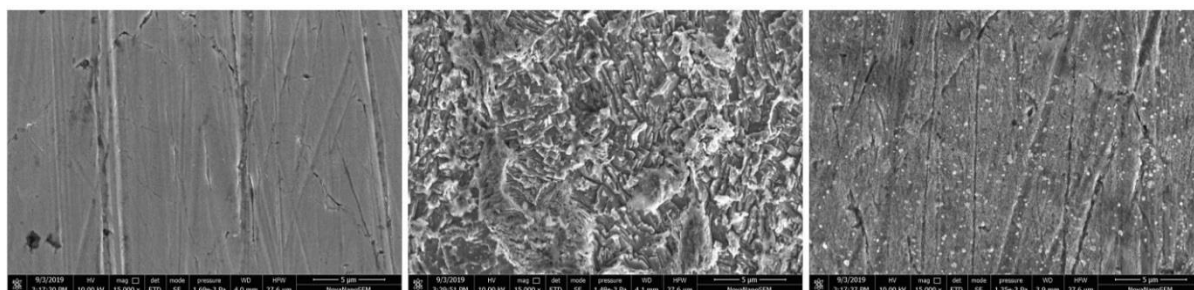


Fig. 4.7.3: SEM images of MSS: (a) before immersion in corrosive solution; (b) after immersion in 1 M HCl for 6 h; (c) after immersion in 1M HCl solution containing 5 g/L *Mentha piperita* extracted oils for 6 h.

4.7.4 *Eryngium foetidum*.

SEM pictures of the metal surface before and after three hours of immersion in 1 N HCl with and without *Eryngium foetidum* extracted oil are recorded at 5 μm resolution 15000 magnifications for both Fig. 4.7.4 (a) & (b) and 10000 for Fig. 4.7.4 (c) MSS disintegration in a corrosive medium in the absence of plant oils causes the substrate surface to become rough and damaged (Singh et al., 2012). The addition of 5g L⁻¹ of plant extracts, on the other hand, results in a noticeable change in the surface chemistry of MSS. The formation of a protective film on the metal surface keeps the metal from dissolving in corrosive liquids and gives the surface a smooth appearance that is easy to compare to an unpolished surface.

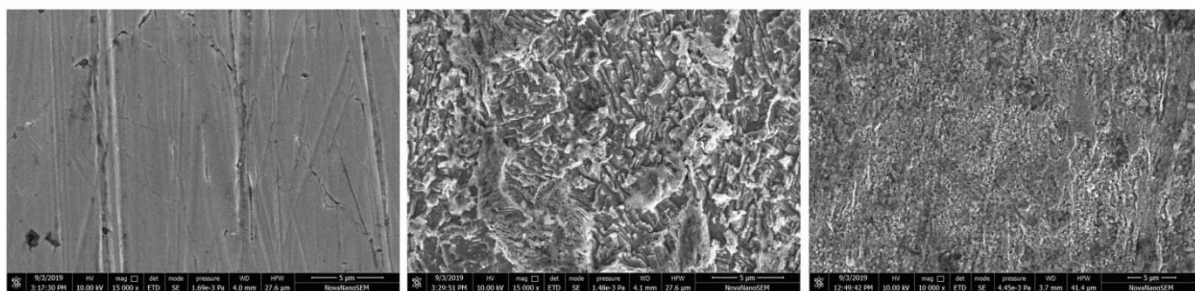


Fig. 4.7.4: SEM images of MSS: (a) before immersion in corrosive solution; (b) after immersion in 1 M HCl for 6h; (c) after immersion in 1M HCl solution containing 5 g/L *Eryngium foetidum* extracted oils for 6 h.

4.7.5 *Allium sativum*

SEM pictures of the metal surface before and after three hours of immersion in 1 N HCl with and without Garlic oil are recorded at 5 μm resolution and 15000 magnification in Fig. 4.7.5 The substrate surface becomes rough and harmed when MSS disintegrates in corrosive media in the absence of plant oils (Zakeri et al., 2022). However, a noticeable change in the surface chemistry of MSS is brought about by adding 5g L⁻¹ of plant extracts. The development of a protective film on the metal surface keeps it from dissolving in corrosive liquids and gives the surface a smooth look that is easy to compare to an unpolished surface.

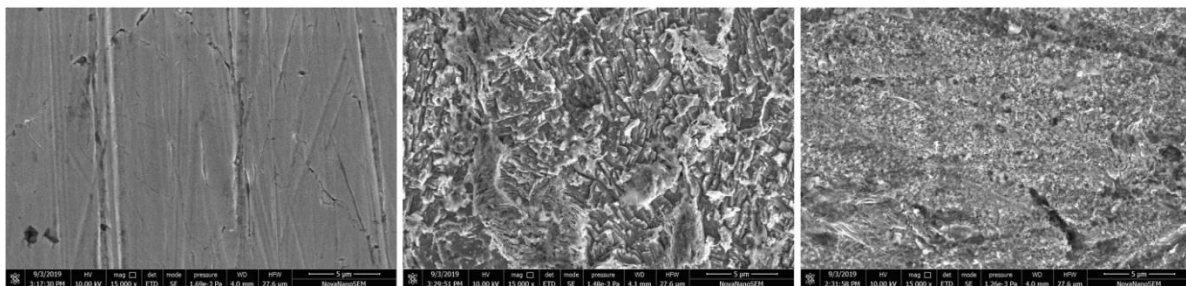


Fig. 4.7.5: SEM images of MSS: (a) before immersion in corrosive solution; (b) after immersion in 1 M HCl for 6 h; (c) after immersion in 1N HCl solution containing 5 g/L *Allium sativum* extracted oils for 6 h.

Based on the surface's roughness, we can conclude that the level of protection has followed the following pattern: *Allium sativum* < *Eryngium foetidum* < *Mentha piperita* < *Zingiber officinale* < *Zingiber mioga*.

4.8 Mechanism of Corrosion Inhibition

4.8.1 Mechanism of Corrosion Inhibition of ZM Extract

The adsorption of inhibitor molecules on the surface of MS has two steps: (i) diffusion of inhibitor molecules from the aqueous phase to the double layer and (ii) inhibitor adsorption over the MS surface. The phytochemical analysis from GC-MS and FT-IR studies shows various organic compounds in the ZM extract. In an acidic medium, these compounds may exist as protonated species, which interact with Cl⁻ on a metallic surface (Figure 4.8.1). Potentiodynamic polarization curves indicate that these inhibitor molecules retarded the corrosion by controlling both anodic and cathodic reactions. Protonated molecules adsorb on cathodic sites of MS to retard the H₂ evolution process, whereas π -system adsorb on anodic sites of MS to prevent the diffusion of metal ions into the aqueous phase (Yadav et al., 2015)

Figure 4.8.1 shows a plausible inhibition mechanism of corrosion inhibition by adsorption of phytochemicals of ZM extracts on the MS surface (Guo et al.,

2014). The interaction between organic molecules present in EOs of ZM is attributed as follows:

- (i) Charge-transfer-type interaction between unshared electron pairs presents in terpineol derivative or π -electrons with empty low energy d- orbitals of Fe atom present on MS surface.
- (ii) Columbic interactions between π -clouds and MS surface/solution interface or between protonated hydroxy and adsorbed Cl^- ions at cathodic sides.

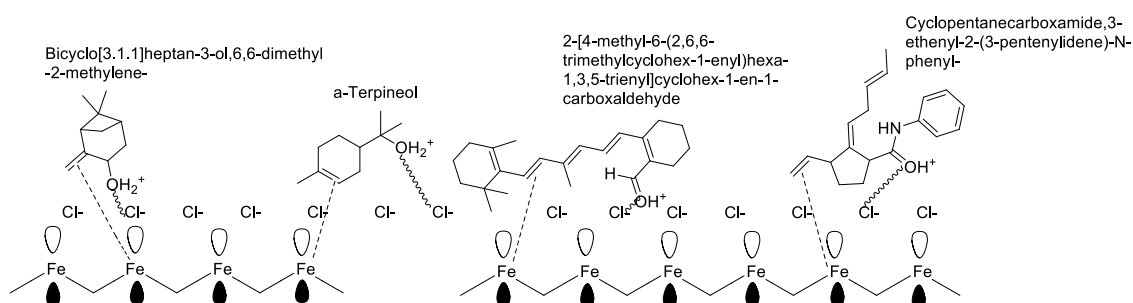


Fig. 4.8.1: Postulated corrosion inhibition mechanism of main constituent compounds in ZM extract

The proposed adsorption mechanism is indicatively understood by the FT-IR study discussed above. FT-IR spectroscopy analysis (Figure 3.3.9) also reveals that the shifting in peaks of -OH and C=C vibration is due to physical interaction between charged metal surface with protonated terpineol, diallyl derivatives, and myrtenol, etc.

4.8.2 Mechanism of Corrosion Inhibition of ZO Extract

The phytochemical analysis from GC-MS and FT-IR studies shows various types of organic compounds in the ZO extract. The inhibitive action of ZO extract on MS in a corroding medium is attributed to the adsorption of these components containing oxygen atoms in functional groups -OH, -CHO, -OR, and octadienal

through C=C and many more. A molecule of small size as a verbinol derivative diffused rapidly and covered the MS surface.

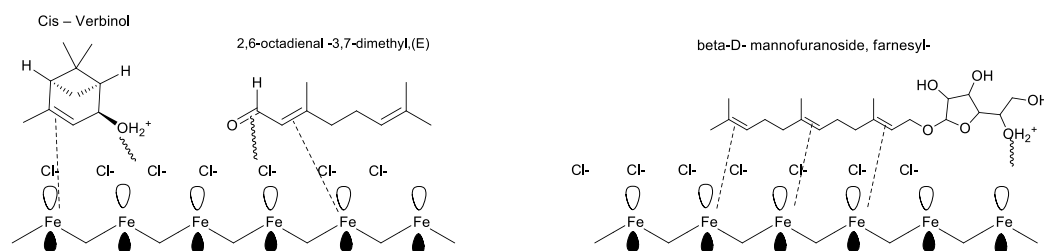


Fig. 4.8.2: Postulated corrosion inhibition mechanism of main constituent compounds in ZO extract

In an acidic medium, these compounds may exist as protonated species, which interact with Cl⁻ on metallic surfaces (Figure 4.8.2). Potentiodynamic polarization curves indicate that these inhibitor molecules retarded the corrosion by controlling both anodic and cathodic reactions. Protonated molecules adsorb on cathodic sites of MS to retard the H₂ evolution process, whereas π-system adsorb on anodic sites of MS to prevent the diffusion of metal ions into the aqueous phase (Yadav et al., 2015).

The proposed adsorption mechanism is indicatively understood by the FT-IR study discussed above. FT-IR spectroscopy analysis (Figure 4.8.2) also reveals that the shifting in peaks of -OH and C=C vibration is due to physical interaction between charged metal surface with protonated verbinol and mannofuranoside etc.

4.8.3 Mechanism of Corrosion Inhibition of EF Extract

The phytochemical analysis from GC-MS and FT-IR studies shows various organic compounds in the EF extract. The inhibitive action of ZO extract on MS in a corroding medium is attributed to the adsorption of these components containing oxygen atoms in functional groups -OH, -COOR, -OR, and dodecatetraene through

C=C and many more. Molecules of small size as camphene, pinene, verbinol, and eucalyptol, diffused rapidly and covered the MS surface.

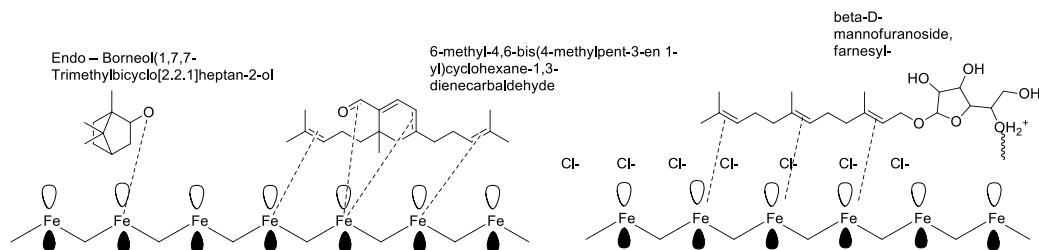


Fig. 4.8.3: Postulated corrosion inhibition mechanism of main constituent compounds in EF extract

In an acidic medium, these compounds may exist as protonated species, which interact with Cl^- on metallic surfaces (Figure 4.8.3). Potentiodynamic polarization curves indicate that these inhibitor molecules retarded the corrosion by controlling both anodic and cathodic reactions. Protonated molecules adsorb on cathodic sites of MS to retard the H_2 evolution process, whereas π -system adsorb on anodic sites of MS to prevent the diffusion of metal ions into the aqueous phase (Yadav et al., 2015).

The proposed adsorption mechanism is indicatively understood by the FT-IR study discussed above. FT-IR spectroscopy analysis (Figure 4.8.3) also reveals that the shifting in peaks of -OH and C=C vibration is due to physical interaction between charged metal surfaces with protonated verbenol, borneol, and mannofuranoside, etc.

4.8.4 Mechanism of Corrosion Inhibition of MP Extract

The phytochemical analysis from GC-MS and FT-IR studies shows various organic compounds in the MP extract. The inhibitive action of MP extract on MS in a corroding medium is attributed to the adsorption of these components containing oxygen atoms in functional groups -OH, -COOR and carveol, carveone through C=C,

and many more. A molecule of small size as carveol, carvone diffused rapidly and covered the MS surface.

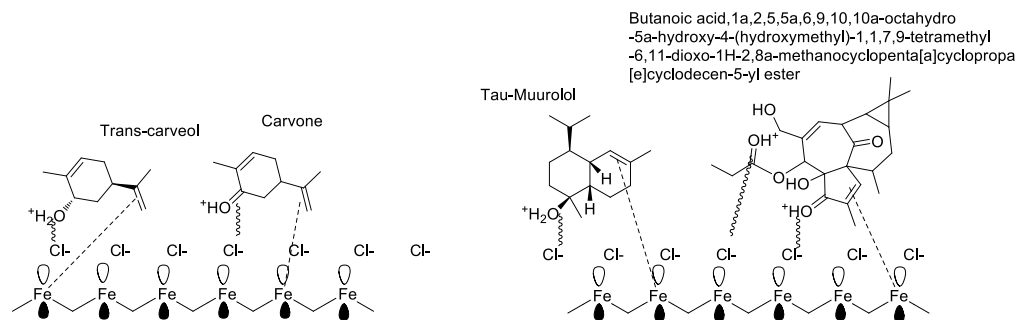


Fig. 4.8.4: Postulated corrosion inhibition mechanism of main constituent compounds in MP extract

In an acidic medium, these compounds may exist as protonated species, which interact with Cl^- on metallic surfaces (Figure 4.8.4). Potentiodynamic polarization curves indicate that these inhibitor molecules retarded the corrosion by controlling both anodic and cathodic reactions. Protonated molecules adsorb on cathodic sites of MS to retard the H_2 evolution process, whereas π -system adsorb on anodic sites of MS to prevent the diffusion of metal ions into the aqueous phase (Yadav et al., 2015).

The proposed adsorption mechanism is indicatively understood by the FT-IR study discussed above. FT-IR spectroscopy analysis (Figure 4.8.4) also reveals that the shifting in peaks of $-\text{OH}$ and $\text{C}=\text{C}$ vibration is due to physical interaction between charged metal surfaces with protonated carveol, carvone, and butanoic acid derivatives, etc.

4.8.5 Mechanism of Corrosion Inhibition of AS Extract

The phytochemical analysis from GC-MS and FT-IR studies shows various organic compounds in the AS extract. The inhibitive action of MP extract on MS in a

corroding medium is attributed to the adsorption of these components containing oxygen atoms in functional groups -OH, -COOR, and diallyl sulfide, dithiine through C=C, -S- and many more. A molecule of small size as diallyl sulfide, dithiine diffused rapidly and covered the MS surface.

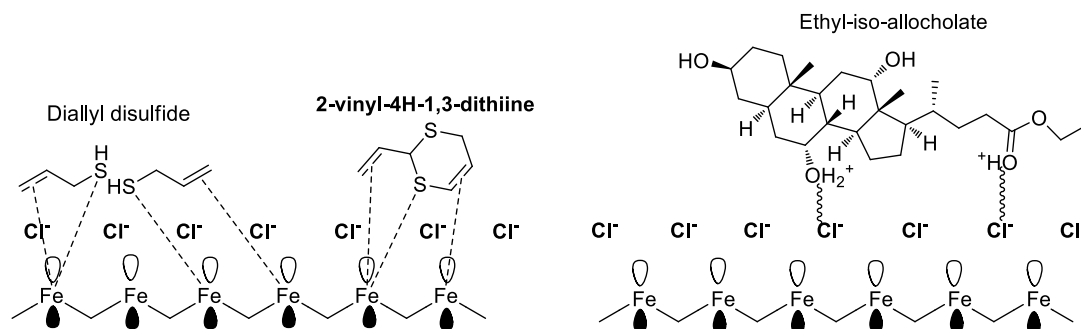


Fig. 4.8.5: Postulated corrosion inhibition mechanism of main constituent compounds in AS extract

In an acidic medium, allochololate-like compounds may exist as protonated species, which interact with Cl^- on metallic surfaces (Figure 4.8.5). Potentiodynamic polarization curves indicate that these inhibitor molecules retarded the corrosion by controlling both anodic and cathodic reactions. Protonated molecules adsorb on cathodic sites of MS to retard the H_2 evolution process, whereas π -system adsorb on anodic sites of MS to prevent the diffusion of metal ions into the aqueous phase (Yadav et al., 2015)

The proposed adsorption mechanism is indicatively understood by the FT-IR study discussed above. FT-IR spectroscopy analysis (Figure 4.8.5) also reveals that the shifting in peaks of -OH and C=C vibration is due to physical interaction between charged metal surface with protonated allochololate etc.

5. SUMMARY AND CONCLUSION

The applicable interpretation and the significant conclusion of the present study of corrosion efficiency effect on corrosion inhibition of mild steel in an acidic medium using different oils extracted from some selected plants are summarized. In this chapter, the most important findings are discussed from the investigation result are thrashed out.

Maintenance and cleaning of mild steel interconnected equipment or machines are required for environmental protection and pollution-free production. When clean and maximized corrosion resistance is present, the machinery gives the most excellent appearance; on the other hand, washing agents cause the corroding apparatus, raising operational and maintenance expenditures (Romero et al., 2010). During cleaning processes, the transportation of MS and processing of some chemical industry corrosion inhibitors are used to minimize the corrosion to maximize the production of good quality products (Rähse, 2014).

Zingiber Myoga (ZM) Extract

The present studies elaborate an exhaustive phytochemical analysis of ZM extract using GC-MS, which helps to identify its major inhibitive components. The essential oil was characterized by the high content of α -Terpineol, (-) -myrtenol, α -Pinene, Trisulphide, di-2-propenyl, Caryophyllene, followed by small amounts of α -Longipinene, Cyclopentanecarboxamide with O and N, 3-ethenyl-2-(3-pentenylidene)-N-phenyl. The major components were Allyl disulfide with sulfur atoms and π -bonds of oils extracted, and it reveals that π -bond and lone pair interact with the vacant -d orbital of Fe atoms.

The weight loss measurements indicated that the corrosion rate of Mild steel in 1 M HCl was observed as 0.174 mg/cm²h, which was decreased to 0.011 mg/cm² h in the presence of 5 g/L ZM oil extract with 93.74% corrosion inhibition efficiency over MS surface.

Langmuir adsorption isotherm studies show that the value of K_{ads} decreases with an increase in temperature. It indicates that the strength of the adsorption bond on the metal surface is decreased and hence shows lower inhibition efficiency at higher temperatures. The obtained value of standard free energy in temperatures (300 K-330 K) is less negative standard free energy around (-15 kJ/mol), usually characteristic of the physical adsorption of inhibitor molecule onto the metal surface.

Arrhenius-type dependence on thermodynamic parameters for the corrosion inhibition process shows that activation energy increases in addition of extract on the metal surface. It is generally interpreted as an indication of the formation of an adsorptive film. The positive sign of ΔH_a reflects the dissolution of MS is slower in the presence of an inhibitor. The entropy of activation ΔS_a in the absence of an inhibitor is mainly due to more extent of metal dissociation.

Potentiodynamic polarization measurements show that ZM oils extract suppressed both the anodic and cathodic reactions. The cathodic curves shifted towards lower current densities (I_{corr}), and corrosion potential (E_{corr}) turned markedly towards negative value in addition of oils extract as compared to the blank solution. This phenomenon indicates that the presence of inhibitors in an acid medium affects the rate of cathodic hydrogen evolution without causing any considerable decrease in the value of corrosion potential and the anodic rate of dissolution of mild steel. However, there was no specific relation between corrosion potential and the inhibitors' concentrations, indicating that the *Zingiber Myoga* EO inhibitors act as mixed-type inhibitors. These consequences are interrelated to the adsorption of the inhibitors compound on the electrode surface at the active sites, which slows down the corrosion reaction at the corrosive medium. The higher value of anodic slopes (β_a) are relatively more affected when compared to the lower values of cathodic slopes (β_c), indicating that the investigated functionalized ZM oils extract predominantly acts as an anodic type.

The vibration spectra bands in the range from 1800 to 800 cm^{-1} accurately reflected the chemical contents of *Zingiber Myoga* oil extracts, particularly lipids, proteins, polysaccharides, and polyphenols.

The primary bands in the infrared spectra of metal surfaces coated with ZM oils correspond to the hydroxyl and carbonyl groups. When compared to the pure extract, the carbonyl band's intensity rose with a slight shift in position (1624 cm^{-1}), and a broad peak attributable to hydroxyl group appeared at 3398 cm^{-1} . In comparison to pure oil, the combined intensities of the individual peaks are extremely low, clearly suggesting the creation of a thin layer on the metal surface.

Zingiber Officinale (ZO) Extract

The analysis of GC-MS data of essential oils extract of ZO revealed the presence of Geraniol (23.30 %), Camphene (12.59 %), Eucalyptol (12.87 %), and α -terpineol (7.38 %) and followed by other structures of few organic molecules with their molecular weight. Ginger extracted oils, and its constituent's α -terpineol, cis-verbinol, and 2, 4-dihydroxybenzoic acid 3TMS derivative acts as benzene derivatives exhibited an anti-corrosive effect under 1 M HCl solution on uniform corrosion for MS corrosion.

The weight loss measurement reveals the corrosion rate of MS in 1M HCl. It was observed that the weight loss of MS corrosion rate was decreased from $0.157\text{ mg/cm}^2\text{h}$ to $0.009\text{ mg/cm}^2\text{ h}$ in the presence of 5g/L of ZO extract with 94.27% corrosion inhibition efficiency over mild steel surface. The corresponding value of standard free energy is between -12.59 to -13.21 kJ/mol , which suggests that the adsorption of ZO extracts over the MS surface is spontaneous. And the low enthalpies tell that it is physical adsorption along with the electrostatic interactions between the inhibitor and the charged metal surface.

It is also noticed from the weight loss data that the corrosion rate for mild steel in 1 M HCl is increased with an increase in temperature from 303 K to 333 K. The inhibitor molecules diffuse back into the solution from the mild steel surface with an increase in temperature; hence, more surface area of mild steel is exposed to the acid medium.

It is observed from the polarization curves that I_{corr} decreases with increasing the concentration of ZO extract in acidic media. It indicates that the inhibitor suppresses the dissolution of iron. In contrast, the variation of the cathodic Tafel slope suggests that the presence of ZO extract significantly suppresses the hydrogen evolution reaction.

Further, the Nyquist plots possess a single semicircle capacitance loop, which indicates the charge transfer corrosion process. The diameter of the capacitive loop increases with an increase in the concentration of inhibitor. It suggests the decrease of corrosion rate due to the adsorption of inhibitor species or species like H^+ on the electrode surface. It is also found that there is a significant decrease in C_{dl} with the addition of an inhibitor, but the value increases with increasing the inhibitor concentration. This result leads to a decline in the local dielectric constant or an increase in the thickness of the electrical double layer. It suggests that the inhibitor molecules form a protective layer at the MS metal surface.

The *Zingiber Officinale* also exhibits the band corresponding to aliphatic groups of proteins and lipids which are major constituents. Intriguingly, FTIR analysis of plant extracts coated on MS surface shows that, due to the interaction of polar functional group to the metal surface, the constituents connected on the surface of metal largely comprise -OH and carbonyl functional group

In an acidic medium, these compounds exist as protonated species interacting with a charged metallic surface. Potentiodynamic polarization curves indicate that these inhibitor molecules retard the corrosion by controlling both anodic and cathodic processes. Protonated molecules adsorb on cathodic sites of MS to retard the H_2 -evolution process. In contrast, the π -system adsorbs on anodic sites of MS to prevent the diffusion of metal ions into the aqueous phase.

***Eryngium foetidum* (EF) Extract**

A combined GC-MS spectral data analysis of EF leaves oil extracts revealed that the constituents of phytochemical obtained have the potential to inhibit the acid corrosion of mild steel. The significant phytochemicals camphene and α -Pinene

(C₁₀H₁₆) are bicyclic monoterpene. Followed by the organic compounds Trifluoroacetyl- α - Terpineol, α -Citral, E-Citral, Duraldehyde, Phenylalanine acts as the presence of oxygen, Nitrogen, aromatic rings, and pie-bond can donate electrons to vacant d orbital to the metal complex.

The weight loss result indicates the effect of EF extract on the C_{rate}, and there is a significant decrease as the concentration of EF oil extract increases. It was due to an increase in the extent of adsorption of inhibitors from EF oil extract to the MS surface in 1M HCl medium. The obtained standard free energy values are around (-12 kJ/mol) and generally, the less negative value of standard free energy approximately (-15 kJ/mol) is usually characteristic of physical adsorption.

The increase in the corrosion rate with an increase in temperature is due to the desorption of the inhibitor molecules, and the adsorption at higher temperatures indicated to physical adsorption of the inhibitor onto the MS surface. The higher value of E_a in the presence of EF oil extract solution suggests the physical adsorption of inhibitor molecules and the formation of a physical barrier at the MS surface/solution interface.

The positive value of ΔH_a indicates that the corrosion process is endothermic. At the same time, a negative correlation was found between the values of ΔS_a and the concentration of inhibitor in the corrosive medium. The higher values of ΔS_a for the inhibition solution are due to an increase in solvent entropy.

The Tafel polarization curves decreased for both anodic and cathodic I_{corr} for all investigated concentrations. The displacement of E_{corr} was around 98 mV towards the cathodic direction with respect to the blank, which showed the inhibitive effect of examined inhibitor. It concludes that the inhibitor is of mixed type. The β_c value was shifted toward the more negative side of the E_{corr} value, whereas β_a was slightly shifted toward the lower E_{corr} side.

The EIS data indicates that the value of C_{dl} decreases, whereas the value of R_{ct} increases with inhibitor concentration in the presence of a larger amount of green inhibitor. The decrease in C_{dl} values is interpreted as either strengthening in

inhibitive film onto the metal surface, i.e., an increase in thickness of the electrical double layer, a decrease in the dielectric constant of the solution, or both.

FTIR spectra of *Eryngium foetidum* oil show the presence of aliphatic C-H in plant extract (See chapter 2 for phytochemical analysis) as major constituent. Low intensity peaks with slight shift ($2\text{-}5\text{ cm}^{-1}$) are observed when the plant extracts are coated on MSS surface, which is indication for formation of thin layer on metal surface. In most of the cases, a broad IR band is observed 3398 cm^{-1} due to OH group form on the surface of MS by atmospheric oxidation. In addition, peaks observed at 685 cm^{-1} is due to formation of the metal-oxygen (functional group) bond. The peak at $\sim 1633\text{ cm}^{-1}$ is due to carbonyl groups of acid/ester and ketonic group present in phytochemicals of *Eryngium foetidum* oil.

Hence, IR spectroscopic studies suggest that in different plant oils mainly lipids and proteins are present. However, carbonyl and hydroxyl group containing phytochemicals are mainly attached to the surface of metal and protect the metal from corrosion.

The interaction between organic molecules present in oils extract of EF is attributed to a charge-transfer-type interaction between unshared electron pairs present in oxygen in carotenoids derivative or π -electrons of carotenoids and empty low energy d orbitals of Fe atom present on MS surface and columbic interactions between aromatic π -clouds and MS surface/solution interface or between protonated β -carotenoids and adsorbed Cl^- ions at cathodic sides.

***Mentha Piperita* (MP) oils extract**

The analysis of GC-MS data of MP oils extracted helps to identify several organic elements of various structures present in inhibitors. It was characterized by components of Trans-carveol, Carvone, Caryophyllene, Germacrene-D, and Cis-calamenene. They inhibited the corrosion effect on mild steel due to the presence of aromatic loops, sulfur, and nitrogen atoms and followed by some amounts of Heptasiloxane, 1,1,3,3,5,5,7,7,9,9,11,11,13,13-tetradecamethyl, Chlorpyrifos, Heptadecanoic acid, 9-methyl ester, Butanoic acid, 1a,2,5,5a,6,9,10,10a-octa, Hydro-

5a-hydroxy-4-(hydroxymethyl)-1,1,7,9-tetramethyl-6,11-dioxo-1H-2, 8a
methanocyclopenta[a]Cyclopropa [e]cyclodecan-5-yl esters. It acts as an inhibitor due to the presence of long-chain fatty acid, which can prevent corrosion attack, and π – bonds reveal that pi-bond and lone pair interact with the vacant d-orbital of Fe atoms.

Weight loss results for MS in 1M HCl for MP oils extract revealed the increase in inhibition efficiency with the increase in MP extract concentrations, eventually decreasing the corrosion rate. This behaviour is due to the increase in surface area covered by the adsorbed molecules on the MS surface with an increase in MP oils extract concentrations having a maximum inhibition efficiency of 94.59%, as is achieved at the concentration of 5 g/L.

Inhibition of MS corrosion in 1M HCl in the presence of oils extract was attributed due to the adsorption of the phytochemical constituents of the extracted oils of peppermint leaves on the mild steel surface and forming a protective layer. It is also observed from the polarization curves that the addition of the inhibitors affected both the anodic and cathodic processes as the curves are shifted towards a lower corrosion current density region with respect to the blank. It is due to inhibitor molecules inhibiting the anodic and cathodic corrosion process of the electrode in the electrolytic solution.

The shifts in corrosion current densities appear more dominant for the anodic curves than the cathodic curves. It suggests that the inhibitor predominantly suppressed the anodic reaction more than the cathodic reaction. These results indicate that inhibitor molecules are adsorbed on the metal surface and retarded the electrode processes. It is considered due to the mixed-type behavior of the studied inhibitors. The obtained inhibitors' efficiency by the electrochemical method is also supported by the weight loss method.

An FTIR spectrum of *Mentha piperita* oils extracted matches well with the reported literatures. Oils coating on metal surface reveal peak corresponding to hydroxyl and carbonyl groups of proteins and lipids. In addition, peaks observed at 721 cm^{-1} is due to formation of the metal-oxygen (functional group) bond. The peak

at $\sim 1627\text{ cm}^{-1}$ is due to carbonyl groups of acid/ester and ketonic group present in phytochemicals of peppermint oil

***Allium Sativum* (AS) oils extract**

The results of GC/MS revealed that SA oils extracts are mainly composed of different organic compounds with various molecular weights, such as 3H-1,2-Dithiole, Dimethyl trisulfide, Diallyl disulfide, Trisulfide, methyl-2-propenyl, 2-vinyl-4H-1,3-dithiine, Allyl trisulfide, Ethyl-iso-allocholate, and chlorpyrifos. Therefore, it can be concluded that the oils extracted from ginger bulbs contain long-chain fatty acids. It can also confirm the presence of the organic compounds containing hetero-atoms containing sulfur and the presence of oxygen and aromatic loop. These compounds can be used as inhibitors in acidic media. Inspection of the structure of the present compound reveals that the π bonds almost protected the metal, and protonated oxygen atoms are involved in the formation of a protective layer on the metal surface.

The gravimetric results indicated a rapid decrease in corrosion rate with an increase in AS extract concentrations. This is because more inhibitor molecules are adsorbed on the MS surface, which protects MS surfaces from an aggressive acidic medium. The corrosion rate of MS in 1M HCl is observed as $0.154\text{ mg/cm}^2\text{h}$, which decreases to $0.008\text{ mg/cm}^2\text{h}$ in the presence of 5 g/L of SA extract with 94.81% corrosion inhibition efficiency over MS. Further, the increase in temperature caused to decrease the corrosion inhibition process.

The Langmuir adsorption isotherm is fitted well in the present system, indicating the monolayer coverage of adsorbed molecules onto the mild steel surface. No lateral interactions are involved between the adsorbed molecules.

The value of standard free energy was found to be less than -20 kJ/mol . The negative value of standard free energy is due to the electrostatic interactions between the inhibitor molecules and the metal surface. Thus, the obtained value of standard free energy suggests physical adsorption on the MS surface in an acidic solution.

The polarization curve was shifted to more negative and more positive potentials with respect to the blank polarisation curve by increasing the concentration of AS oils extract. These observations indicate that the AS oils are a mixed-type inhibitor for the corrosion of mild steel. It is also noted that the cathodic polarization curves slightly shifted toward the negative region, whereas the anodic polarisation curve shifted toward a greater extent, which means that the inhibition of corrosion reaction predominates with inhibitive anodic dissolution reaction in an acidic medium.

It is also seen that the presence of AS extract enhances the values of R_{ct} . The increase in R_{ct} is due to the adsorption of AS oils extract on a metal surface exposed in a corrosive medium and forming a protective film. The intact protective thin film acts as a barrier for intimate interaction of water, oxygen, and corrosive anions on the metal surface. All Nyquist plots exhibit one single capacitive loop, indicating the corrosion of MS in 1M HCl with and without protection is mainly controlled by the charge transfer process and double-layer capacitance. The low C_{dl} values at higher concentrations of AS extract are associated with slower corroding processes, which decrease with the local dielectric constant and cause an increase in the thickness of the electrical double layer.

FTIR spectrum of garlic oil shows the presence of aliphatic C-H as the primary ingredient (See chapter 2 for phytochemical analysis). When plant extracts are coated on MSS, broad peaks are observed at 3498 and 1622 cm^{-1} due to carbonyl groups of acid/ester and ketonic group present in phytochemicals of garlic oil.

The C=C stretching vibration of the allyl group is responsible for the intense peak that can be found at $\sim 1636 \text{ cm}^{-1}$. This was caused by the *Allium Sativum* oil and was identified as belonging to the conjugated double bond of the Diallyldisulphide. Symmetric CH_3 bending modes of the methyl groups of proteins may be detected at $\sim 1400 \text{ cm}^{-1}$.

Future Work

The present study is a starting point for the corrosion inhibition study using plant extracts. The study already established the plant extract as effective corrosion inhibitive agent, but the application of only a few of them is explored. The natural products derived from plants are important from biological and organo-metallic-chemistry points of view.

A limited number of plant extracts are used in metal protection and recognized as corrosive inhibition in acid medium. It also explored the main phytochemical constituent compounds in plant extract that bond with the metal surface.

Further, using the established methodology, large quantities of particular phyto-organic compounds must be explored. The phytochemical is expected to be important from biological, chemical, and other industrial points of view.

Methodology for anti-corrosive studies are established, which may further be commercialized for more significant implications. The efficient inhibitor was tested as a promising alternative for organic substances by comparing the structures of the inhibitors with that of encapsulated coating. An application of natural inhibitors for prevention from the crevice, inter-granular and stress corrosion processes could be investigated and a green corrosion inhibitor could be developed. New techniques need to be employed to interpret corrosion and inhibition mechanisms. The surface analysis could be conducted with the help of new analytical methods, which provides a better understanding of inhibition processes in the different corrosive mediums.

LIST OF PUBLICATIONS

1. **Lalrintluangi**, Ved Prakash Singh, Ashish Kumar Singh, 2022. "Plants and oils extract as corrosion inhibitors for steel corrosion in acid media - A review." (Communicated).
2. **Lalrintluangi**, Jay Prakash Rajan, Manisha Malviya, Raghvendu Pathak, Raj Kumar Mishra. 2022. "Study on essential oils extracted from *Zingiber Mioga* (Aidu) as green inhibitors for corrosion of steel on 1M HCl." (Communicated).

CONFERENCES AND SEMINAR

1. Presented poster entitled, “***Melocanna baccifera* (Bamboo) Leaves as Corrosion Inhibitors for Iron in Acidic Media.**” at 18th National symposium in chemistry, Chemical Research Society of India (CRSI-2016), organised by Institute of Nano Science and Technology and Punjab University, Chandigarh, India held from February 5th – 7th, 2016.
2. Presented paper entitled, “**Study on essential oils extracted from *Zingiber Mioga* (Aidu) as a green inhibitors for corrosion of steel of 1M HCl**” at International Conference on innovation and Application in Science & Technology (ICIAST-2021)-(Zoom Online mode), organised by Deptt. Of Applied Sciences. Galgothias College of Engineering and Technology, Greater Noida UP, India held on 21st - 23rd December 2021.

PARTICULARS OF THE CANDIDATE

NAME OF CANDIDATE : Lalrintluangi
DEGREE : Doctor of Philosophy (Ph.D)
DEPARTMENT : Departmet of Industrial Chemistry
TITLE OF THESIS : Study on corrosion inhibition efficiency of essential oils extracted from some selected plants available in Mizoram.

DATE OF ADMISSION : 13th August, 2014

APPROVAL OF RESEARCH PROPOSAL:

- 1. BOS** : 1st May 2015
- 2. SCHOOL BOARD** : 11th May 2015
- 3. MZU REGN. NO.** : 5440 of 2013
- 4. Ph.D REGN. NO. &DATE:** MZU/Ph.D/732 of 11.05.2015
- 5. EXTENSION** : Extension period 30.06.2022 to 31.12.2022
(No.12-4/MZU(Acad)/20/142)

Head

Department of Industrial Chemistry

REFERENCES:

- Abboud, Y., Abourriche, A., Ainane, T., Charrouf, M., Bennamara, A., Tanane, O., & Hammouti, B. (2009). Corrosion inhibition of carbon steel in acidic media by *Bifurcaria bifurcata* extract. *Chemical Engineering Communications*, 196(7), 788–800.
- Abdel-Gaber, A. M., Abd-El-Nabey, B. A., & Saadawy, M. (2009). The role of acid anion on the inhibition of the acidic corrosion of steel by lupine extract. *Corrosion Science*, 51(5), 1038–1042. <https://doi.org/10.1016/j.corsci.2009.03.003>
- Abe, M., Ozawa, Y., Morimitsu, Y., & Kubota, K. (2008). Mioganal, a novel pungent principle in myoga (*Zingiber mioga* Roscoe) and a quantitative evaluation of its pungency. *Bioscience, Biotechnology, and Biochemistry*, 72(10), 2681–2686.
- Abiola, O. K., Oforka, N. C., Ebenso, E. E., & Nwinuka, N. M. (2007). Eco-friendly corrosion inhibitors: The inhibitive action of *Delonix Regia* extract for the corrosion of aluminium in acidic media. *Anti-Corrosion Methods and Materials*, 54(4), 219–224. <https://doi.org/10.1108/00035590710762357>
- Acharya, G. C., Ponnamp, N., Kumari, M., Roy, T. K., Shivashankara, K. S., & Sahoo, M. R. (2021). Phytochemical profiling of spiny coriander (*Eryngium foetidum* L.)—A potential perennial spicing-culinary herb of eastern India. *Acta Chromatographica*, 34(2), 197–202.
- Afrokh, M., Baroud, S., Kerroum, Y., Hatimi, A., Tahrouch, S., Sadki, I., Warad, I., Guenbour, A., Bellaouchou, A., & Tabyaoui, M. (2021). Green approach to corrosion inhibition of carbon steel by *fucus spiralis* extract in 1 M HCl medium. *Biointerface Research in Applied Chemistry*, 12(5), 7075–7091.
- Ahamad, I., Prasad, R., & Quraishi, M. A. (2010). Adsorption and inhibitive properties of some new Mannich bases of Isatin derivatives on corrosion of mild steel in acidic media. *Corrosion Science*, 52(4), 1472–1481.
- Akinbulumo, O. A., Odejebi, O. J., & Odekanle, E. L. (2020). Thermodynamics and adsorption study of the corrosion inhibition of mild steel by *Euphorbia heterophylla* L. extract in 1.5 M HCl. *Results in Materials*, 5, 100074. <https://doi.org/10.1016/j.rinma.2020.100074>
- Al-Sehaibani, H. (2000). Evaluation of Extracts of Henna Leaves as Environmentally Friendly Corrosion Inhibitors for Metals. *Materialwissenschaft und Werkstofftechnik*, 31(12), 1060–1063. [https://doi.org/10.1002/1521-4052\(200012\)31:12<1060::AID-MAWE1060>3.0.CO;2-K](https://doi.org/10.1002/1521-4052(200012)31:12<1060::AID-MAWE1060>3.0.CO;2-K)

- Al-Senani, G. M. (2016). Corrosion inhibition of carbon steel in acidic chloride medium by Cucumis sativus (cucumber) peel extract. *Int. J. Electrochem. Sci*, 11(1), 291–302.
- Aribo, S., Olusegun, S. J., Ibhadiyi, L. J., Oyetunji, A., & Folorunso, D. O. (2017). Green inhibitors for corrosion protection in acidizing oilfield environment. *Journal of the Association of Arab Universities for Basic and Applied Sciences*, 24, 34–38.
- Avwiri, G. O., & Igho, F. O. (2003). Inhibitive action of Vernonia amygdalina on the corrosion of aluminium alloys in acidic media. *Materials Letters*, 57(22–23), 3705–3711. [https://doi.org/10.1016/S0167-577X\(03\)00167-8](https://doi.org/10.1016/S0167-577X(03)00167-8)
- Bammou, L., Belkhaouda, M., Salghi, R., Benali, O., Zarrouk, A., Zarrok, H., & Hammouti, B. (2014). Corrosion inhibition of steel in sulfuric acidic solution by the Chenopodium Ambrosioides Extracts. *Journal of the Association of Arab Universities for Basic and Applied Sciences*, 16, 83–90.
- Bayol, E., Gürten, A. A., Dursun, M., & Kayakirilmaz, K. (2008). Adsorption behavior and inhibition corrosion effect of sodium carboxymethyl cellulose on mild steel in acidic medium. *Acta Physico-Chimica Sinica*, 24(12), 2236–2243.
- Behpour, M., Ghoreishi, S. M., Khayatkashani, M., & Soltani, N. (2012). Green approach to corrosion inhibition of mild steel in two acidic solutions by the extract of Punica granatum peel and main constituents. *Materials Chemistry and Physics*, 131(3), 621–633. <https://doi.org/10.1016/j.matchemphys.2011.10.027>
- Benali, O., Selles, C., & Salghi, R. (2014). Inhibition of acid corrosion of mild steel by Anacyclus pyrethrum L. extracts. *Research on Chemical Intermediates*, 40(1), 259–268.
- Bhuvaneshwari, T. K., Vasantha, V. S., & Jeyaprabha, C. (2018). Pongamia Pinnata as a Green Corrosion Inhibitor for Mild Steel in 1N Sulfuric Acid Medium. *Silicon*, 10(5), 1793–1807. <https://doi.org/10.1007/s12633-017-9673-3>
- Block, E. (2010). Allium botany and cultivation, ancient and modern. *Garlic and Other Alliums: The Lore and the Science*, 1–32.
- Bommersbach, P., Alemany-Dumont, C., Millet, J.-P., & Normand, B. (2005). Formation and behaviour study of an environment-friendly corrosion inhibitor by electrochemical methods. *Electrochimica Acta*, 51(6), 1076–1084.
- Boonsong, E. (2005). *Seed development and umbel order contribution on eryngio (Eryngium foetidum L.) seed yield and quality* [PhD Thesis]. PhD Thesis, The Graduate School, Kasetsart University, Chatuchak, Bangkok

- Chalchat, J.-C., Garry, R.-P., Michet, A., Benjlali, B., & Chabart, J. L. (1993). Essential Oils of Rosemary (*Rosmarinus officinalis* L.). The Chemical Composition of Oils of Various Origins (Morocco, Spain, France). *Journal of Essential Oil Research*, 5(6), 613–618. <https://doi.org/10.1080/10412905.1993.9698293>
- Chaubey, N., Yadav, D. K., Singh, V. K., & Quraishi, M. A. (2017). A comparative study of leaves extracts for corrosion inhibition effect on aluminium alloy in alkaline medium. *Ain Shams Engineering Journal*, 8(4), 673–682. <https://doi.org/10.1016/j.asej.2015.08.020>
- Chetouani, A., & Hammouti, B. (2014). Salvia officinalis essential oil and the extract as green corrosion inhibitor of mild steel in hydrochloric acid. *Journal of Chemical and Pharmaceutical Research*, 6(7), 1401–1416.
- Coskun, O. (2016). Separation Techniques: CHROMATOGRAPHY. *Northern Clinics of Istanbul*. <https://doi.org/10.14744/nci.2016.32757>
- Da Rocha, J. C. (2010). José Antônio da Cunha Ponciano Gomes, Eliane D’Elia. *Corros. Sci*, 52, 2341.
- Da Rocha, J. C., Gomes, J. A. da C. P., & D’Elia, E. (2010). Corrosion inhibition of carbon steel in hydrochloric acid solution by fruit peel aqueous extracts. *Corrosion Science*, 52(7), 2341–2348.
- Dafaalla, D. M. M. E. (2022). *Phytochemistry and GC-MS Analysis of some Plant Products and Evaluation of their Biological Effects Using Mosquitoes Larvae as Bioindicators* [PhD Thesis]. University of Gezira.
- Dalia Mustafa M Elbashir, Mutaman AA Kehail, Abdalla I Abdalla Mohamed, & Abdelmonem Eltiyab H Ali. (2021). Phytochemistry and GC-MS Screening and Biocidal Potentiality of Ginger (*Zingiber officinale*) Rhizome against Mosquito’s Larvae. *International Journal of Science and Research Archive*, 3(2), 090–096. <https://doi.org/10.30574/ijrsra.2021.3.2.0137>
- Davis, J. R. (1989). *Metals Handbook: Machining*. ASM International.
- Deng, S., & Li, X. (2012). Inhibition by Ginkgo leaves extract of the corrosion of steel in HCl and H₂SO₄ solutions. *Corrosion Science*, 55, 407–415. <https://doi.org/10.1016/j.corsci.2011.11.005>
- Deng, S., Li, X., & Xie, X. (2014). Hydroxymethyl urea and 1,3-bis(hydroxymethyl) urea as corrosion inhibitors for steel in HCl solution. *Corrosion Science*, 80, 276–289. <https://doi.org/10.1016/j.corsci.2013.11.041>

- Deyab, M. A. (2014). Adsorption and inhibition effect of Ascorbyl palmitate on corrosion of carbon steel in ethanol blended gasoline containing water as a contaminant. *Corrosion Science*, 80, 359–365. <https://doi.org/10.1016/j.corsci.2013.11.056>
- Deyab, M. A., Osman, M. M., Elkholy, A. E., & El-Taib Heikal, F. (2017). Green approach towards corrosion inhibition of carbon steel in produced oilfield water using lemongrass extract. *RSC Advances*, 7(72), 45241–45251. <https://doi.org/10.1039/C7RA07979F>
- Dillon, E. P., Andreoli, E., Cullum, L., & Barron, A. R. (2015). Polyethyleneimine functionalised nanocarbons for the efficient adsorption of carbon dioxide with a low temperature of regeneration. *Journal of Experimental Nanoscience*, 10(10), 746–768. <https://doi.org/10.1080/17458080.2014.894256>
- Dinodi, N., & Shetty, A. N. (2014). Alkyl carboxylates as efficient and green inhibitors of magnesium alloy ZE41 corrosion in aqueous salt solution. *Corrosion Science*, 85, 411–427.
- Divya, B. J., Suman, B., Venkataswamy, M., & Thyagaraju, K. (2017). A study on phytochemicals, functional groups and mineral composition of *Allium sativum* (garlic) cloves. *Int J Curr Pharm Res*, 9(3), 42–45.
- Dixit, P. (2021). MEDICINAL IMPORTANCE OF PLANTS: AN OVERVIEW. *ECONOMIC IMPORTANCE OF DIFFERENT CLASSES OF PLANTS*, 113.
- Eddy, N. O., Ameh, P., Gimba, C. E., & Ebenso, E. E. (2011). GCMS studies on Anogessus leocarpus (Al) gum and their corrosion inhibition potential for mild steel in 0.1 M HCl. *International Journal of Electrochemical Sciences*, 6, 5815–5829.
- Eddy, N. O., & Odoemelam, S. A. (2009). Inhibition of corrosion of mild steel in acidic medium using ethanol extract of Aloe vera. *Pigment & Resin Technology*.
- El Ouali, I., Chetouani, A., Hammouti, B., Aouniti, A., Touzani, R., El Kadiri, S., & Nlate, S. (2013). Thermodynamic study and characterization by electrochemical technique of pyrazole derivatives as corrosion inhibitors for C38 steel in molar hydrochloric acid. *Portugaliae Electrochimica Acta*, 31(2), 53–78.
- El Ouariachi, E., Paolini, J., Bouklah, M., Elidrissi, A., Bouyanzer, A., Hammouti, B., Desjobert, J. M., & Costa, J. (2010). Adsorption properties of Rosmarinus officinalis oil as green corrosion inhibitors on C38 steel in 0.5 M H₂SO₄. *Acta Metal. Sin.(Engl. Lett.)*, 23(1), 13–20.

- El-Etre, A. Y. (2007). Inhibition of acid corrosion of carbon steel using aqueous extract of olive leaves. *Journal of Colloid and Interface Science*, *314*(2), 578–583. <https://doi.org/10.1016/j.jcis.2007.05.077>
- Fawzy, A., & Toghan, A. (2021). Inhibition Evaluation of Chromotrope Dyes for the Corrosion of Mild Steel in an Acidic Environment: Thermodynamic and Kinetic Aspects. *ACS Omega*, *6*(5), 4051–4061.
- Florez-Frias, E. A., Barba, V., Lopez-Sesenes, R., Landeros-Martínez, L. L., los Ríos, J. P., Casales, M., & Gonzalez-Rodriguez, J. G. (2021). Use of a metallic complex derived from Curcuma longa as green corrosion inhibitor for carbon steel in sulfuric acid. *International Journal of Corrosion*, 2021.
- Fockaert, L. I., Würger, T., Unbehau, R., Boelen, B., Meißner, R. H., Lamaka, S. V., Zheludkevich, M. L., Terry, H., & Mol, J. M. C. (2020). ATR-FTIR in Kretschmann configuration integrated with electrochemical cell as in situ interfacial sensitive tool to study corrosion inhibitors for magnesium substrates. *Electrochimica Acta*, *345*, 136166. <https://doi.org/10.1016/j.electacta.2020.136166>
- Fouda, A. E.-A. S., Abd El-Maksoud, S. A., El-Sayed, E. H., Elbaz, H. A., & Abousalem, A. S. (2021). Experimental and surface morphological studies of corrosion inhibition on carbon steel in HCl solution using some new hydrazide derivatives. *RSC Advances*, *11*(22), 13497–13512.
- Fouda, A. E.-A. S., & Haleem, E. A. (2020). Tussilago farfara extract (TFE) as green corrosion inhibitor for aluminum in hydrochloric acid solution. *Biointerface Res. Appl. Chem*, *10*, 7023–7041.
- G, B. (1989). Non-conventional machining processes. *Fundamentals of Machining and Machine Tools*, 491. <https://cir.nii.ac.jp/crid/1572261549959938944>
- Gadiyar, H. S., Das Chintamani, & Gaonkar, K. B. (1991). *Chemical cleaning, decontamination and corrosion* (p. 21).
- Gadow, H. S., & Fakeeh, M. (2022). Green inhibitor of carbon steel corrosion in 1 M hydrochloric acid: *Eruca sativa* seed extract (experimental and theoretical studies). *RSC Advances*, *12*(15), 8953–8986. <https://doi.org/10.1039/D2RA01296K>
- Garcia-Arriaga, V., Alvarez-Ramirez, J., Amaya, M., & Sosa, E. (2010). H₂S and O₂ influence on the corrosion of carbon steel immersed in a solution containing 3M diethanolamine. *Corrosion Science*, *52*(7), 2268–2279. <https://doi.org/10.1016/j.corsci.2010.03.016>
- Garverick, L. (1994). *Corrosion in the Petrochemical Industry*. ASM International.

- Groysman, A. (2014). *Corrosion in Systems for Storage and Transportation of Petroleum Products and Biofuels: Identification, Monitoring and Solutions*. Springer Science & Business Media.
- Gupta, R. K., Malviya, M., Verma, C., Gupta, N. K., & Quraishi, M. A. (2017). Pyridine-based functionalized graphene oxides as a new class of corrosion inhibitors for mild steel: An experimental and DFT approach. *RSC Advances*, 7(62), 39063–39074.
- Gutzeit, J., Merrick, R. D., & Scharfstein, L. R. (1987). Corrosion in petroleum refining and petrochemical operations. *ASM Handbook.*, 13, 1262–1287.
- Haldhar, R., Prasad, D., Saxena, A., & Singh, P. (2018). *Valeriana wallichii* root extract as a green & sustainable corrosion inhibitor for mild steel in acidic environments: Experimental and theoretical study. *Materials Chemistry Frontiers*, 2(6), 1225–1237. <https://doi.org/10.1039/C8QM00120K>
- Hasyim, M. R., Ma, D., Rajagopalan, R., & Randall, C. (2017). Prediction of charge-discharge and impedance characteristics of electric double-layer capacitors using porous electrode theory. *Journal of The Electrochemical Society*, 164(13), A2899.
- Heitz, E., Henkhaus, R., & Rahmel, A. (1992). *Corrosion Science: An Experimental Approach*. Ellis Horwood Limited.
- Hoseizadeh, A. R., Danaee, I., & Maddahy, M. H. (2014). Adsorption and corrosion inhibitive properties of 2-Mercaptobenzothiazole on AISI steel 4130 alloy in hydrochloric acid solution. *Kovove Mater*, 52, 35–45.
- Hossain, N., Chowdhury, M. A., Iqbal, A. P., Islam, M. S., Omar, N. Y. S., & Saifullah, A. Z. A. (2021). *Paederia Foetida* leaves extract as a green corrosion inhibitor for mild steel in hydrochloric acid solution. *Current Research in Green and Sustainable Chemistry*, 4, 100191.
- Hosseini, S. M. A., Salari, M., Jamalizadeh, E., Khezripor, S., & Seifi, M. (2010). Inhibition of mild steel corrosion in sulfuric acid by some newly synthesized organic compounds. *Materials Chemistry and Physics*, 119(1–2), 100–105.
- Hussein, U. K., Hassan, N. E.-H. Y., Elhalwagy, M. E., Zaki, A. R., Abubakr, H. O., Nagulapalli Venkata, K. C., Jang, K. Y., & Bishayee, A. (2017). Ginger and propolis exert neuroprotective effects against monosodium glutamate-induced neurotoxicity in rats. *Molecules*, 22(11), 1928.
- Ikpeseni, S. C., Odu, G. O., Owamah, H. I., Onochie, P. U., & Ukala, D. C. (2021). Thermodynamic parameters and adsorption mechanism of corrosion inhibition in mild

- steel using jatropa leaf extract in hydrochloric acid. *Arabian Journal for Science and Engineering*, 46(8), 7789–7799.
- IWASHITA, K., YAMAKI, K., & TSUSHIDA, T. (2001). Mioga (*Zingiber mioga* Rosc.) extract prevents 3T3-L1 differentiation into adipocytes and obesity in mice. *Food Science and Technology Research*, 7(2), 164–170.
- Jafari, N., Ahmadi, S. A., & Razavi, R. (2022). *Experimental and computational study of Trachyspermum leaves extract as a green inhibitor for corrosion inhibition of mild steel in HCl*.
- Ji, G., Dwivedi, P., Sundaram, S., & Prakash, R. (2013). Inhibitive effect of chlorophytum borivilianum root extract on mild steel corrosion in HCl and H₂SO₄ solutions. *Industrial & Engineering Chemistry Research*, 52(31), 10673–10681.
- Johnsirani, V., Sathiyabama, J., Rajendran, S., Christy, S. L., & Jeyasundari, J. (2013). The effect of *Eclipta alba* leaves extract on the corrosion inhibition process of carbon steel in sea water. *Portugaliae Electrochimica Acta*, 31(2), 95–106.
- Kakino, M., Izuta, H., Ito, T., Tsuruma, K., Araki, Y., Shimazawa, M., Oyama, M., Iinuma, M., & Hara, H. (2010). Agarwood induced laxative effects via acetylcholine receptors on loperamide-induced constipation in mice. *Bioscience, Biotechnology, and Biochemistry*, 74(8), 1550–1555.
- Karthik, G., Sundaravadivelu, M., & Rajkumar, P. (2015). Corrosion inhibition and adsorption properties of pharmaceutically active compound esomeprazole on mild steel in hydrochloric acid solution. *Research on Chemical Intermediates*, 41(3), 1543–1558.
- Kavitha, N., Manjula, P., & Kumar, N. A. (2014). Syneristic effect of C. Papaya leaves extract-Zn²⁺ in corrosion inhibition of mild steel in aqueous medium. *Research Journal of Chemical Sciences*, 4(8), 88–93.
- Khadom, A. A. (2013). Effect of corrosive solution motion on copper–nickel alloy pipe in presence of naphthylamine as a corrosion inhibitor. *Journal of Materials and Environmental Science*, 4(4), 510–519.
- Khaled, K. F. (2010). Electrochemical investigation and modeling of corrosion inhibition of aluminum in molar nitric acid using some sulphur-containing amines. *Corrosion Science*, 52(9), 2905–2916. <https://doi.org/10.1016/j.corsci.2010.05.001>
- Kim, Y.-S., & Kim, J.-G. (2017). Evaluation of corrosion fatigue and life prediction of lower arm for automotive suspension component. *Metals and Materials International*, 23(1), 98–105.

- Kliškić, M., Radošević, J., Gudić, S., & Katalinić, V. (2000). Aqueous extract of *Rosmarinus officinalis* L. as inhibitor of Al–Mg alloy corrosion in chloride solution. *Journal of Applied Electrochemistry*, *30*(7), 823–830. <https://doi.org/10.1023/A:1004041530105>
- Kosari, A., Moayed, M. H., Davoodi, A., Parvizi, R., Momeni, M., Eshghi, H., & Moradi, H. (2014). Electrochemical and quantum chemical assessment of two organic compounds from pyridine derivatives as corrosion inhibitors for mild steel in HCl solution under stagnant condition and hydrodynamic flow. *Corrosion Science*, *78*, 138–150.
- Kovács, L., Csupor, D., Lente, G., & Gunda, T. (2014). *100 chemical myths: Misconceptions, misunderstandings, explanations*. Springer.
- Kumar, C. P., & Mohana, K. N. (2014). Phytochemical screening and corrosion inhibitive behavior of *Pterolobium hexapetalum* and *Celosia argentea* plant extracts on mild steel in industrial water medium. *Egyptian Journal of Petroleum*, *23*(2), 201–211.
- Kumari, P. P., Shetty, P., & Rao, S. A. (2017). Electrochemical measurements for the corrosion inhibition of mild steel in 1 M hydrochloric acid by using an aromatic hydrazide derivative. *Arabian Journal of Chemistry*, *10*(5), 653–663.
- Lai, G. Y. (1990). *High temperature corrosion of engineering alloys*. <https://www.osti.gov/biblio/5465166>
- Lavanya, D. K., Priya, F. V., & Vijaya, D. P. (2020). Green approach to corrosion inhibition of mild steel in hydrochloric acid by 1-[Morpholin-4-yl (thiophen-2-yl) methyl] thiourea. *Journal of Failure Analysis and Prevention*, *20*(2), 494–502.
- Lebrini, M., Robert, F., Vezin, H., & Roos, C. (2010). Electrochemical and quantum chemical studies of some indole derivatives as corrosion inhibitors for C38 steel in molar hydrochloric acid. *Corrosion Science*, *52*(10), 3367–3376. <https://doi.org/10.1016/j.corsci.2010.06.009>
- Lewandowski, D. A. (2017). *Design of Thermal Oxidation Systems for Volatile Organic Compounds* (D. A. Lewandowski, Ed.; 1st ed.). CRC Press. <https://doi.org/10.1201/9781315141060>
- Li, J., Fan, T., Xu, Y., & Wu, X. (2016). Ionic liquids as modulators of physicochemical properties and nanostructures of sodium dodecyl sulfate in aqueous solutions and potential application in pesticide microemulsions. *Physical Chemistry Chemical Physics*, *18*(43), 29797–29807.
- Li, X., Deng, S., & Fu, H. (2012). Inhibition of the corrosion of steel in HCl, H₂SO₄ solutions by bamboo leaf extract. *Corrosion Science*, *62*, 163–175.

- Li, X., Deng, S., Fu, H., & Xie, X. (2014). Synergistic inhibition effects of bamboo leaf extract/major components and iodide ion on the corrosion of steel in H₃PO₄ solution. *Corrosion Science*, 78, 29–42.
- Li, X., Deng, S., & Xie, X. (2014). Experimental and theoretical study on corrosion inhibition of oxime compounds for aluminium in HCl solution. *Corrosion Science*, 81, 162–175.
- Li, X., Xie, X., Deng, S., & Du, G. (2014). Two phenylpyrimidine derivatives as new corrosion inhibitors for cold rolled steel in hydrochloric acid solution. *Corrosion Science*, 87, 27–39.
- Lopedota, A. A., Arduino, I., Lopalco, A., Iacobazzi, R. M., Cutrignelli, A., Laquintana, V., Racaniello, G. F., Franco, M., la Forgia, F., & Fontana, S. (2021). From oil to microparticulate by prilling technique: Production of polynucleate alginate beads loading *Serenoa Repens* oil as intestinal delivery systems. *International Journal of Pharmaceutics*, 599, 120412.
- Loto, R. T., & Solomon, M. M. (2022). Application of ginger and grapefruit essential oil extracts on the corrosion inhibition of mild steel in dilute 0.5 M H₂SO₄ electrolyte. *Scientific African*, e01489.
- Machnikova, E., Whitmire, K. H., & Hackerman, N. (2008). Corrosion inhibition of carbon steel in hydrochloric acid by furan derivatives. *Electrochimica Acta*, 53(20), 6024–6032.
- Mahmou, C., Bouissoui, E. M., Bouhlal, F., Labjar, N., Merimi, I., Kaya, S., El Ibrahim, B., Chellouli, M., Dahrouch, A., & El Hajjaji, S. (2021). Synergistic effects of aminotris (methylene phosphonic acid) and Zn²⁺ on the carbon steel corrosion in acid media: An experimental and theoretical approach. *International Journal of Corrosion and Scale Inhibition*, 10(3), 1245–1281.
- Mai, W., Soghrati, S., & Buchheit, R. G. (2016). A phase field model for simulating the pitting corrosion. *Corrosion Science*, 110, 157–166.
- Maqbool, F., Bahadar, H., & Abdollahi, M. (2014). Science for the benefits of all: The way from idea to product. *Journal of Medical Hypotheses and Ideas*, 8(2), 74–77. <https://doi.org/10.1016/j.jmhi.2014.02.002>
- Marimuthu, S., Padmaja, B., & Nair, S. (2013). Phytochemical screening studies on *Melia orientalis* by GC-MS analysis. *Pharmacognosy Research*, 5(3), 216.
- Miksic, B. M., Furman, A. Y., & Kharshan, M. A. (2009, March 22). *Effectiveness Of The Corrosion Inhibitors For The Petroleum Industry Under Various Flow Conditions*.

CORROSION 2009. <https://onepetro.org/NACECORR/proceedings-abstract/CORR09/All-CORR09/126686>

- Miralrio, A., & Espinoza Vázquez, A. (2020). Plant extracts as green corrosion inhibitors for different metal surfaces and corrosive media: A review. *Processes*, 8(8), 942.
- Mobin, M., & Rizvi, M. (2017). Polysaccharide from *Plantago* as a green corrosion inhibitor for carbon steel in 1M HCl solution. *Carbohydrate Polymers*, 160, 172–183. <https://doi.org/10.1016/j.carbpol.2016.12.056>
- Mouhsine, G., Tarfaoui, K., Ouakki, M., Nehiri, M., Touhami, M. E., Barhada, N., & Ouhssine, M. (2019). Valorization of the essential oil of *Zingiber officinale* by its Use as inhibitor against the corrosion of the carbon steel in acid medium hydrochloric acid 1M. *Mediterranean Journal of Chemistry*, 8(1), 17–24.
- Mourya, P., Banerjee, S., & Singh, M. M. (2014a). Corrosion inhibition of mild steel in acidic solution by *Tagetes erecta* (Marigold flower) extract as a green inhibitor. *Corrosion Science*, 85, 352–363.
- Mourya, P., Banerjee, S., & Singh, M. M. (2014b). Corrosion inhibition of mild steel in acidic solution by *Tagetes erecta* (Marigold flower) extract as a green inhibitor. *Corrosion Science*, 85, 352–363.
- Mulder, K. F. (2007). Innovation for sustainable development: From environmental design to transition management. *Sustainability Science*, 2(2), 253–263. <https://doi.org/10.1007/s11625-007-0036-7>
- Murthy, Z. V. P., & Vijayaragavan, K. (2014). Mild steel corrosion inhibition by acid extract of leaves of *Hibiscus sabdariffa* as a green corrosion inhibitor and sorption behavior. *Green Chemistry Letters and Reviews*, 7(3), 209–219.
- Naemnezhad, A., Isari, A. A., Khayer, E., & Esfandiari Birak Olya, M. (2017). Consequence assessment of separator explosion for an oil production platform in South of Iran with PHAST Software. *Modeling Earth Systems and Environment*, 3(1), 43. <https://doi.org/10.1007/s40808-017-0297-9>
- Nair, K. P. (2019). *Turmeric (Curcuma Longa L.) and Ginger (Zingiber Officinale Rosc.)- World's Invaluable Medicinal Spices: The Agronomy and Economy of Turmeric and Ginger*. Springer.
- Ng, J. Y., & Gilotra, K. (2020). Complementary medicine mention and recommendations are limited across hypertension guidelines: A systematic review. *Complementary Therapies in Medicine*, 50, 102374.

- Noor, E. A. (2008). Comparative study on the corrosion inhibition of mild steel by aqueous extract of Fenugreek seeds and leaves in acidic solutions. *Journal of Engineering and Applied Sciences*, 3(1), 23–30.
- Odiongenyi, A. O., Odoemelam, S. A., & Eddy, N. O. (2009). Corrosion inhibition and adsorption properties of ethanol extract of *Vernonia amygdalina* for the corrosion of mild steel in H₂SO₄. *Portugaliae Electrochimica Acta*, 27(1), 33–45.
- Oguzie, E. E. (2006). Adsorption and corrosion inhibitive properties of *Azadirachta indica* in acid solutions. *Pigment & Resin Technology*.
- Okewale, A. O., & Olaitan, A. (2017). The use of rubber leaf extract as a corrosion inhibitor for mild steel in acidic solution. *International Journal of Materials and Chemistry*, 7(1), 5–13.
- Olasunkanmi, L. O., Obot, I. B., Kabanda, M. M., & Ebenso, E. E. (2015). Some quinoxalin-6-yl derivatives as corrosion inhibitors for mild steel in hydrochloric acid: Experimental and theoretical studies. *The Journal of Physical Chemistry C*, 119(28), 16004–16019.
- Ouahrani, M. R., Gherraf, N., lamine Sekirifa, M., & Baameur, L. (2014). Anticorrosive action study of retama retam extracts on mild steel X 52 in 20% H₂SO₄ solution. *Energy Procedia*, 50, 401–405.
- Pandey, A., Soccol, C. R., & Larroche, C. (2008). *Current Developments in Solid-state Fermentation*. Springer Science & Business Media.
- Papavinasam, S. (2021). Electrochemical polarization techniques for corrosion monitoring. In *Techniques for Corrosion Monitoring* (pp. 45–77). Elsevier. <https://doi.org/10.1016/B978-0-08-103003-5.00003-5>
- Park, S.-J., Lee, M., Yun, J.-M., Kim, D., Lee, J., & Lee, Y.-H. (2021). Zingiber mioga extract improves moisturization and depigmentation of skin and reduces wrinkle formation in UVB-irradiated HRM-2 hairless mice. *Applied Sciences*, 11(3), 976.
- Patel, K., Patel, J., Patel, M., Rajput, G., & Patel, H. (2010). Introduction to hyphenated techniques and their applications in pharmacy. *Pharmaceutical Methods*, 1(1), 2. <https://doi.org/10.4103/2229-4708.72222>
- Petek, A., & Kovačič, S. (2014). The influence of Ce³⁺ ions on the corrosion rate of stainless steel in acidic solutions of different pH-values. *Green Chemistry Letters and Reviews*, 7(4), 337–341.

- Prabhu, D., Prabhu, P. R., & Rao, P. (2021). Thermodynamics, adsorption, and response surface methodology investigation of the corrosion inhibition of aluminum by Terminalia chebula Ritz. Extract in H₃PO₄. *Chemical Papers*, 75(2), 653–667.
- Rähse, W. (2014). Industrial product design: Materials for the machinery. *ChemBioEng Reviews*, 1(3), 117–132.
- Raja, P. B., Qureshi, A. K., Abdul Rahim, A., Osman, H., & Awang, K. (2013). Neolamarckia cadamba alkaloids as eco-friendly corrosion inhibitors for mild steel in 1M HCl media. *Corrosion Science*, 69, 292–301. <https://doi.org/10.1016/j.corsci.2012.11.042>
- Raja, P. B., & Sethuraman, M. G. (2008). Natural products as corrosion inhibitor for metals in corrosive media—A review. *Materials Letters*, 62(1), 113–116. <https://doi.org/10.1016/j.matlet.2007.04.079>
- RAJA, P., RAHIM, A., Osman, H., & Awang, K. (2010). Inhibitory effect of kopsia singapurensis extract on the corrosion behavior of mild steel in acid media. *Acta Physico-Chimica Sinica*, 26(8), 2171–2176.
- Rajeswari, V., Kesavan, D., Gopiraman, M., Viswanathamurthi, P., Poonkuzhali, K., & Palvannan, T. (2014). Corrosion inhibition of Eleusine aegyptiaca and Croton rottleri leaf extracts on cast iron surface in 1 M HCl medium. *Applied Surface Science*, 314, 537–545.
- Rao, J. S. (2000). Iron Age of Ancient India. In M. Ceccarelli (Ed.), *International Symposium on History of Machines and Mechanisms Proceedings HMM 2000* (pp. 217–224). Springer Netherlands. https://doi.org/10.1007/978-94-015-9554-4_25
- Romero, I., Ruiz, E., Castro, E., & Moya, M. (2010). Acid hydrolysis of olive tree biomass. *Chemical Engineering Research and Design*, 88(5–6), 633–640.
- Roy, P., Karfa, P., Adhikari, U., & Sukul, D. (2014). Corrosion inhibition of mild steel in acidic medium by polyacrylamide grafted Guar gum with various grafting percentage: Effect of intramolecular synergism. *Corrosion Science*, 88, 246–253. <https://doi.org/10.1016/j.corsci.2014.07.039>
- Sabirneeza, A., & Subhashini, S. (2014). Poly (vinyl alcohol–proline) as corrosion inhibitor for mild steel in 1M hydrochloric acid. *International Journal of Industrial Chemistry*, 5(3), 111–120.
- Salleh, S. Z., Yusoff, A. H., Zakaria, S. K., Taib, M. A. A., Seman, A. A., Masri, M. N., Mohamad, M., Mamat, S., Sobri, S. A., & Ali, A. (2021). Plant extracts as green

- corrosion inhibitor for ferrous metal alloys: A review. *Journal of Cleaner Production*, 304, 127030.
- Sanghavi, M. J., Shukla, S. K., Misra, A. N., Padh, M. R., & Mehta, G. N. (1996). Corrosion inhibition of mild steel in hydrochloric acid by acid extracts of *Sapindus trifolianus*, *Acacia Concian* and *Trifla*. *Transactions of the Metal Finishers' Association of India(India)*, 5(3), 143–147.
- Sastri, V. S. (2011). *Green Corrosion Inhibitors: Theory and Practice*. John Wiley & Sons, Inc. <https://doi.org/10.1002/9781118015438>
- Satapathy, A. K., Gunasekaran, G., Sahoo, S. C., Amit, K., & Rodrigues, P. V. (2009). Corrosion inhibition by *Justicia gendarussa* plant extract in hydrochloric acid solution. *Corrosion Science*, 51(12), 2848–2856.
- Sethuraman, M. G., & Raja, P. B. (2005). Corrosion inhibition of mild steel by *Datura metel* in acidic medium. *Pigment & Resin Technology*.
- Shabani-Nooshabadi, M., Hoseiny, F. S., & Jafari, Y. (2015). Green approach to corrosion inhibition of copper by the extract of *Calligonum comosum* in strong acidic medium. *Metallurgical and Materials Transactions A*, 46(1), 293–299.
- Sharifi-Rad, M., Varoni, E. M., Salehi, B., Sharifi-Rad, J., Matthews, K. R., Ayatollahi, S. A., Kobarfard, F., Ibrahim, S. A., Mnayer, D., & Zakaria, Z. A. (2017). Plants of the genus *Zingiber* as a source of bioactive phytochemicals: From tradition to pharmacy. *Molecules*, 22(12), 2145.
- Sin, H. L. Y., Rahim, A. A., Gan, C. Y., Saad, B., Salleh, M. I., & Umeda, M. (2017). *Aquilaria subintergra* leaves extracts as sustainable mild steel corrosion inhibitors in HCl. *Measurement*, 109, 334–345.
- Singh, A., Ebenso, E. E., & Quraishi, M. A. (2012). Theoretical and electrochemical studies of *Cuminum cyminum* (Jeera) extract as green corrosion inhibitor for mild steel in hydrochloric acid solution. *Int. J. Electrochem. Sci*, 7, 8543–8559.
- Singh, B. K., Ramakrishna, Y., & Ngachan, S. V. (2014). Spiny coriander (*Eryngium foetidum* L.): A commonly used, neglected spicing-culinary herb of Mizoram, India. *Genetic Resources and Crop Evolution*, 61(6), 1085–1090.
- Singh, M., Pant, G., Hossain, K., & Bhatia, A. K. (2017). Green remediation. Tool for safe and sustainable environment: A review. *Applied Water Science*, 7(6), 2629–2635. <https://doi.org/10.1007/s13201-016-0461-9>
- Singh, P., Ebenso, E. E., Olasunkanmi, L. O., Obot, I. B., & Quraishi, M. A. (2016). Electrochemical, theoretical, and surface morphological studies of corrosion

- inhibition effect of green naphthyridine derivatives on mild steel in hydrochloric acid. *The Journal of Physical Chemistry C*, 120(6), 3408–3419.
- Soltani, N., Tavakkoli, N., Khayatkashani, M., Jalali, M. R., & Mosavizade, A. (2012). Green approach to corrosion inhibition of 304 stainless steel in hydrochloric acid solution by the extract of *Salvia officinalis* leaves. *Corrosion Science*, 62, 122–135. <https://doi.org/10.1016/j.corsci.2012.05.003>
- Stratmann, M., Frankel, G. S., & Bard, A. J. (2003). *Corrosion and oxide films (Encyclopedia of Electrochemistry, Vol. 4)*. Weinheim Wiley-VCH.
- Thirupathi, P., & Venkatraman, B. R. (2021). Corrosion inhibition behaviour on carbon steel in well-water by Ethanolic extract of *Portulaca quadrifida* (Chicken weed) leaves. *Indian Journal of Science and Technology*, 14(18), 1488–1504.
- Trabanelli, G. (1991). **1991 Whitney Award Lecture:** Inhibitors—An Old Remedy for a New Challenge. *CORROSION*, 47(6), 410–419. <https://doi.org/10.5006/1.3585271>
- Turcio-Ortega, D., Pandiyan, T., Cruz, J., & Garcia-Ochoa, E. (2007). Interaction of imidazoline compounds with Fe_n (n= 1- 4 ATOMS) as a model for corrosion inhibition: DFT and electrochemical studies. *The Journal of Physical Chemistry C*, 111(27), 9853–9866.
- Umoren, S. A., & Ebenso, E. E. (2008). Studies of the anti-corrosive effect of *Raphia hookeri* exudate gum-halide mixtures for aluminium corrosion in acidic medium. *Pigment & Resin Technology*, 37(3), 173–182. <https://doi.org/10.1108/03699420810871020>
- Umoren, S. A., Gasem, Z. M., & Obot, I. B. (2013). Natural products for material protection: Inhibition of mild steel corrosion by date palm seed extracts in acidic media. *Industrial & Engineering Chemistry Research*, 52(42), 14855–14865.
- Umoren, S. A., Ogbobe, O., Igwe, I. O., & Ebenso, E. E. (2008). Inhibition of mild steel corrosion in acidic medium using synthetic and naturally occurring polymers and synergistic halide additives. *Corrosion Science*, 50(7), 1998–2006. <https://doi.org/10.1016/j.corsci.2008.04.015>
- Valdez, B. (2012). *Food Industrial Processes: Methods and Equipment*. BoD – Books on Demand.
- Verma, C. B., Reddy, M. J., & Quraishi, M. A. (2014). Microwave assisted eco-friendly synthesis of chalcones using 2, 4-dihydroxy acetophenone and aldehydes as corrosion inhibitors for mild steel in 1M HCl. *ANALYTICAL & BIOANALYTICAL ELECTROCHEMISTRY*, 6(3), 321–340.

- Wanklyn, J. N. (1982). Corrosion Monitoring in the Oil, Petrochemical and Process Industries. *Oyez Scientific and Technical Services Ltd, Norwich House, 11-13 Norwich Street, London EC 4 A 1 AB, England, 1982.*
- Wiart, C. (2012). *Medicinal Plants of China, Korea, and Japan: Bioresources for Tomorrow's Drugs and Cosmetics.* CRC Press.
- Wilbertz, J. (2013). *Evaluating societal relevance of research.* s.n.
- Yadav, D. K., & Quraishi, M. A. (2012). Application of Some Condensed Uracils as Corrosion Inhibitors for Mild Steel: Gravimetric, Electrochemical, Surface Morphological, UV–Visible, and Theoretical Investigations. *Industrial & Engineering Chemistry Research*, 51(46), 14966–14979. <https://doi.org/10.1021/ie301840y>
- Yousefi, A., Javadian, S., Dalir, N., Kakemam, J., & Akbari, J. (2015). Imidazolium-based ionic liquids as modulators of corrosion inhibition of SDS on mild steel in hydrochloric acid solutions: Experimental and theoretical studies. *RSC Advances*, 5(16), 11697–11713.
- Yuan, B.-F. (2014). 5-Methylcytosine and Its Derivatives. In *Advances in Clinical Chemistry* (Vol. 67, pp. 151–187). Elsevier. <https://doi.org/10.1016/bs.acc.2014.09.003>
- Zakeri, A., Bahmani, E., & Aghdam, A. S. R. (2022). *Corrosion Communications.*
- Zarras, P., & Stenger-Smith, J. D. (2015). Smart Inorganic and Organic Pretreatment Coatings for the Inhibition of Corrosion on Metals/Alloys. In *Intelligent Coatings for Corrosion Control* (pp. 59–91). Elsevier. <https://doi.org/10.1016/B978-0-12-411467-8.00003-9>
- Zehra, B. F., Said, A., Eddine, H. M., Hamid, E., Najat, H., Rachid, N., & Toumert, L. I. (2022). Crataegus oxyacantha leaves extract for carbon steel protection against corrosion in 1M HCl: Characterization, electrochemical, theoretical research, and surface analysis. *Journal of Molecular Structure*, 1259, 132737. <https://doi.org/10.1016/j.molstruc.2022.132737>
- Zhang, Q. B., & Hua, Y. X. (2009). Corrosion inhibition of mild steel by alkylimidazolium ionic liquids in hydrochloric acid. *Electrochimica Acta*, 54(6), 1881–1887.
- Zhou, L., Li, H., & Shi, C. (2008). Materials research in China. *Nature Materials*, 7(8), Article 8. <https://doi.org/10.1038/nmat2234>
- Zhou, Y., Guo, L., Zhang, S., Kaya, S., Luo, X., & Xiang, B. (2017). Corrosion control of mild steel in 0.1 M H₂SO₄ solution by benzimidazole and its derivatives: An experimental and theoretical study. *RSC Advances*, 7(39), 23961–23969. <https://doi.org/10.1039/C7RA02192E>

ABSTRACT
STUDY ON CORROSION INHIBITION EFFICIENCY OF ESSENTIAL
OILS EXTRACTED FROM SOME SELECTED PLANTS AVAILABLE
IN MIZORAM

AN ABSTRACT SUBMITTED IN PARTIAL FULFILLMENT OF THE
REQUIREMENTS FOR THE DEGREE OF DOCTOR OF
PHILOSOPHY

LALRINTLUANGI

MZU REGISTRATION NO. : 5440 OF 2013

Ph.D REGISTRATION NO. : MZU/Ph.D./732 of 11.05.2015



DEPARTMENT OF INDUSTRIAL CHEMISTRY

SCHOOL OF PHYSICAL SCIENCES

JUNE, 2023

**STUDY ON CORROSION INHIBITION EFFICIENCY OF ESSENTIAL OILS
EXTRACTED FROM SOME SELECTED PLANTS
AVAILABLE IN MIZORAM**

BY

Lalrintluangi

Department of Industrial Chemistry

Under the supervision of

Dr. VED PRAKASH SINGH

Joint supervisors

Prof., RAJ KUMAR MISHRA

Dr. RAGHVENDU PATHAK

Dr. ASHISH KUMAR SINGH

Submitted

**In partial fulfillment of the requirement of the Degree of Doctor of Philosophy in
Industrial Chemistry of Mizoram University, Aizawl.**

ABSTRACT

Corrosion is a subject of interest to interdisciplinary research communities, combining fields of materials science, chemistry, physics, metallurgy, and chemical engineering. To understand the mechanisms of corrosion and the function of corrosion inhibitors, the reactions at the interfaces between the corrosive electrolyte and a steel surface, particularly at the initial stages of the corrosion process, need to be studied. Here is a study on corrosion inhibitive properties of various plant extracts obtained from Mizoram. Characterizing corrosion products on corroded metal surfaces helps with corrosion inhibition processes. The analysis of plant constituents is considered a very large number of natural products present in the crude extract of plants. The extraction technique establishment for the active compounds associated with the metal surface and the inhibitor molecule adsorption thermodynamics is studied to understand the corrosion inhibitive mechanism. Mild steel Metals have been extensively studied in the corrosive medium using chemical and quantum calculations to understand their nature of corrosion and the molecular structure of inhibitor molecules under equilibrium and non-equilibrium thermodynamic conditions.

The present study uses corrosion inhibitors to protect metals and alloys in aggressive environments. Large numbers of organic compounds were investigating their corrosion inhibition potential. Literature studies revealed that organic compounds, especially with heteroatoms, such as nitrogen, sulfur, oxygen, and multiple bonds containing compounds, inhibit the corrosion reaction.

Considering this, the global interest has increased to utilize wild plant resources for alternative and valuable natural products used for prevention in the corrosive medium for minimizing metal dissolutions. This scenario has led us to search for new alternatives application.

Chapter 1 deals with a detailed survey of the literature, which includes the importance of iron, its alloys used for industrial and domestic purposes, the scope of the study, their degradation properties in industrial operational conditions, thermodynamics inhibition process. Also, describe one or more of the corrosion protection methods implemented to reduce the corrosion process and extend the lifetime of the structural iron materials.

Chapter 2, the medicinal plant, and the present work are devoted to phytochemical analysis of the essential oil of some commonly available medicinal plants in Mizoram, India.

We selected the following plants for the present study to evaluate their anti-corrosive property, commonly used in Mizoram. Such as buds of *Zingiber mioga* (ZM), the rhizome of *Zingiber officinale* (ZO), leaves of *Eryngium foetidum* (EF), leaves of *Mentha piperita* (MP), and scaly bulb of *Allium sativum* (AS).

Extraction of oils from some selected plants was done by the Cleavenger apparatus using the Hydro-distillation method used for extraction of active phytoconstituents from plants.

In this chapter, we have discussed the significant phytochemicals present in the samples. GC-MS characterized ZM essential oil. The major components are Diallyl disulfide with sulfur atoms and π -bond of extracted oils, and it reveals that π -bond and lone pair interact with the vacant d orbital of Fe atoms. ZM oil extract primarily included aliphatic phytochemicals, and it is evident from FTIR studies that only phytochemicals having hydroxyl/carbonyl groups of alcohol/acid/ester/aldehyde/ketonic group were able to form a protective layer on metal surfaces.

In the analysis of the essential oil of ZO, the most abundant components are Geranial (23.30 %), Camphene (12.59 %), Eucalyptol (12.87 %), and alpha-terpineol (7.38 %). Ginger extracted oils, and its constituent's α -terpineol, cis- verbinol, and 2, 4-dihydroxybenzoic acid

3TMS derivative acts as benzene derivatives exhibited an anti-corrosive effect under 1 M HCl solution on uniform corrosion for MS corrosion.

The ZO also exhibits the band corresponding to aliphatic groups of proteins and lipids, which are major constituents. Intriguingly, FTIR analysis of plant extracts coated on MS surface shows that, due to the interaction of the polar functional group to the metal surface, the constituents connected on the metal surface largely comprise -OH and carbonyl functional group.

A combined GC-MS spectral data analysis of EF leaves extracted, Phenylalanine acts as the presence of oxygen, nitrogen, aromatic rings, and π -bond can donate electrons to vacant d orbital to the metal complex. IR spectroscopic study of EF suggests that in different plant oils, mainly lipids and proteins are present. However, carbonyl and hydroxyl groups containing phytochemicals are primarily attached to the surface of the metal and protect the metal from corrosion.

MP essential oil was characterized by components that inhibit the corrosion effect on mild steel due to the presence of aromatic loops, sulfur, and nitrogen atoms. Butanoic acid acts as long-chain fatty acid capable of preventing corrosion attacks. It reveals that π -bond and lone pair interact with the vacant d orbital of Fe atoms. FTIR peaks observed at 721 cm^{-1} are due to forming of the metal-oxygen (functional group) bond. The peak at $\sim 1627\text{ cm}^{-1}$ is due to carbonyl groups of acid/ester and ketonic group present in phytochemicals of peppermint oils.

AS (Garlic bulb) extracted oils were used in GC-MS analysis. A combined GC-MS spectral data analysis of AS bulb extracted, 3-H-1,2-Dithiole, Dimethyl trisulfide, Diallyldisulfide acts as a lone pair donor in the presence of sulphur, aromatic rings, and π -bond can donate electrons to vacant d orbital to the metal complex. This essential oil contain mainly Oxygen, Sulfur, Phosphorus and Silicon containing phytochemicals. IR spectroscopic

study of AS suggests that in different plant oils, mainly lipids and proteins are present. However, carbonyl, ether, ester and hydroxyl groups containing phytochemicals are primarily attached to the surface of the metal and protect the metal from corrosion.

It can be concluded that the oils extracted from ginger buds contain long-chain fatty acid; it can also confirm the presence of the organic compounds containing hetero-atoms containing sulfur and oxygen and aromatic loops. These compounds can be used as inhibitors in acidic media. In FT-IR studies, the C=C stretching vibration of the allyl group is responsible for the intense peak found at $\sim 1636\text{ cm}^{-1}$ and belongs to the conjugated double bond of the Diallyl disulfide.

In Chapter 3, corrosion inhibition is studied in 1M HCl in mild steel using weight loss, potentiodynamic polarization, and the A.C impedance method.

The weight loss method is the simplest way to measure the corrosion rate and directly determine the quantity corrosion rate in a corrosive medium. Here the test specimens were weighed before and after exposure to the corrosion medium. The weight loss measurements reveal that the inhibition efficiency linearly increases with increasing concentration of plant extract.

The potentiodynamic measurement results show that corrosion potential shifted towards a more negative value, and cathodic curves shifted towards lower current densities in the presence of ZM plant extract compared to blank. It means that the cathodic inhibition reaction is predominant.

Inspection of the polarization curves of ZO reveals that anodic branches shifted towards lower corrosion current density with increasing inhibitor concentration and higher value of β_a over β_c . It means that the anodic reaction is the predominantly observed phenomenon, indicating that the inhibitor could suppress the dissolution of iron. In contrast,

the variation of the cathodic tafel slope suggests the suppression of the hydrogen evaluation reaction by ZO extract.

The obtained results from weight loss measurements illustrate that the corrosion rate of mild steel in 1M HCl was observed as 0.170 mg/cm²/h, which decreases to 0.005 mg/cm²/h in the presence of 5 g/L EOs extracts of EF with 97.06 % corrosion inhibition efficiency over mild steel.

It can be seen from polarization curves that there is a decrease in both anodic and cathodic I_{corr} , most significantly in the cathodic region at all investigated concentrations, and the displacement of E_{corr} was around 99.07 mV towards the cathodic direction with respect to the blank, which shows the mixed type of inhibitive effect of examined inhibitor corrosion rate.

Weight loss results for mild steel in 1M HCl revealed increased inhibition efficiency with the concentration of MP extract and corrosion rate decreases. This behavior can be attributed to the increase in surface area covered by the adsorbed molecules on the mild steel surface with an increase in the concentration of MP extract. The maximum efficiency of 94.59 % of MP extract was achieved at the concentration of 5 g/L.

It could be observed from the polarization curves that shift in corrosion current densities appear to be more dominant for the anodic curves than the cathodic curves. It suggests that the inhibitors might have more predominant effects on the anodic reaction than the cathodic one.

From the EIS study from AS oils extract, the diameter of the depressed semicircle becomes more significant with increasing the inhibitor concentration as obtained from leading to the fall of corrosion rate through adsorption of inhibitor species like H⁺ atoms on the surface of electrodes and the surface coverage gradually increases.

In Chapter 4, we discussed the surface characterization of the MS by SEM image before and after immersion in the presence and absence of inhibitors concentration of 5g/L. The morphology (SEM image) of the mild steel with all the above oil extract shows a significant difference from the blank MS without inhibitor in an acidic solution. The extent of the rough surface formed on the metal surface is reduced due to the adsorptions of inhibitor molecules.

The inhibitor particles disperse into 1M HCl solution from the surface of the metal with the temperature rise. The surface area of mild steel exposed to a corrosive medium becomes more significant, then the inhibition efficiency decreases. To confirm the adsorption-desorption of corrosion inhibitors on the metal surface. At the entire temperature, a high R^2 correlation coefficient and the graph plot gives a straight line that reveals that inhibitors obey the Langmuir-adsorption isotherm.

Moreover, the negative sign of Gibb's free adsorption energy indicates that the adsorption is spontaneous. The small value of K_{ads} indicates the inhibitor molecule and the charge ions held together by weak interaction on the metal surface. All these indicate that the inhibition process is exposed by physical adsorption.

In Chapter 5, we have shown the summary and conclusion obtained from the result and discussion. Now we conclude that all studied plants show similar Langmuir adsorption isotherm behavior in the presence of oils extract.

In all circumstances, the inhibition efficiency increases with increasing the concentration of inhibitor, and the curves from weight loss, Nyquist, and Tafel have similar results supporting each other. In all the corrosion rate calculations and thermodynamic properties, the important parameters of phytoconstituents have been used for corrosion inhibitors.